ENGINEERING AND INDUSTRIAL RESEARCH STATION

FACILITY FORM 602

N65-29675
(ACCESSION NUMBER)

(THRU)

121
(PAGES)

1
(CODE)

CR 64055
(NASA CR OR TMX OR AD NUMBER)

12
(CATEGORY)

Annual Report

NAS8-11334

RESEARCH STUDY FOR DETERMINATION OF LIQUID SURFACE PROFILE IN A CRYOGENIC TANK DURING GAS INJECTION

June 18, 1964 - June 17, 1965

GPO PRICE $ ____

CFSTI PRICE(S) $ ____

Hard copy (HC) 4.00

Microfiche (MF) 1.00

ff 653 July 65

COLLEGE OF ENGINEERING

MISSISSIPPI STATE UNIVERSITY
STATE COLLEGE, MISSISSIPPI

Engineering and Industrial Research Station
College of Engineering
Mississippi State University
P.O. Box 147, State College, Mississippi 39762

Annual Report, NAS8-11334
RESEARCH STUDY FOR DETERMINATION OF LIQUID SURFACE
PROFILE IN A CRYOGENIC TANK
DURING GAS INJECTION

Period Covered: June 18, 1964 - June 17, 1965

Authors

Dr. E. H. Bishop
Dr. W. D. McCain, Jr.

Contributors

Mr. R. E. Forbes
Mr. H. P. Horner
Dr. W. A. Kennedy
Dr. C. W. Bouchillon
Dr. E. W. Hough

Annual Report:
Contract Number: NAS8-11334
Control Number: DCN 1-4-50-01218-01 (1F)
CPB 02-1277-64

June 17, 1965

This report was prepared by Mississippi State University under NAS8-11334, RESEARCH STUDY FOR DETERMINATION OF LIQUID SURFACE PROFILE IN A CRYOGENIC TANK DURING GAS INJECTION, for the George C. Marshall Space Flight Center of the National Aeronautics and Space Administration. The work was administered under the technical direction of the Propulsion and Vehicle Engineering Laboratory of the George C. Marshall Space Flight Center with Mr. Hugh M. Campbell acting as project manager.

TABLE OF CONTENTS

TABLE OF CONTENTS -- Continued

LIST OF FIGURES

LIST OF FIGURES -- Continued

NOMENCLATURE

a	Bubble radius
A	x dimension of ellipsoid
B	y dimension of ellipsoid
C	z dimension of ellipsoid
d	Bubble diameter
D'	Distance between bubble centers
D	Dimensionless distance between bubble centers, $D = \frac{D'}{a}$
DEQ	Equivalent bubble diameter
$f(r)$	An arbitrary function used in equation (40); for this work $f(r) = \sqrt{1-r^2}$
$F(r)$	Function as defined by equation (9)
g	Acceleration of gravity
g_c	Dimensional constant
h_f	Height of fluid above reference plane
H'	Upper limit of integration in equation (7)
H	Dimensionless upper limit of integration in equation (9), $H = \frac{H'}{a}$
i	Unit vector
j	Unit vector
K	Defined by equation (17), $K = \frac{F(r)}{U^2}$
N_{Re}	Bubble Reynolds Number, $N_{Re} = \frac{Ud}{\nu_L}$
K.E.	Kinetic energy
P.E.	Potential energy
P	Pressure
P_{atm}	Atmospheric pressure

r'	Cylindrical radial coordinate
R'	Spherical radial coordinate
r	Dimensionless cylindrical radial coordinate, $r = \frac{r'}{a}$
R	Dimensionless spherical radial coordinate, $R = \frac{R'}{a}$
u	Vertical velocity component
u_o	Tangential velocity component for real solution in spherical coordinate system, defined by equation (43b)
u_o'	Perturbed vertical velocity component
U	Bubble terminal velocity
U_o	Potential vertical velocity component
UC	Vertical velocity component for the real solution, defined by equation (50)
v	Radial velocity component
$\bar{v}$	Velocity $= \sqrt{u^2 + v^2}$
v_o	Radial velocity component for real solution in spherical coordinate system, defined by equation (43a)
v_o'	Perturbed radial velocity component
$\vec{v}_o'$	Perturbed velocity field, see equation (8a)
V_o	Potential radial velocity component
$\vec{V}_o$	Potential velocity field, see equation (8b)
$\overline{v^2}$	Time average of velocity squared
VC	Radial velocity component for the real solution, defined by equation (49)
VOL	Volume of ellipsoid
y	$(R'-a)$, distance from the bubble surface
z'	Vertical coordinate

z	Dimensionless vertical coordinate, $z = \frac{z'}{a}$
$Z(r)$	Dimensionless surface profile defined by equation (3c)
Z_s	Dimensional surface profile defined by equation (3e)
Z_c	Height of free surface above the undisturbed free liquid surface computed by correlation procedure, equation (28)
Φ_c	Potential function in cylindrical coordinates
Φ_s	Potential function in spherical coordinates
ζ_o	A function of Reynolds number and position in the perturbed region, defined by equation (46)
μ_g	Viscosity of gas
μ_L	Viscosity of liquid
ρ_g	Density of gas
ρ_L	Density of liquid
ν_L	Dynamic viscosity of liquid, $\nu_L = \frac{\mu_L}{\rho_L}$
θ	Angle in spherical coordinate system
π	Constant, 3.14159
α	Degree of penetration of bubble into surface, defined by equation (28a)
erf	Error function, see Appendix IV
erfc	Complimentary error function, see Appendix IV
ierfc	Integral of complimentary error function, see Appendix IV

ANALYSIS OF PROGRESS

By applying the principle of conservation of energy to the fluid surrounding a rectilinearly rising spherical bubble, or column of non-interfering bubbles, an equation for the free liquid surface profile caused by injection of gas bubbles into a tank of liquid was developed. In dimensionless form the surface profile is given by

$$Z(r) = \frac{F(r)}{2HU^2} , \tag{3d}$$

and in dimensional form by

$$Z_s = \frac{U^2 Z(r)}{g} , \tag{3e}$$

where

$$\frac{F(r)}{U^2}$$

is a dimensionless time mean kinetic energy distribution and

$$F(r) \equiv \int_{\sqrt{1 - r^2},\, 0}^{H} \bar{v}^2 (r,Z)dZ \quad . \tag{9}$$

Calculations of $\frac{F(r)}{U^2}$ utilizing a potential flow model and a flow model based upon the research of B. T. Chao (11) were made. A comparison of the results showed that certain undesirable features obtained by use of the potential flow model were eliminated or reduced by the Chao model. Thus, the potential flow model was dropped from further consideration.

Plots of Z(r) and Z_s have been made for several Reynolds numbers to demonstrate the behavior of the surface profile as the bubble rise velocity is varied. The results for Z(r) showed that the dimensionless surface profile was not a strong function of Reynolds number for $N_{Re} \leq 450$. Thus, utilizing a least squares method, the following equation for Z(r), independent of N_{Re} in this range, was developed:

$$2HZ(r) = .182907 + .086949r - .245937r^2 + .102929r^3 - .012489r^4. \quad (21)$$

In dimensional form

$$Z_s = \frac{N_{Re}^2 \; \nu_L^2}{g d^2}\left[.0091453 + .0043475\left(\frac{r'}{a}\right) - .0122968\left(\frac{r'}{a}\right)^2 + .0051464\left(\frac{r'}{a}\right)^3 - .0006244\left(\frac{r'}{a}\right)^4\right] . \quad (24)$$

Comparison of the surface profiles computed by the previous equations with those predicted by numerical integration of F(r) showed that satisfactory results were obtained by equations (21) and (24).

Limited progress has been made in the area of bubble-to-bubble interference. A direct superposition method was employed to obtain a first approximation to the velocity field generated by two bubbles of equal size, rising side by side at the same velocity. The results of this method are presented in graphical form.

The surface disturbance caused by a single column of non-interfering bubbles has been photographically recorded. Sequence photographs taken from the frames of high speed motion picture film were made which show the build-up and collapse of the surface disturbance. Images of the maximum disturbance have been measured at a magnification, with reference to true size, of about 35 to 1.

The maximum surface disturbances due to several different bubbles have been averaged and presented graphically.

Comparisons between these experimental profiles and those predicted analytically were made for bubbles of various Reynolds numbers. A surface profile correlating procedure, modifying the analytically based equation by accounting for bubble surface penetration, was developed utilizing the results of the photographic work. The resulting equation was

$$Z_c = Z_s H + \alpha a \sqrt{1-r^2} \tag{28}$$

where

$$\alpha = 0.00122 N_{Re} - 0.305 \quad . \tag{29}$$

An interesting adjunct to this work was the discovery of the origin of the spray droplets which appear above the liquid surface. These droplets are formed when the gas bubbles break at the free liquid surface. A sequence taken from the high speed motion picture film showing this phenomenon is given.

INTRODUCTION

This is the first Annual Progress Report for NAS8-11334, RESEARCH STUDY FOR DETERMINATION OF LIQUID SURFACE PROFILE IN A CRYOGENIC TANK DURING GAS INJECTION. The period covered is June 18, 1964 to June 17, 1965. This report constitutes a compilation of the salient features of all previous monthly and quarterly progress reports for the period covered. The material is not presented in chronological order, but has been arranged for purposes of clarity. The reader may wish to refer to previous quarterly reports for certain details, such as Quarterly Progress Report #1 for abstracts of many of the articles given in the Bibliography.

PROGRESS

When bubbles are admitted into the bottom of a tank containing a stagnant liquid, surface disturbances develop which may be detrimental under conditions where the height of the liquid surface is critical. Initiation of the process entails complex transient phenomena which are difficult to analyze. In an attempt to predict the surface profile, for given gas input rates, the problem is greatly simplified if only the steady state case is considered. The assumption of steady state may be justified for some cases where the total time of operation is large in comparison with the time lapse of the initiation transient. In other cases, the initiation conditions may be critical and thereby impose the necessity for consideration of the transient behavior.

In order to better understand the phenomena under consideration, it will be assumed that analysis of the steady state case will yield useful results regarding the free surface profile. All subsequent discussion will be concerned with steady state.

ANALYTICAL

Formulation of the Theory for Surface Profile Predictions

Consider a continuous stream or swarm of gas bubbles rising in an initially stagnant liquid with a free surface. As a result of the rising bubbles, the liquid will be set in motion, and after a period of time, definite circulation patterns will be established. Prior to the injection of the gas bubbles into the liquid, the free liquid surface would be flat and possess a certain potential energy with respect to an arbitrary reference plane. As a result of the rising bubbles, the free liquid surface will be raised and distorted from the initial flat profile, indicating a change in potential energy of the liquid at the surface over that which it possessed prior to the initiation of the bubble injection. This change in the potential energy distribution at the liquid surface is caused by the kinetic energy imparted to the liquid by the rising bubbles.

That the above is the case may be seen by applying the conservation of energy principle to the system. If we neglect friction and consider that no work is done on or by the system, this principle may be stated simply as

$$\sum \text{K.E.} \quad + \quad \sum \text{P.E.} \quad = \quad \text{Constant}$$

where

K.E. is kinetic energy and

P.E. is potential energy.

For any point in the liquid regime the equation representing the conservation of energy principle may be written by considering

$$K.E. = \frac{1}{2} \frac{\rho v^2}{g_c}$$

$$(P.E)_{Pressure} = P_{atm} + \frac{\rho gh}{g_c}$$

$$(P.E.)_{gravity} = \frac{\rho gz}{g_c}$$

where ρ is the fluid density (the fluid is considered to be incompressible), v is the fluid velocity, P is atmospheric pressure, g is the acceleration of gravity, g_c is a dimensional constant, h is the height of the liquid above the point in question, and z is the vertical coordinate measured from some arbitrary reference plane; and observing that

$$\left[(K.E.) + (P.E.)_{pressure} + (P.E.)_{gravity}\right] = \text{Constant.} \qquad (1)$$

We shall now consider a single spherical gas bubble rising rectilinearly in a cylindrical tank, filled with liquid, where the inside radius of the tank is large in comparison to the bubble radius. A reference plane for potential energy due to gravitational effects is taken as a plane located at section 1-1 which is sufficiently removed from the bottom that entrance effects have subsided and terminal velocity has been achieved. The plane is located so that it passes through the center of the bubble. This may be seen in Figure 1.

At a given radial position the energy passing a given plane, for instance, plane 1-1 in Figure 1, may be time averaged in order to predict the mean value of the energy passing during a given time interval. This is tantamount to taking a space average at a given instant. This procedure will thus

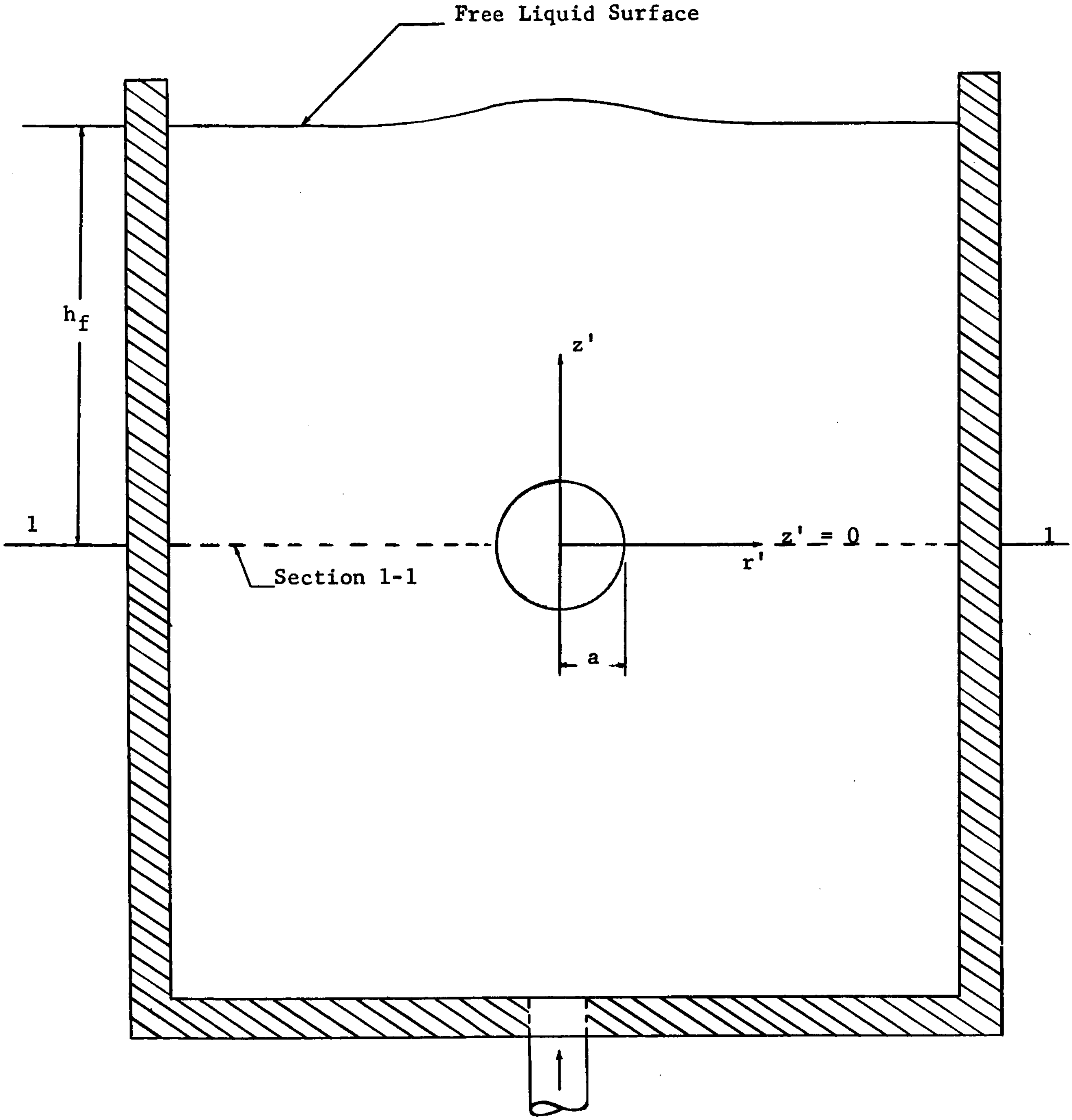

Figure 1. Single Spherical Bubble Rising Rectilinearly in a Large Cylindrical Tank

yield a time mean kinetic energy level at plane 1-1 as a function of radial location.

Writing equation (1) in terms of the time average kinetic energy and evaluating it at plane 1-1 and at the free surface, yields

$$\frac{1}{2}\,\frac{\rho \overline{V^2}}{g_c} + P_{atm} + \frac{\rho g h_f}{g_c} = P_{atm} + \frac{\rho g\ Z_s}{g_c}\ , \tag{2}$$

or

$$Z_s = h_f + \frac{1}{2}\,\frac{\overline{V^2}}{g}\ , \tag{3}$$

where $\overline{V^2}$ is the time average of the velocity squared and Z_s is the profile of the free surface with respect to reference plane 1-1. The following assumptions have been made in arriving at equation (3):

$$P = P(z'), \tag{4}$$

$$\overline{V^2}\ \text{wall} = 0 \tag{5}$$

and

$$\overline{V^2}\ \text{surface} = 0\ . \tag{6}$$

Equation (3) is made dimensionless by multiplying each term by $\frac{2g}{U^2}$ to obtain

$$\frac{2\ g\ Z_s}{U^2} = \frac{2\ g\ h_f}{U^2} + \frac{\overline{V^2}}{U^2}\ , \tag{3a}$$

where U is the bubble terminal velocity.

Thus, the height of the free surface is predicted from the time mean kinetic energy distribution within the cylinder for steady state operating conditions.

It should be noted that equation (3) could have also been obtained by considering Bernoulli's equation for an irrotational, incompressible, steady-flow system.

If the reference plane 1-1, shown in Figure 1, is taken where $h_f = 0$, equation (3a) reduces to

$$\frac{2gZ_s}{U^2} = \frac{\overline{V^2}}{U^2} \quad . \tag{3b}$$

Defining a dimensionless surface profile as

$$Z(r) = \frac{gZ_s}{U^2} \quad ,$$

we have

$$Z(r) = \frac{\overline{V^2}}{2U^2} \quad . \tag{3c}$$

Equation (3c) gives the dimensionless surface profile Z(r) in terms of a mean kinetic energy, which is represented in the equation by $\overline{V^2}$. A defining equation for this quantity is developed in the following section.

Time Mean Kinetic Energy Relation

The concept of changing the observer to the bubble center from a stationary position with the bubble going past allows the determination of the mean kinetic energy along the axial direction at a given location. This will later be used in conjunction with the bubble distribution and ascent velocities to predict the gross surface effects.

By the first mean value integral theorum ,

$$(\overline{V^2})H' = \int_{\sqrt{a-r'^2}\,,\,0}^{H'} \overline{v}^2(r',z')\, dz \tag{7}$$

where r', z', and H' are the radial coordinate, vertical coordinate, and upper limit of integration respectively, and $\overline{v}$ is the velocity vector given by

$$\overline{v} = iv + ju. \tag{8}$$

Non-dimensionalizing r', z', and H', with respect to the bubble radius a, equation (7) becomes

$$F(r) \equiv (\overline{V^2})H = \int_{\sqrt{1-r^2},\ 0}^{H} \overline{v}^2(r,z)dz \quad . \tag{9}$$

In equation (9) the lower limit of integration is $\sqrt{1-r^2}$ when $0 \le r \le 1$, in that the kinetic energy of the gas may be neglected, and 0 when $1 \le r \le \infty$. Rewriting equation (9) in terms of the velocity components u and v, we have

$$F(r) \equiv (\overline{V^2})H = \int_{\sqrt{1-r^2},\ 0}^{H} (u^2 + v^2)\ dz. \tag{10}$$

Combining equation (10) with equation (3c) we obtain for the dimensionless surface profile

$$Z(r) = \frac{F(r)}{2HU^2} \tag{3d}$$

and for the dimensional surface profile

$$Z_s = \frac{U^2 Z(r)}{g} \quad . \tag{3e}$$

It now remains to determine appropriate values for F(r) for various combinations of gases and liquids and bubble rise velocity. To do this requires a knowledge of the fluid velocity field, i.e., a solution for the velocity components u and v as functions of the dimensionless coordinates r and z.

Potential Flow Model

The simplified model of potential flow around a sphere rising at a uniform velocity in an otherwise still fluid of infinite extent is taken as a first approximation to the velocity distribution around a rising bubble. The potential function, Φ_s, for this case, as given by Prandtl and Tietjens (78), was transformed into cylindrical coordinates (r',z') for convenience. The transformed potential function, Φ_c, is given by

$$\Phi_c = \frac{a^3 U z'}{2(r'^2 + z'^2)^{3/2}} \tag{11}$$

and, thus, in dimensionless coordinates r, z,

$$V_o = \frac{\partial \Phi_c}{\partial r} = -\frac{3}{2} \frac{Urz}{(r^2 + z^2)^{5/2}} \tag{12}$$

and

$$U_o = \frac{\partial \Phi_c}{\partial z} = -U \frac{(z^2 - \frac{r^2}{2})}{(r^2 + z^2)^{5/2}} \quad . \tag{13}$$

Inserting the above expressions into equation (10), where $u = U_o$ and $v = V_o$ for potential flow, and simplifying, we obtain

$$F(r) = U^2 \int_{\sqrt{1-r^2},\ 0}^{H} \frac{4z^2 + r^2}{4(r^2 + z^2)^4} dz \quad . \tag{14}$$

Appendix I gives the details of the development of equations (11), (12), (13), and (14).

Equation (14) was integrated by numerical techniques and the results are presented in dimensionless form in Figure 2. The upper limit of integration H was set at that z location, for a given r, where the value of the integrand,

$$\frac{4z^2 + r^2}{4(r^2 + z^2)^4} \quad ,$$

was equal to or less than 1×10^{-6}. To verify the results of the numerical integration, equation (14) was integrated by classical mathematical methods (see Appendix II) to give for $r = 0$:

$$\frac{F(r)}{U^2} = \left[-\frac{1}{5} z^{-5} \right]_1^{\infty} = 0.20 \tag{15}$$

and for $r > 0$;

$$\frac{F(r)}{U^2} = \left[- \frac{3z}{24(r^2 + z^2)^3} + \frac{9z}{96r^2(r^2 + z^2)^2} + \frac{27z}{192r^4(r^2 + z^2)} \right.$$

$$\left. + \frac{27 \arctan \frac{z}{r}}{192r^2} \right]_{\sqrt{1-r^2},\ 0}^{\infty} . \qquad (16)$$

The upper limit of integration H in equation (14) has been set equal to ∞, however,

$$\int_{\sqrt{1-r^2},\ 0}^{\infty} \bar{v}^2(r,z)dz = \int_{\sqrt{1-r^2},\ 0}^{H} \bar{v}^2(r,z)dz + \int_{H}^{\infty} \bar{v}^2(r,z)dz , \qquad (9a)$$

but, since

$$\int_{H}^{\infty} \bar{v}^2(r,z)dz \simeq 0, \qquad (9b)$$

then

$$\int_{\sqrt{1-r^2},\ 0}^{\infty} \bar{v}^2(r,z)dz \simeq \int_{\sqrt{1-r^2},\ 0}^{H} \bar{v}^2(r,z)dz , \qquad (9c)$$

and no appreciable difference should be noted between the numerical integration results and the results given by equations (15) and (16). A comparison of these two integrations is shown in Figure 2.

In Figure 2 we see that as $r \to 1$ from the interior the slope of $\frac{F(r)}{U^2}$ appears to approach infinity, i.e., there appears to be a point of discontinuity at $r = 1$. The existence of a point of discontinuity at $r = 1$ may be shown mathematically in the following manner. Rewriting equation (14), for $0 \leq r \leq 1$, as

$$\frac{F(r)}{U^2} = K = \int_{f(r)}^{H} g(z,r)dz \tag{17}$$

w here

$$g(z,r) = \frac{4z^2 + r^2}{4(r^2 + z^2)^4} ,$$

and

$$f(r) = \sqrt{1-r^2},$$

we wish to investigate the derivative of K with respect to r as $r \to 1$ from the interior. Employing Leibnitz' formula for differentiation of an integral to equation (17) we obtain

$$\frac{dK}{dr} = g(H,r)\frac{dH}{dr} - g\left[f(r),r\right]\frac{df(r)}{dr} + \int_{f(r)}^{H} \frac{\partial}{\partial r}\left[g(z,r)\right] dz. \tag{18}$$

Performing the indicated operations, equation (18) becomes, after some simplifications,

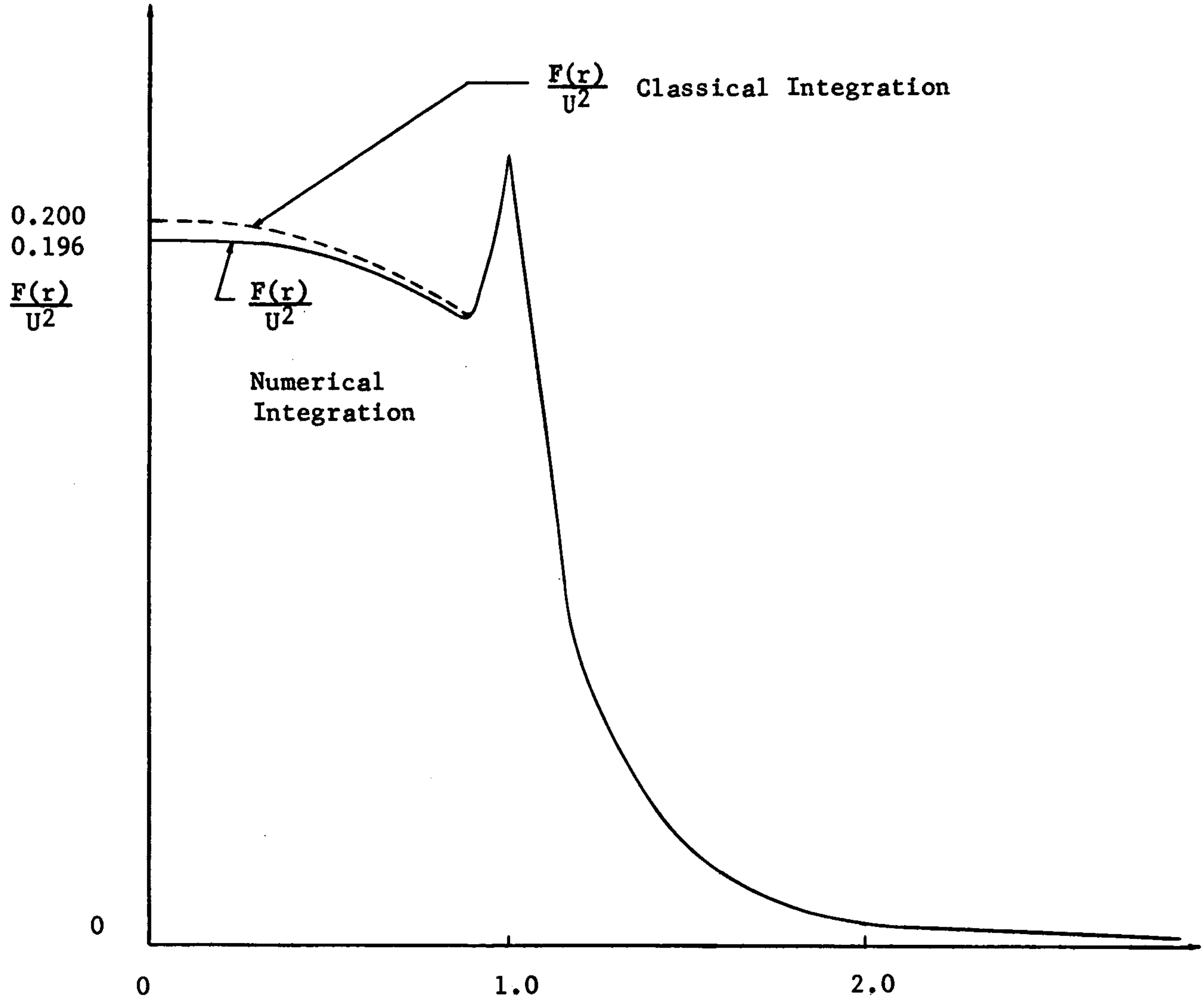

Figure 2. Comparison $\frac{F(r)}{U^2}$, Classical Integration Versus Numerical Integration

$$\frac{dK}{dr} = \frac{4r - 3r^3}{4(1 - r^2)^{\frac{1}{2}}} - \int_{\sqrt{1-r^2},\ 0}^{H} \frac{3r(5z^2 + r^2)}{2(r^2 + z^2)^5}\, dz\ . \tag{19}$$

Taking the limit of equation (19) as $r \rightarrow 1$, it may be shown that $\frac{dK}{dr} \rightarrow \infty$ and that there indeed is, as indicated in Figure 2, a point of discontinuity at $r = 1$. The details of the above development are presented in Appendix III.

Real Fluid Model

The velocity field surrounding a rising bubble deviates only slightly from that predicted by the inviscid theory (potential flow model) except at the vicinity of the bubble surface. Here the radial gradient of the tangential velocity component must be of opposite sign from that predicted by the potential solution.

B. T. Chao(11) considered a fluid sphere rising steadily with constant velocity in a viscous, unbounded liquid. He solves for the velocity field surrounding the bubble by considering that viscous effects (what he refers to as disturbances) are important only in a very thin layer on either side of the bubble surface. Outside these thin layers he postulates, based on other published information, that the flow can be adequately described by potential theory.

Since this research is concerned with the fluid velocity field, only the exterior flow solution presented by Chao will be discussed. Chao assumed that the fluid velocity could be given by

$$\vec{v}_o = \vec{V}_o + \vec{v}\,'_o$$

where

$\vec{v}_o$ is the velocity field,

$\vec{V}_o$ is the velocity field given by the potential solution

$\vec{v}_o'$ is a perturbed velocity field in a thin region immediately adjacent to the bubble surface,

and

$$\left|\vec{v}_o'\right| << \left|\vec{V}_o\right|$$

By certain order of magnitude analysis and other approximations Chao was able to reduce the full equations describing the fluid motion, i.e., the continuity and momentum equations, to forms which enabled solution for the perturbed velocity field. It should be pointed out at this point that Chao, in his order of magnitude analysis, assumed that his arc-length coordinate was of order one, and thus, his analysis cannot be expected to hold in the vicinity of the front stagnation point. This fact is discussed by Chao.

The perturbed velocity field is given by

$$\vec{v}_o' = iv_o' + ju_o' \qquad (8a)$$

where u_o' is the perturbed tangential velocity component and v_o' is the perturbed radial velocity component, and the potential velocity field is given by

$$\vec{V}_o = iV_o + jU_o \qquad (8b)$$

where U_o is the potential tangential velocity component and V_o is the potential radial velocity component discussed in the previous section. Chao's solution for u_o' and v_o', and thus the velocity field $\vec{v}_o$ is given in

Appendix IV. It will be noted that the perturbed tangential velocity component u_o' is essentially zero at $\zeta_o = 2.6$, since ierfc $2.6 \simeq 0$. Thus, the "perturbed" region is considered as that region where $\zeta_o < 2.6$, and the perturbed radial component v_o' is forced to zero if $\zeta_o \geq 2.6$, that is, outside of the perturbed region. Convergence to the potential solution is thus guaranteed for both velocity components for $\zeta_o \geq 2.6$.

Chao's solution does not hold in the rear stagnation region, in fact, as he points out, both u_o' and v_o' increase without limit as the rear stagnation point is approached. Actually, there is flow separation before the rear stagnation point is reached. Even though there is separation of the flow and Chao's solution is invalid in the rear stagnation region, for the purpose of this work, the velocity field will be considered symmetric and Chao's solution utilized.

Chao's solution for $\vec{v}_o$ was transformed into dimensionless cylindrical coordinates and revised expressions for u and v in equation (10) were obtained. Designating the revised velocity components as UC and VC, equation (10) becomes

$$F(r) = (\overline{V^2})H = \int_{\sqrt{1-r^2},\ 0}^{H} \left[(UC)^2 + (VC)^2\right] dz. \qquad (20)$$

The details of this development, as well as the final expressions for the velocity components UC and VC are given in Appendix IV. Equation (20) was integrated by numerical techniques and the results for a distilled water-air system with Reynolds number equal 100 are presented in Figure 3. The Reynolds

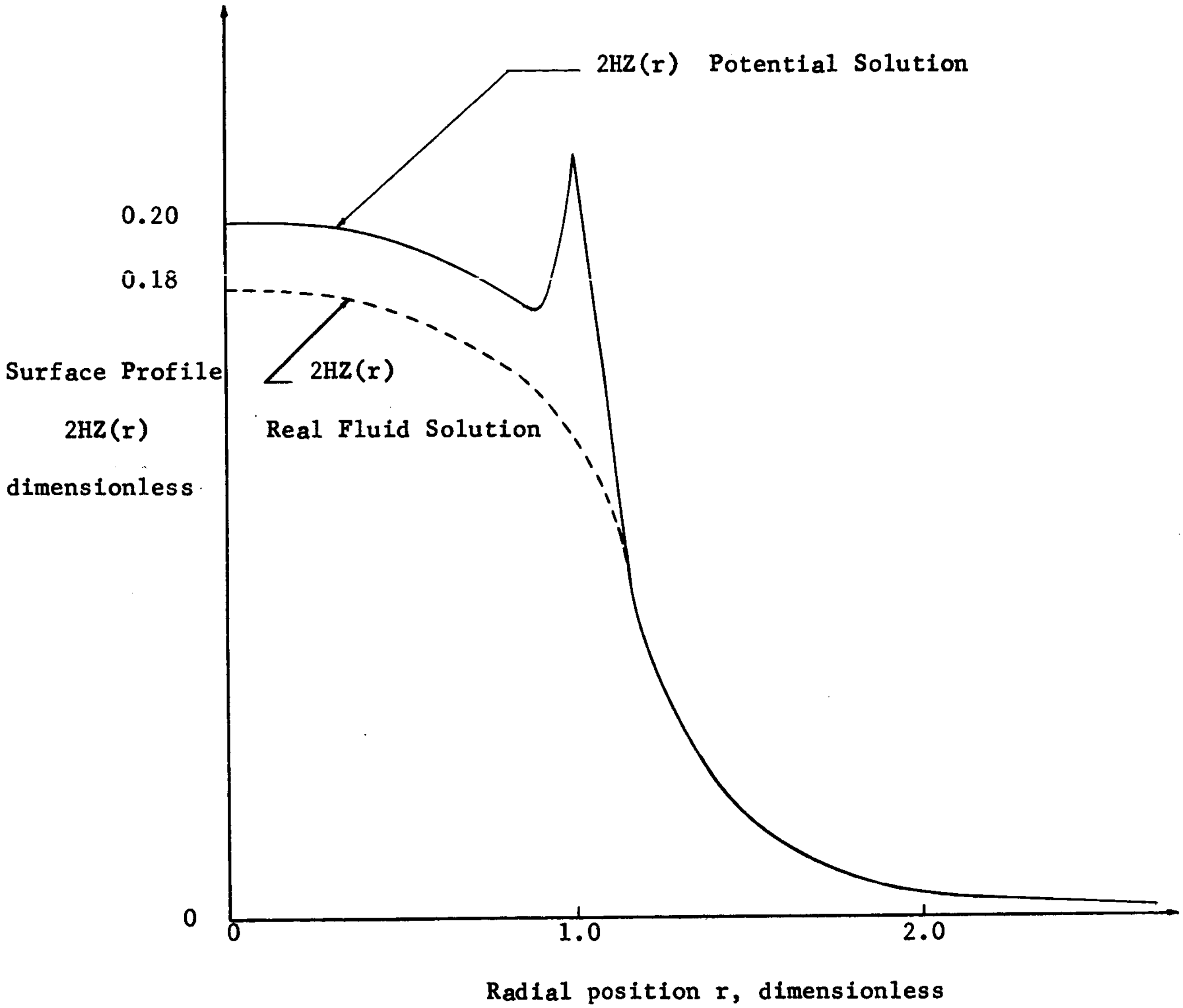

Figure 3. Comparison of 2HZ(r) for the Real Fluid Solution with 2ZH(r) for the Potential Solution. N_{Re} = 100, Air-distilled Water System

number in this instance is defined as

$$N_{Re} = \frac{2Ua}{\nu_L} ,$$

where

U = bubble rise velocity

a = bubble radius

ν_L = liquid kinematic viscosity.

The remaining analysis will be concerned with the real fluid solution, that is, F(r) as given by equation (20).

Development of Surface Profile Predictions

Equation (3d) gives for the dimensionless surface profile

$$Z(r) = \frac{F(r)}{2HU^2} , \tag{3d}$$

where, utilizing Chao's solution for the liquid velocity field, F(r) is given by equation (20). The dimensional surface profile Z_s is given by equation (3e). To demonstrate the behavior of equations (3d) and (3e) as the bubble rise velocity varies, an air-distilled water system was selected, the Reynolds number $N_{Re} = \frac{Ud}{\nu_L}$ varied, and the resulting profiles calculated. The Reynolds number was used as the independet variable since it appears in the perturbed solution for F(r) given by equation (20). The bubble diameter d, and the bubble rise velocity U, used in the determination of N_{Re} were taken from the work of Haberman (37). Figure 4 gives the results for the dimensionless profile (expressed in the form 2HZ(r)) and Figure 5 the results for the dimensional profile.

Figure 4 shows that Z(r) is not strongly dependent upon Reynolds number within the range of Reynolds numbers tested. This was not entirely unexpected, since the Reynolds number as such occurs only in the solution for the velocity field within the perturbed region, which is quite thin when compared to the unperturbed or potential region. Thus, the Reynolds number should have only a slight effect on the dimensionless profile Z(r), and it should be possible to represent the dimensionless surface profile, with acceptable accuracy, by a single curve independent of Reynolds number. Even though the analysis to date is based upon spherical bubbles, which generally occur for $N_{Re} \lesssim 400$, the Reynolds number was extended to include non-spherical bubbles. These results are also shown in Figure 4, however, they will be

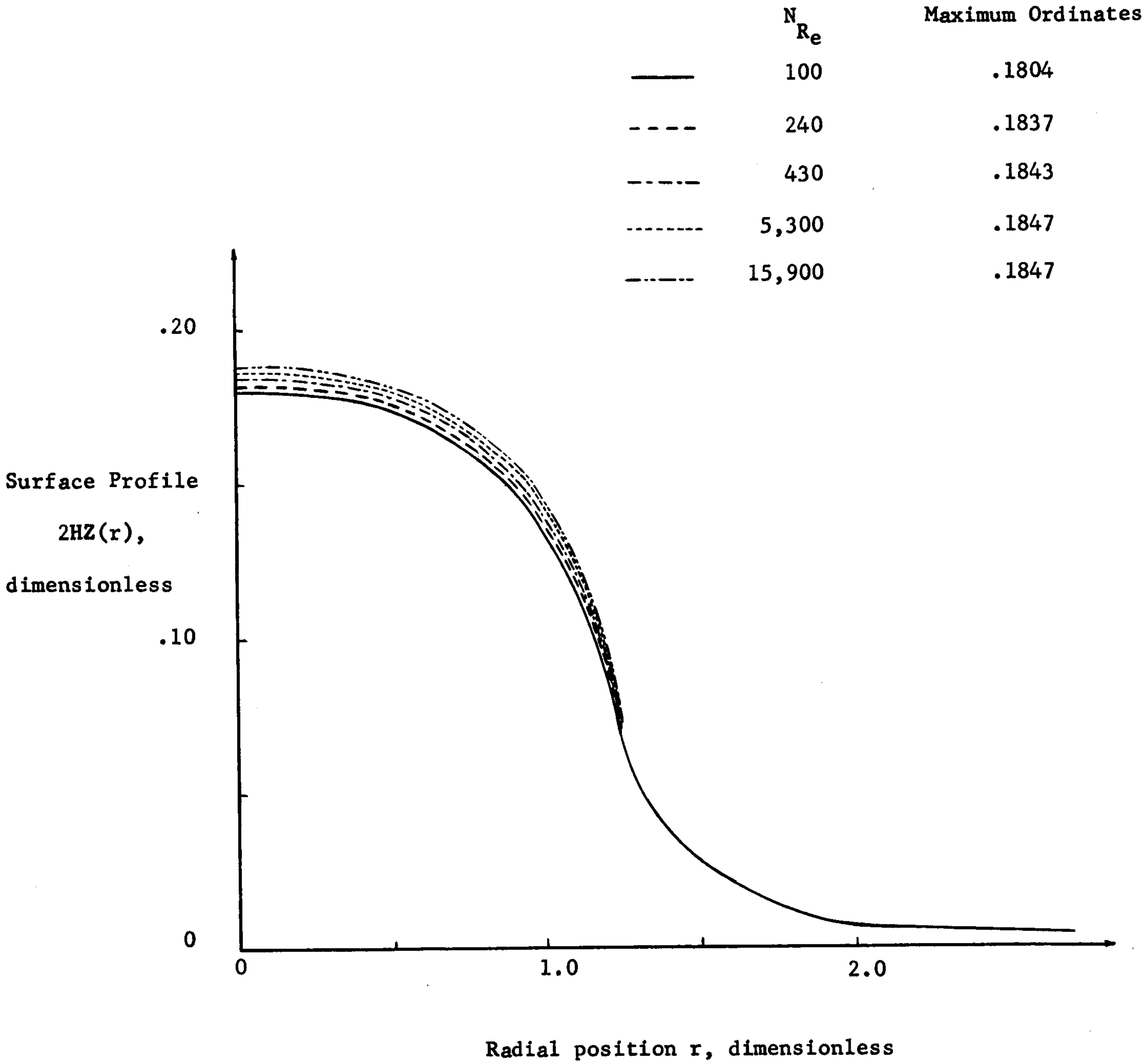

Figure 4. Dimensionless Surface Profile 2HZ(r) Computed from Equation (20), for Various Reynolds Numbers

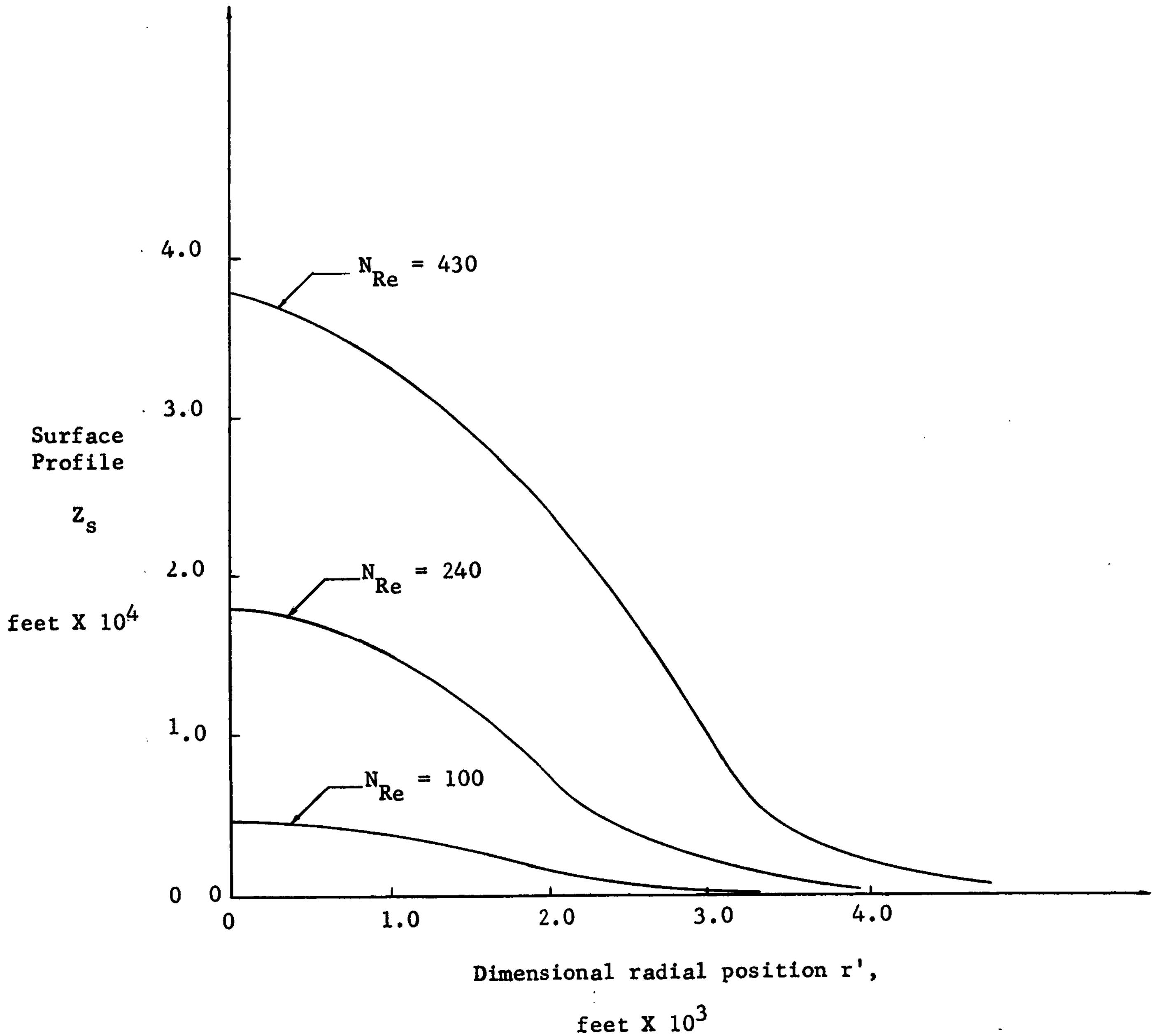

Figure 5. Surface Profiles for Various Reynolds Numbers Computed by Numerical Integration of Equation (20).

excluded from the discussion that follows.

Considering only those profiles for Reynolds number less than or equal to 430, the profile for $N_{Re} = 240$ appears to be the median of the three remaining profiles. Thus, utilizing a least squares method, an attempt was made to fit an equation to this profile. Various degree polynomials, ratio of polynomials, and modified cosine functions were tested with the conclusion that the following fourth degree polynomial best represented the data:

$$2ZH(r) = .182907 + .086949\ r - .245937\ r^2 + .102929\ r^3 - .012489\ r^4. \quad (21)$$

Equation (21) is plotted in Figure 6 together with equation (3d), evaluated by numerical integration of equation (20), for comparison purposes.

The results given by equation (21) are quite good for the following range of the dimensionless radius r:

$$0 \leq r \leq 2.00.$$

For larger values of r, equation (21) gives negative values for 2HZ(r). However, the range of validity is sufficient for the purposes of this analysis.

Utilizing equation (21), equation (3e) for the dimensional surface profile Z_s becomes

$$Z_s = \frac{U^2}{2Hg} \left[.182907 + .086949\ r - .245937\ r^2 + .102929\ r^3 - .012489\ r^4 \right]. \quad (22)$$

H, in equation (22), is equal to that value of the z coordinate where the kinetic energy (represented by $\frac{\overline{V^2}}{U^2}$) is equal to or less than 1×10^{-6}. Even though H is a function of the dimensionless radial coordinate r, it was found that the average value for a given Reynolds number was very nearly ten. Setting H = 10 in equation (22) and replacing r by $\frac{r'}{a}$, we obtain

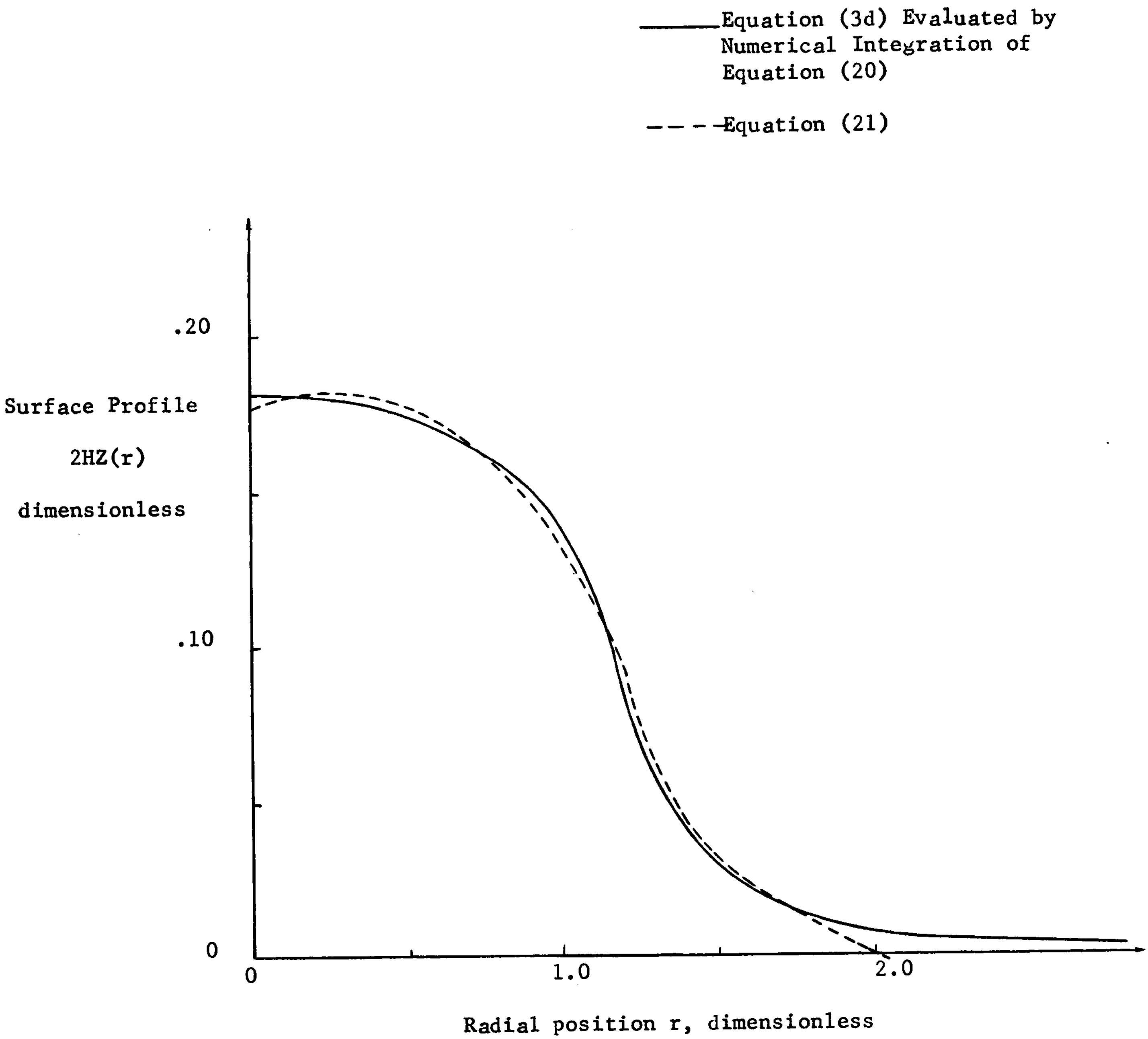

Figure 6. Dimensionless Surface Profile 2HZ(r) for Reynolds Number of 240. Comparison of Result Obtained by Numerical Integration with Result Using Polynomial Fit.

$$Z_s = \frac{U^2}{g}\left[.0091453 + .0043475\left(\frac{r'}{a}\right) - .122968\left(\frac{r'}{a}\right)^2 + .0051464\left(\frac{r'}{a}\right)^3 - .0006244\left(\frac{r'}{a}\right)^4\right] . \qquad (23)$$

Since

$$N_{Re} = \frac{Ud}{\nu_L} ,$$

$$U^2 = \frac{N_{Re}^{\;2}\,\nu_L^{\;2}}{d^2} .$$

Thus, equation (23) may be written

$$Z_s = \frac{N_{Re}^{\;2}\,\nu_L^{\;2}}{gd^2}\left[.0091453 + .0043475\left(\frac{r'}{a}\right) - .0122968\left(\frac{r'}{a}\right)^2 + .0051464\left(\frac{r'}{a}\right)^3 - .0006244\left(\frac{r'}{a}\right)^4\right] . \qquad (24)$$

Figure 7 shows a comparison of the surface profiles given by equation (24) with those obtained by separate numerical integration of equation (20) for each Reynolds number. This figure shows that the surface profiles obtained with equation (24) closely approximate those predicted by the previous theoretical analysis. The values for N_{Re} and d which were used in equation (24) to obtain the results given in Figure 7 were taken from a replot of the data of Haberman and Morton (37) as shown in Figure 25 of Appendix VII.

The development to this point has only considered the kinetic energy above one bubble rising along its centerline. However, the results given by equation (20) may be used for one or more columns of bubbles rising rectilinearly as long as the bubble distribution is such that there is

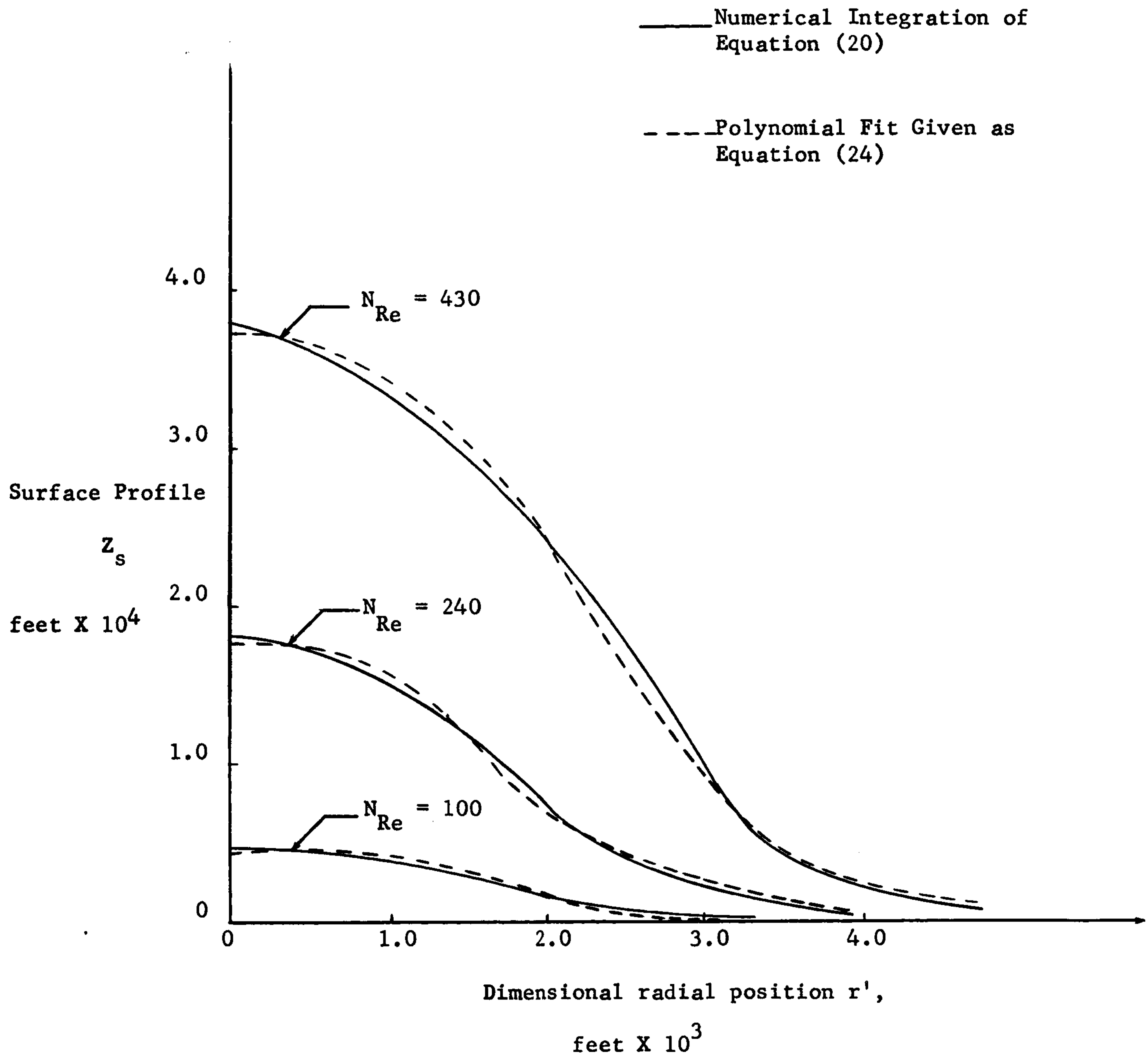

Figure 7. Surface Profiles for Various Reynolds Numbers. Comparison of Result Obtained by Numerical Integration with Result Using Polynomial Fit.

negligible interference of the flow fields associated with each bubble. The minimum vertical bubble spacing for negligible interference may be fixed as twice the vertical distance from the bubble center to the z location where there is a negligibly small contribution to the kinetic energy, for a given r. The upper limit of integration becomes H_{min} in equation (20). A suitable value of H_{min} is found in the following manner:

(a) Equation (20) is integrated numerically for various r's until the integrand reaches a prescribed negligibly small value.

(b) The values of z thus obtained are arithmetically averaged to obtain an average value for H_{min}.

If the bubbles are vertically spaced at a distance D which is greater than $2H_{min}$, then the non-dimensionalized surface profile may be obtained by taking

$$Z(r) = \frac{F(r)}{DU^2} \tag{25}$$

since

$$\overline{v^2}_{\frac{D}{2}} = \int_0^{\frac{D}{2}} \bar{v}^2 \, dz \simeq \int_0^{H} \bar{v}^2 \, dz = F(r) \quad . \tag{26}$$

This is true because

$$\int_H^{\frac{D}{2}} \bar{v}^2 \, dz \simeq 0. \tag{27}$$

The minimum radial spacing allowable may be obtained in a similar manner.

Surface Profile Prediction for Two Columns of Horizontally Interfering Bubbles

As a first approach to the determination of the surface profile upon injection of multiple columns or swarms of bubbles, the following simplified model was considered:

> Two columns of bubbles interfere horizontally, but are spaced so that there is no vertical interference, i.e., one bubble does not affect the velocity field of the bubble directly above or below it but does affect the velocity field of the bubble horizontally adjacent to it, of equal diameters and all rising at the same velocity. Also, the bubbles are horizontally paired, i.e., the bubbles in both columns are rising adjacent to one another with a common horizontal centerline at any instant of time.

As a first approximation to the velocity field generated in the above model, a direct superposition of the velocity fields surrounding each horizontally paired bubble, where the bubbles were considered to be rising singularly, was made. The results of Chao's (11) research were again used in these velocity determinations.

For example, the velocity at point p, shown in Figure 8, below, was computed in the following manner:

(1) The r and z velocity components at point P considering Bubble 1 rising without the presence of Bubble 2, were computed.

(2) The r and z velocity components at point P, considering Bubble 2 rising without the presence of Bubble 1, were computed.

(3) The velocity at point P was then determined by vectorially adding the velocity components computed in steps (1) and (2) above. The horizontal or r components will be in the opposite direction and will be subtractive while the vertical or z components will be in the same direction and thus additive.

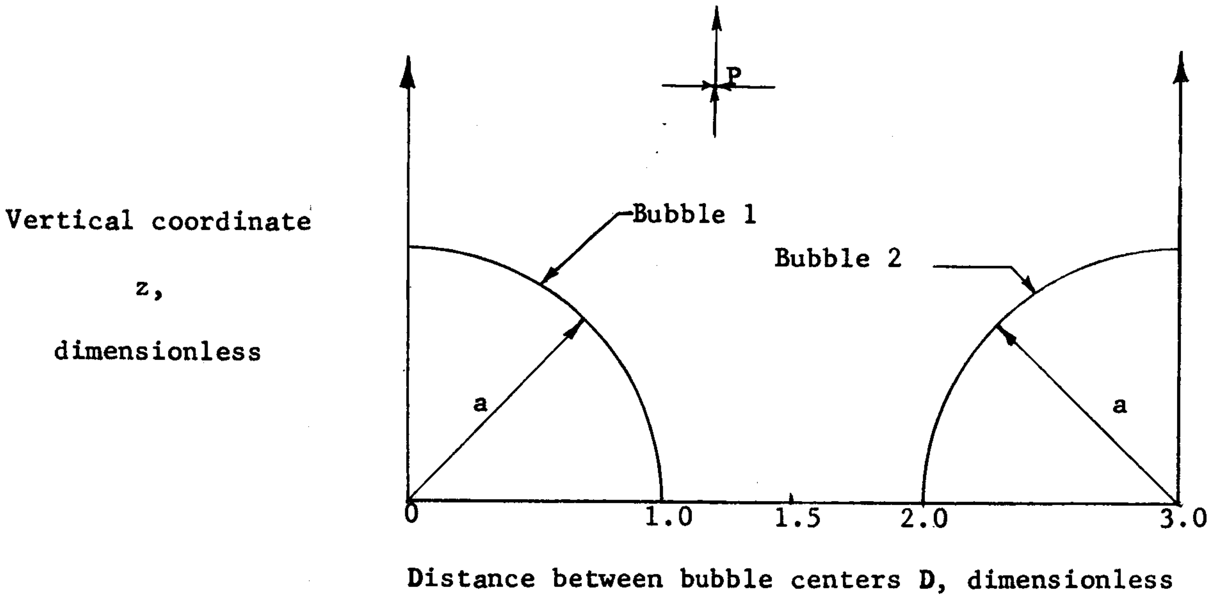

Figure 8. Coordinate System for Two Spherical Bubbles Rising in a Cylindrical Tank.

The dimensionless surface profile $Z(r)$ and the dimensional surface profile Z_s were computed for bubbles three radii apart from center to center, and for a Reynolds number, as previously defined, of 100. These profiles are shown in Figures 9 and 10. Comparing these profiles with those for the single column of bubbles with no vertical interference, shown in Figures 4 and 5, we see that for the region $r < 1.25$ the profiles predicted by the superposition method for the two columns of bubbles interfering horizontally but not vertically lie slightly below those predicted for the single column of non-interfering bubbles.

Since the horizontal components of velocity, i.e., the r components, are subtractive (see item 3, page 29), the resultant velocity in certain regions will be less than that in the single bubble case. This results from the fact that the difference between the final horizontal component of

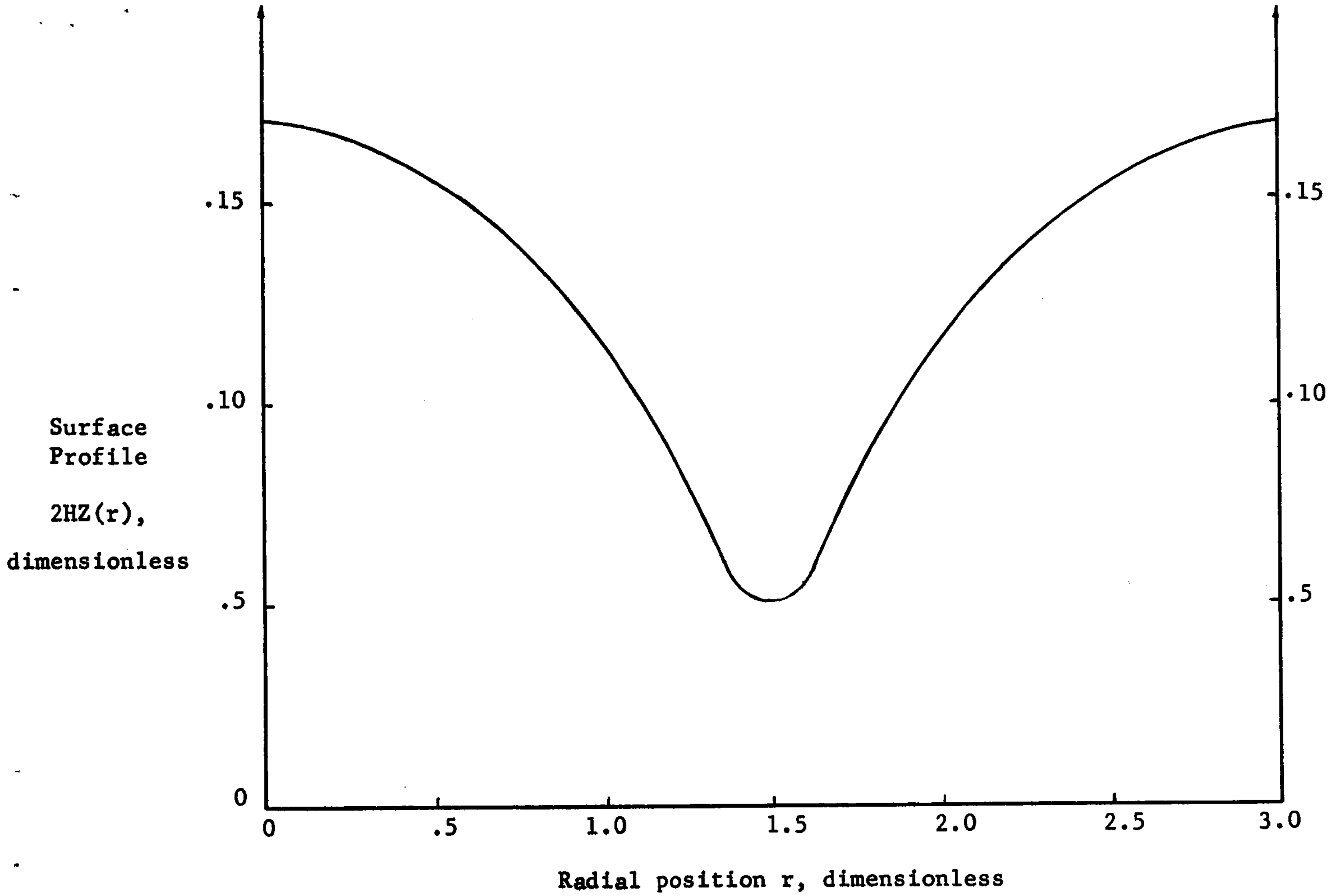

Figure 9. Dimensionless Surface Profile 2HZ(r) for Two Horizontally Interfering Bubbles Three Radii Apart. Reynolds Number of One Hundred.

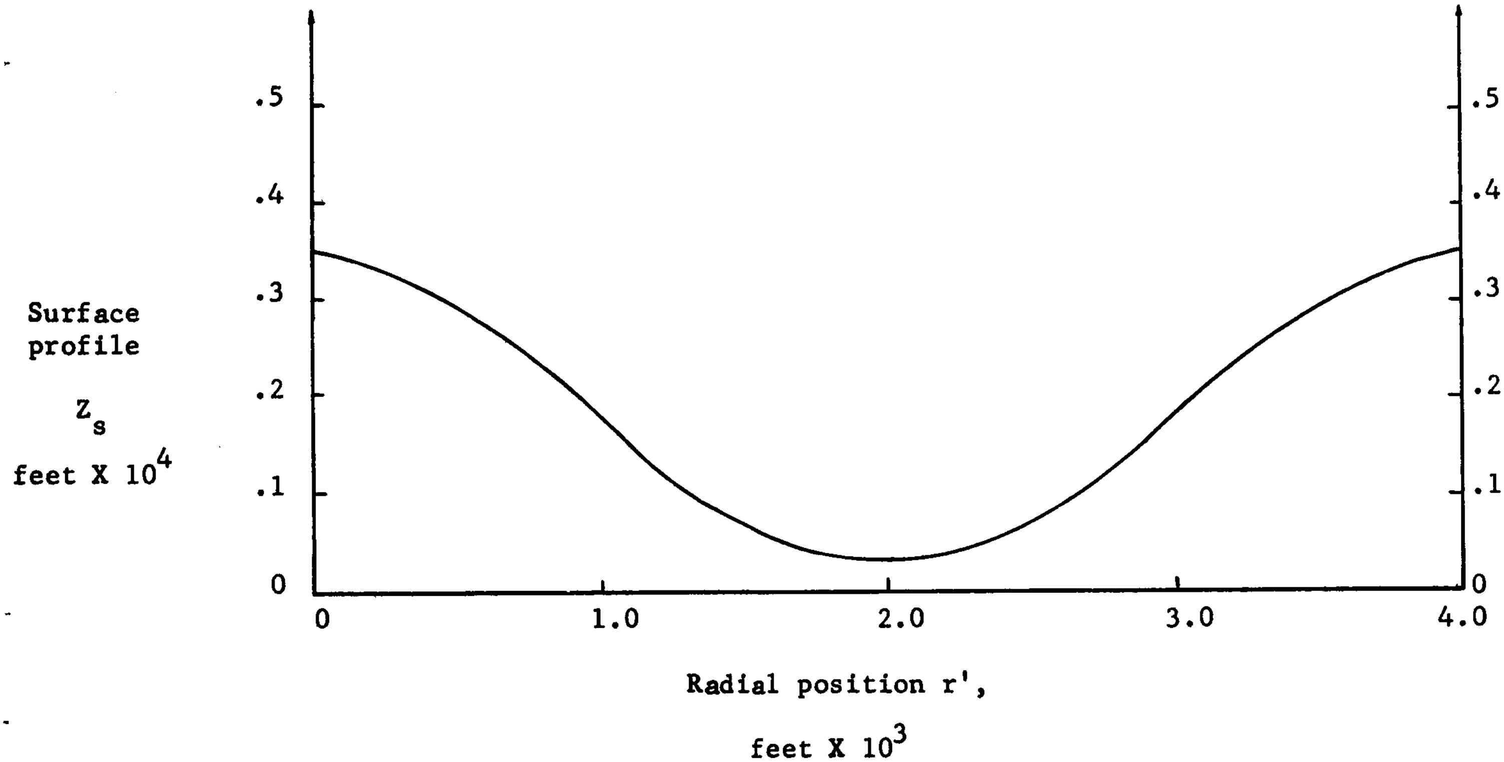

Figure 10. Surface Profile for Two Horizontally Interfering Bubbles Three Radii Apart. Reynolds Number N_{Re} of One Hundred.

velocity and the horizontal component for a single bubble is greater than the additive vertical or z component from the second bubble. That is, the horizontal component may be reduced more than the vertical component is increased.

EXPERIMENTAL

Photographic Work

The surface disturbances caused by a single column of bubbles of nitrogen gas rising in distilled water have been recorded photographically. The equipment used in this work is described in Appendix VIII. Figure 11 shows the buildup and collapse of the disturbance as an individual bubble approaches the liquid surface.

These pictures were reproduced from frames of 16 mm high speed motion picture film. The extreme magnification was achieved by the use of a 155 mm lens which was constructed of locally available material. The focal length necessary to obtain this magnification was such that the depth of field of the pictures is very shallow. The refractive index of water is sufficiently different from that of air so that with a shallow depth of field either the surface profile or the rising bubble can be in focus, but not both. These pictures show the surface profile in focus.

The pictures given in Figure 11 are separated in time by about 1/200 of a second. One can see in frame 11a that the surface disturbance begins well before the bubble reaches the surface. The maximum buildup of liquid ahead of the bubble occurs when the bubble reaches the position shown in frame 11d. The bubble then penetrates the surface and produces a maximum distortion as shown in frame 11g. The remaining frames in Figure 11 show the gas bubble relaxing back to a position mostly under the liquid, and the surface wave beginning to travel radially outward.

Data Reduction

The images on the 16 mm motion picture film were projected and traced onto large sheets of paper at a magnification, with reference to true size,

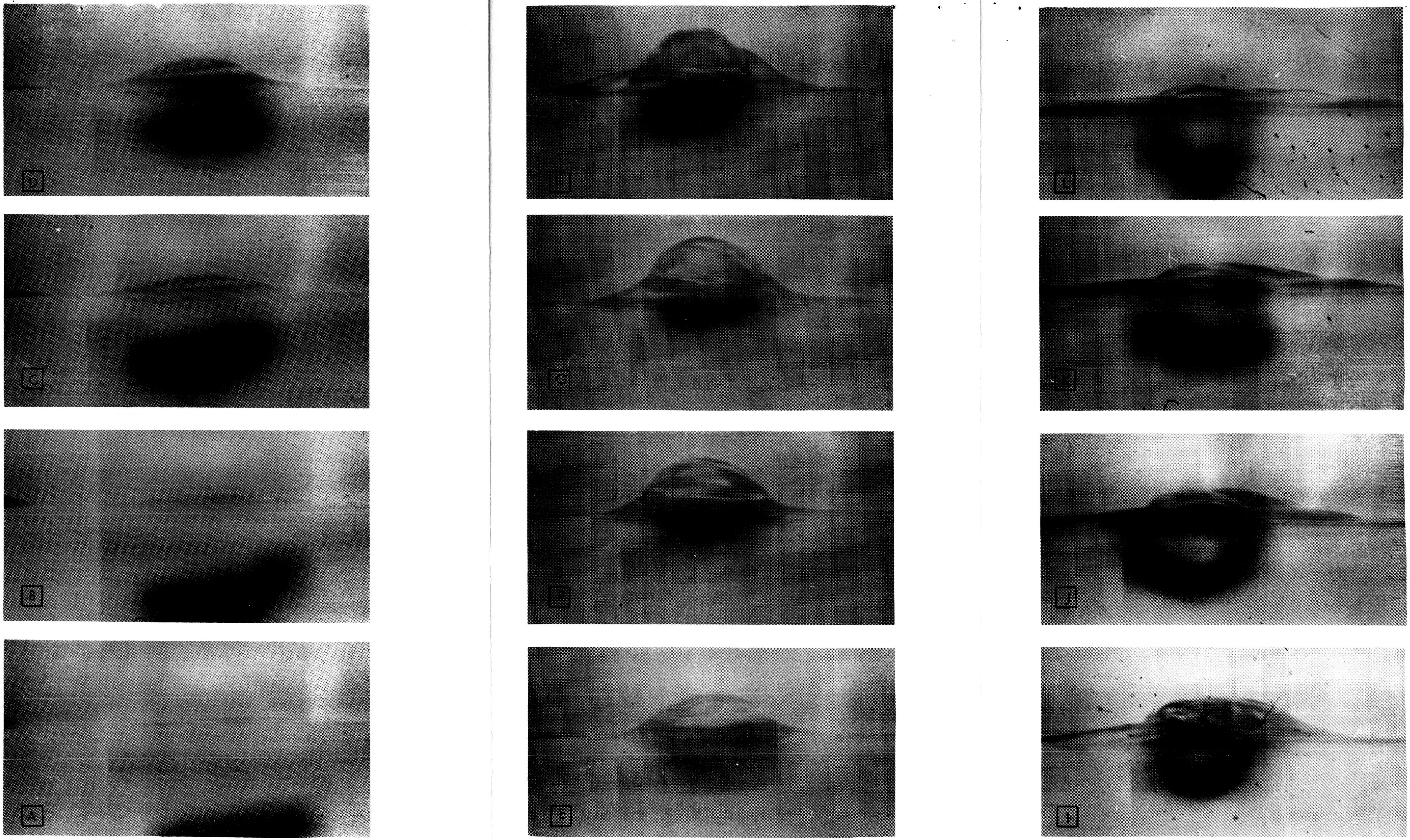

Figure 11. Surface Disturbance Caused by a Single Bubble of Nitrogen Gas Rising in Distilled Water. Taken from Frames of High Speed, 16 mm, Motion Picture Film. Time Interval Between Pictures of 1/200 Second.

of about 35 to 1. Horizontal and vertical scale factors, both above and below the liquid, were taken from a metal scale graduated in 1/100 of an inch which had been photographed at the focal point prior to the start of bubble injection.

Initially, only the frame which recorded the maximum vertical surface distortion was analyzed; for instance, frame 11g, in Figure 11. Thirteen measurements were taken of the height of the surface profile. These measurements were made in both directions away from the point of maximum height at the following values of dimensionless radial coordinate, r

$$r = 0, 0.2, 0.6, 1.0, 1.4, 1.8, 2.4.$$

The equivalent diameter of the bubble which caused each disturbance was also determined. The equivalent diameter is defined as the diameter of a sphere of volume equal to the bubble volume. Appendix X gives the experimental procedure followed to determine the bubble volume and diameter.

The surface profile data were partitioned into groups such that the equivalent diameters of the bubbles in each group differed by less than 0.001 feet. These data were then averaged and are presented in Figure 12. This data is given in Appendix IX. The correlation of bubble rise velocity given in Figure 25 of Appendix VII was used with the average equivalent diameter to determine the corresponding Reynolds number.

Comparison of Experimental Data with Analytical Results

A comparison of the experimentally determined surface profile with the profile resulting from the analytical prediction for a Reynolds number of 803 is given in Figure 13. The shapes of the two curves are similar, however, it is obvious that the magnitudes are greatly different. An examination of Figure 11, especially frames 11g and 11h, shows that one reason for

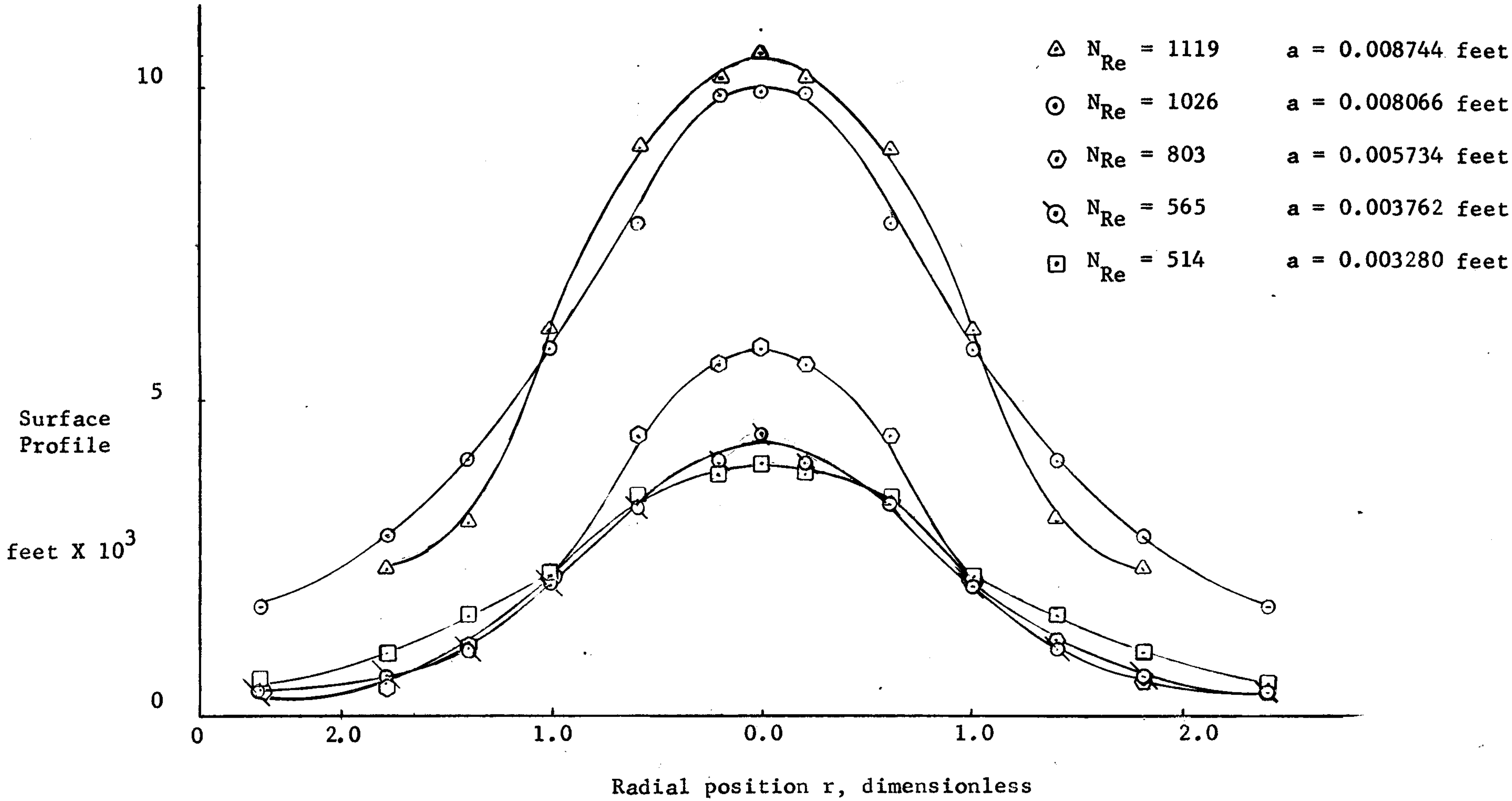

Figure 12. Experimental Surface Profile Data Caused by a Single Bubble of Gas Rising in Distilled Water.

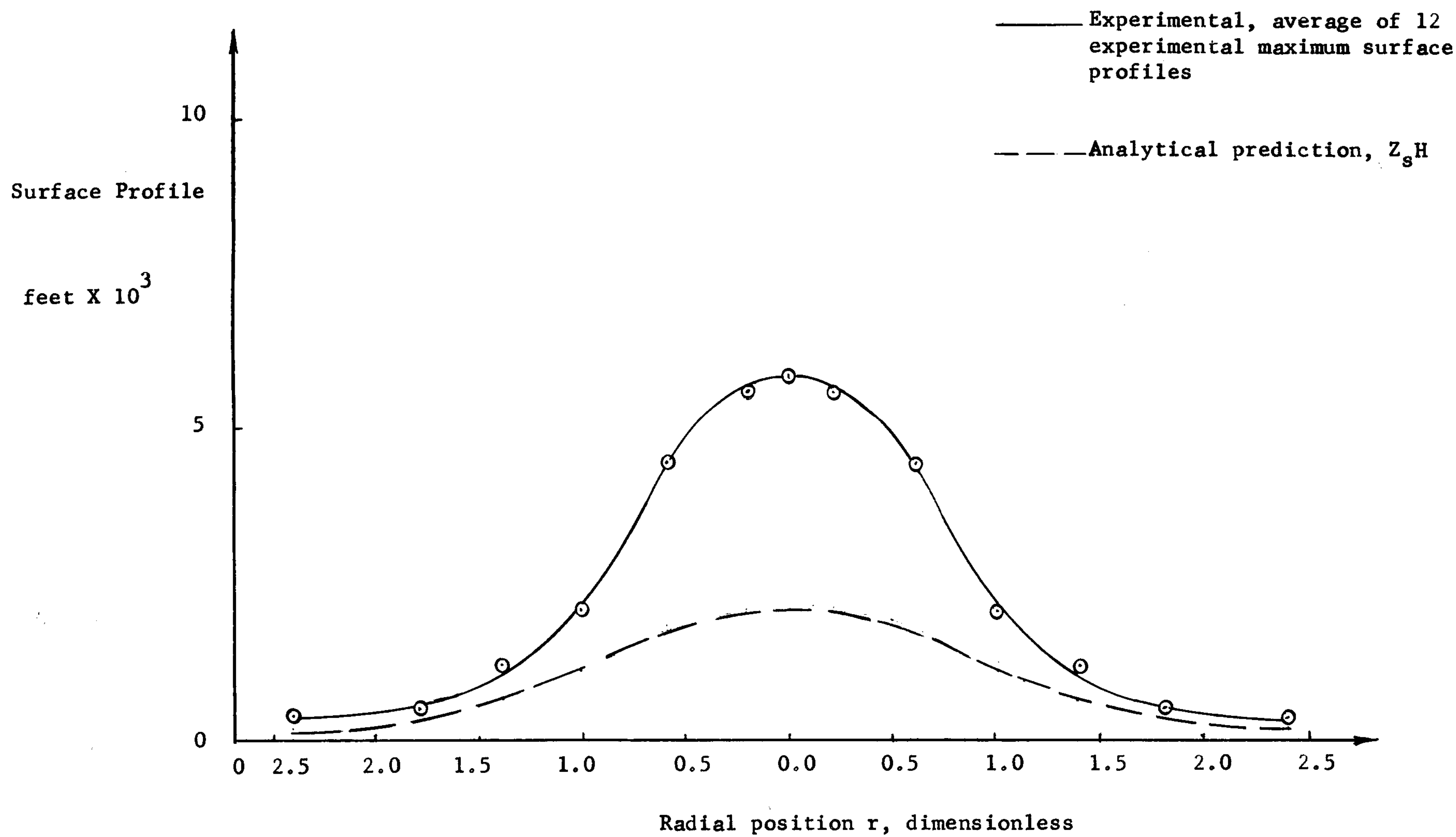

Figure 13. Experimental and Analytical Surface Profile for Reynolds Number N_{Re} = 803 and Equivalent Diameter of 0.01147 Feet.

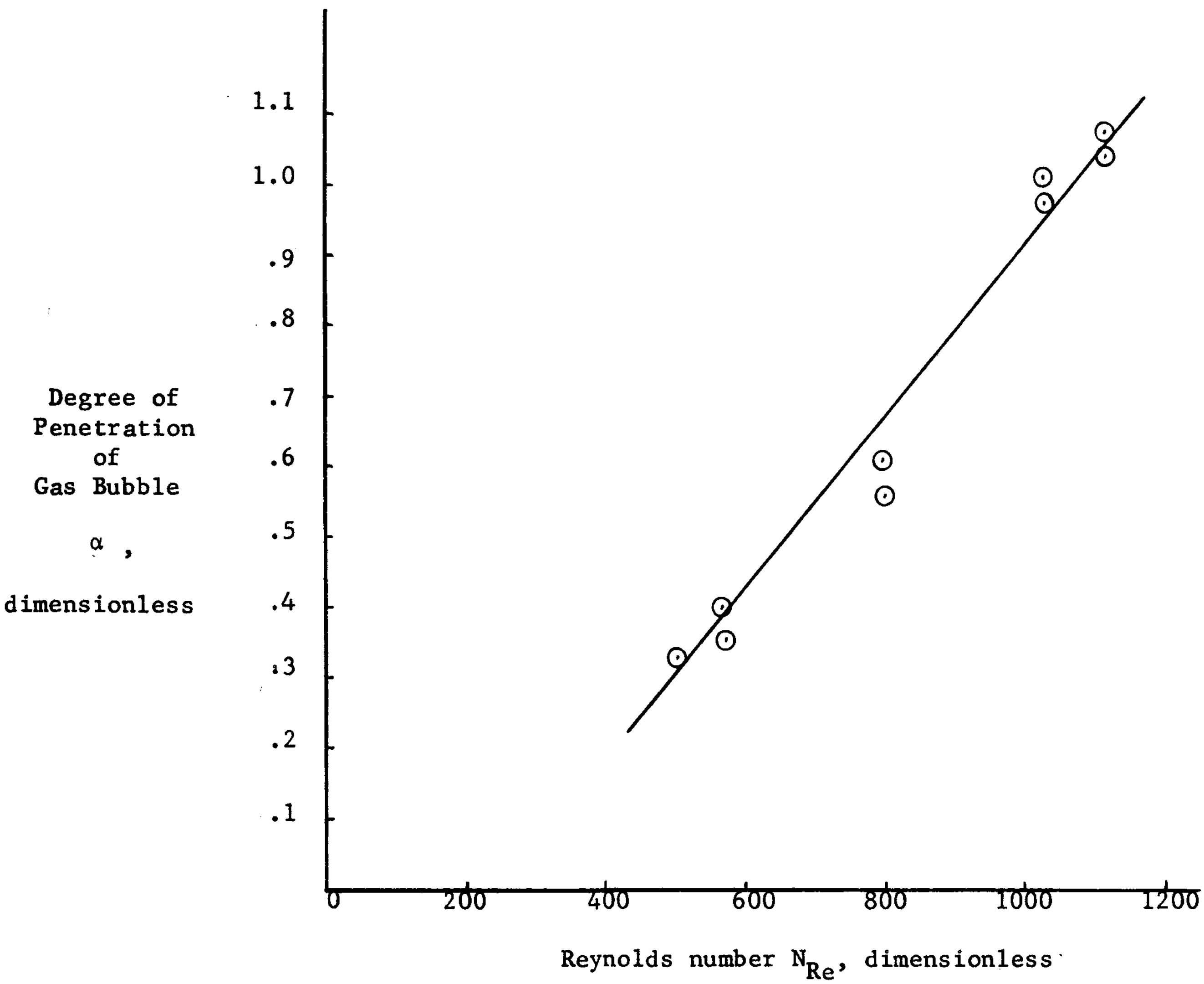

Figure 14. Experimental Correlation of the Degree of Penetration of the Gas Bubble into the Surface Using Data of this Research.

this difference is the penetration of the gas bubbles into the mean surface disturbance.

Thus it appears that a correlation equation could be constructed which would be the sum of the analytical prediction, which would represent the liquid buildup on the surface, and a term to represent the penetration of the gas bubble. This equation is given below.

$$Z_c = Z_s H + \alpha a\sqrt{1-r^2} \tag{28}$$

The term Z_c represents the height of the surface disturbance above the dead liquid surface. Z_c is a function of r. The term $Z_s H$ is the computed maximum surface profile — the product of Z_s, the time average height of the disturbed free surface above the quiescent surface, and H, the upper limit of integration in the equation that is used to compute Z_s. The term $\alpha a\sqrt{1-r^2}$ is the product of $a\sqrt{1-r^2}$, the vertical dimension from the horizontal center line to the edge of a spherical bubble at a particular value of dimensionless radial coordinate r, and α, which represents the degree of penetration of the bubble.

The degree of penetration of the bubble into the surface disturbance must depend on the velocity of rise, the size of the bubble, and the properties of the fluid. Therefore, one would expect α to be a function of Reynolds number, N_{Re}. Figure 14 shows this to be a direct and approximately linear correlation. The values of α given in Figure 14 were computed by inserting experimental values of a and Z_c into equation (28a).

$$\alpha = \frac{Z_c - Z_s H}{a\sqrt{1-r^2}} \quad . \tag{28a}$$

Utilizing a least squares fitting procedure the following equation was obtained for the degree of penetration α :

$$\alpha = 0.00122N_{Re} - 0.305. \qquad (29)$$

Figures 15 through 19 give a graphic comparison of the five experimental surface profiles previously shown in Figure 12, with the results predicted with the correlation equation, equation (28). The values of Z_s and H were obtained from equations (24) and (14) respectively, the values of α were determined by equation (29), and Figure 25 was used to give the relationship between Reynolds number N_{Re} and equivalent bubble diameter d.

The experimental and analytical results seem to be in good agreement at the maximum point and out to about eight-tenths of the bubble radius. However, Figures 15 through 19 show that the experimental profile lies above the predicted profile from eight-tenths to about twice the bubble radius. Figure 11, particularly frames 11h, 11i, and 11j, indicates that this excess of liquid forms the surface wave that moves radially outward from the disturbance.

This difference between the computed and experimental surface profiles for a radial coordinate in the range of $0.8 \leq r \leq 2.0$ is undoubtedly due to one of the assumptions involved in the derivation of the equation for Z_s, probably the assumption that the kinetic energy at the surface is negligible.

The most important part of the surface disturbance as far as this research is concerned occurs at and near the maximum. The computation of this part of the profile may be accomplished with very good accuracy using equation (28), equation (24), equation (29), and Figure 25.

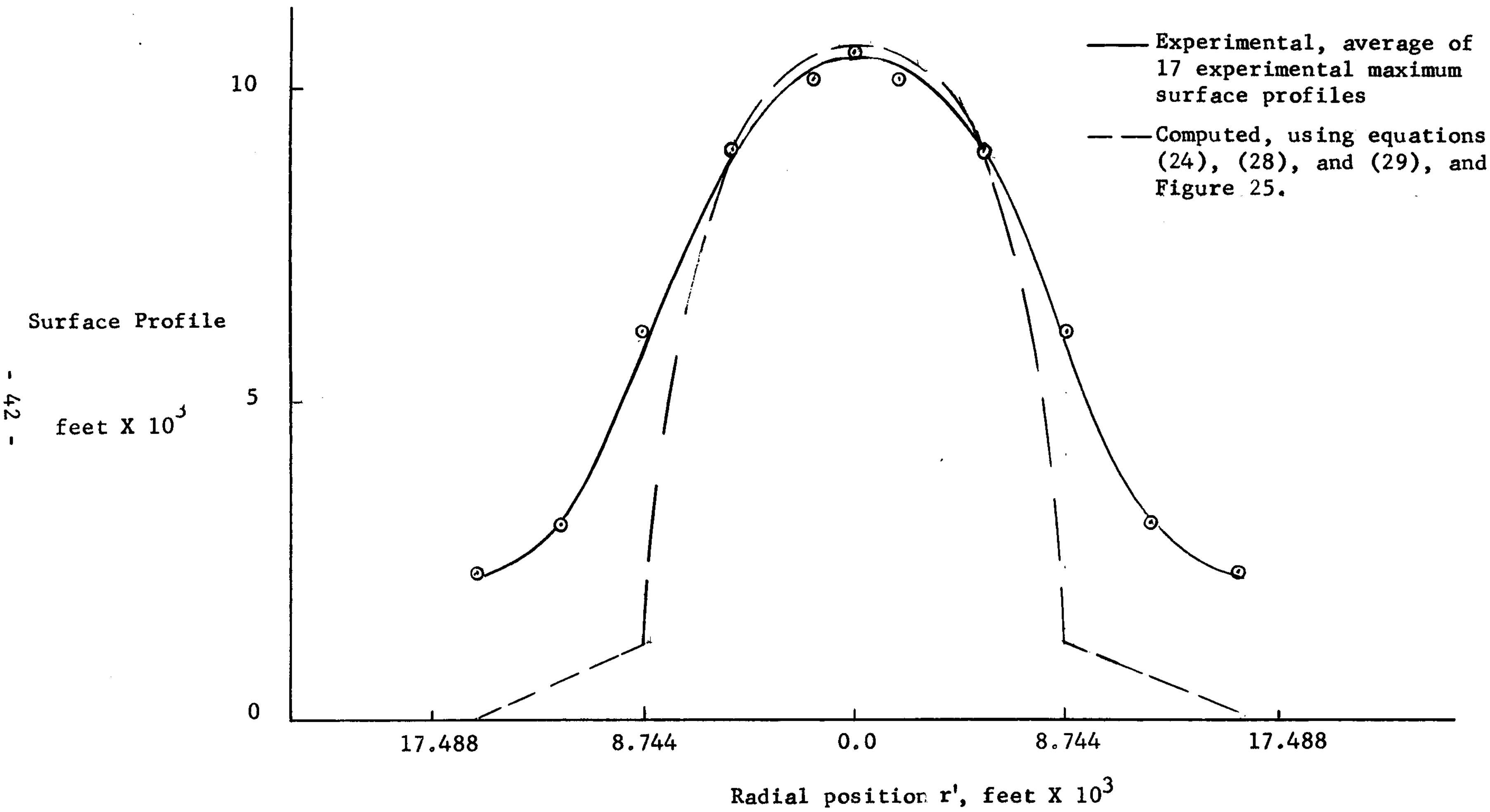

Figure 15. Comparison of Experimental Surface Profile with Profile Computed with Correlation Procedure for Reynolds Number of 1119 and Bubble Diameter of 0.017488 Feet. Nitrogen Gas in Distilled Water.

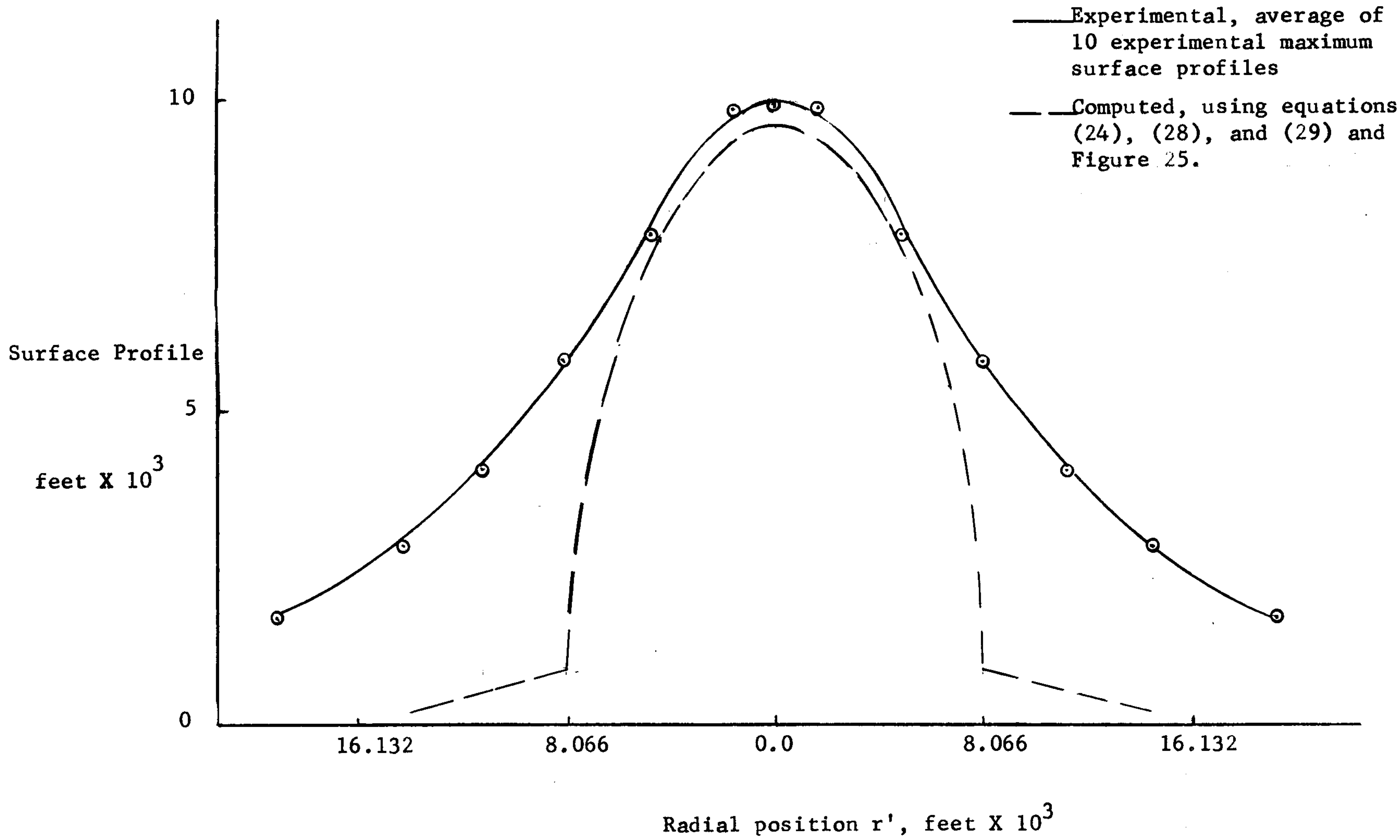

Figure 16. Comparison of Experimental Surface Profile with Profile Computed with Correlation Procedure for Reynolds Number of 1026 and Bubble Diameter of 0.016132 Feet. Nitrogen Gas in Distilled Water.

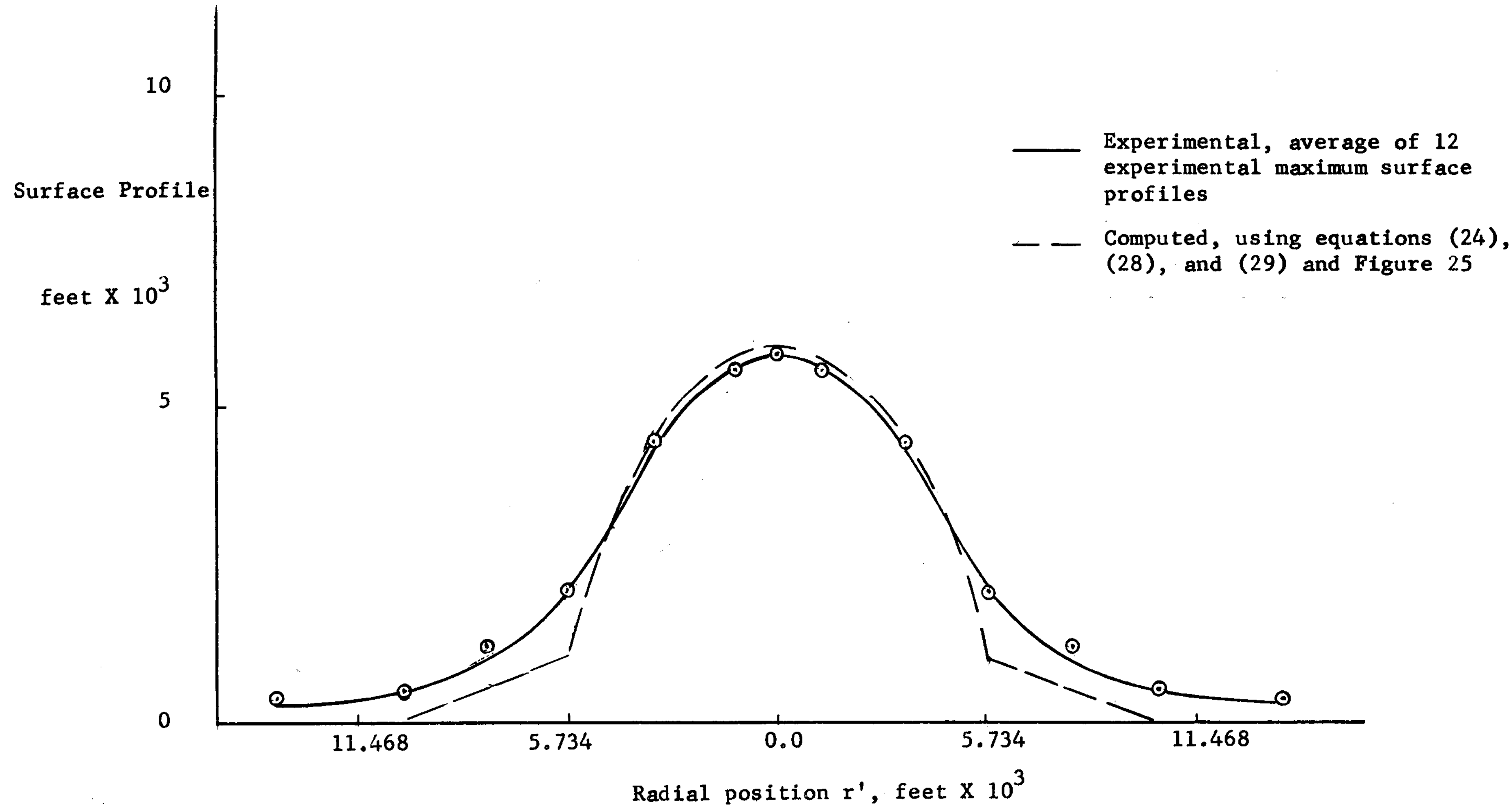

Figure 17. Comparison of Experimental Surface Profile with Profile Computed with Correlation Procedure for Reynolds Number of 803 and Bubble Diameter of 0.011468 Feet. Nitrogen Gas in Distilled Water.

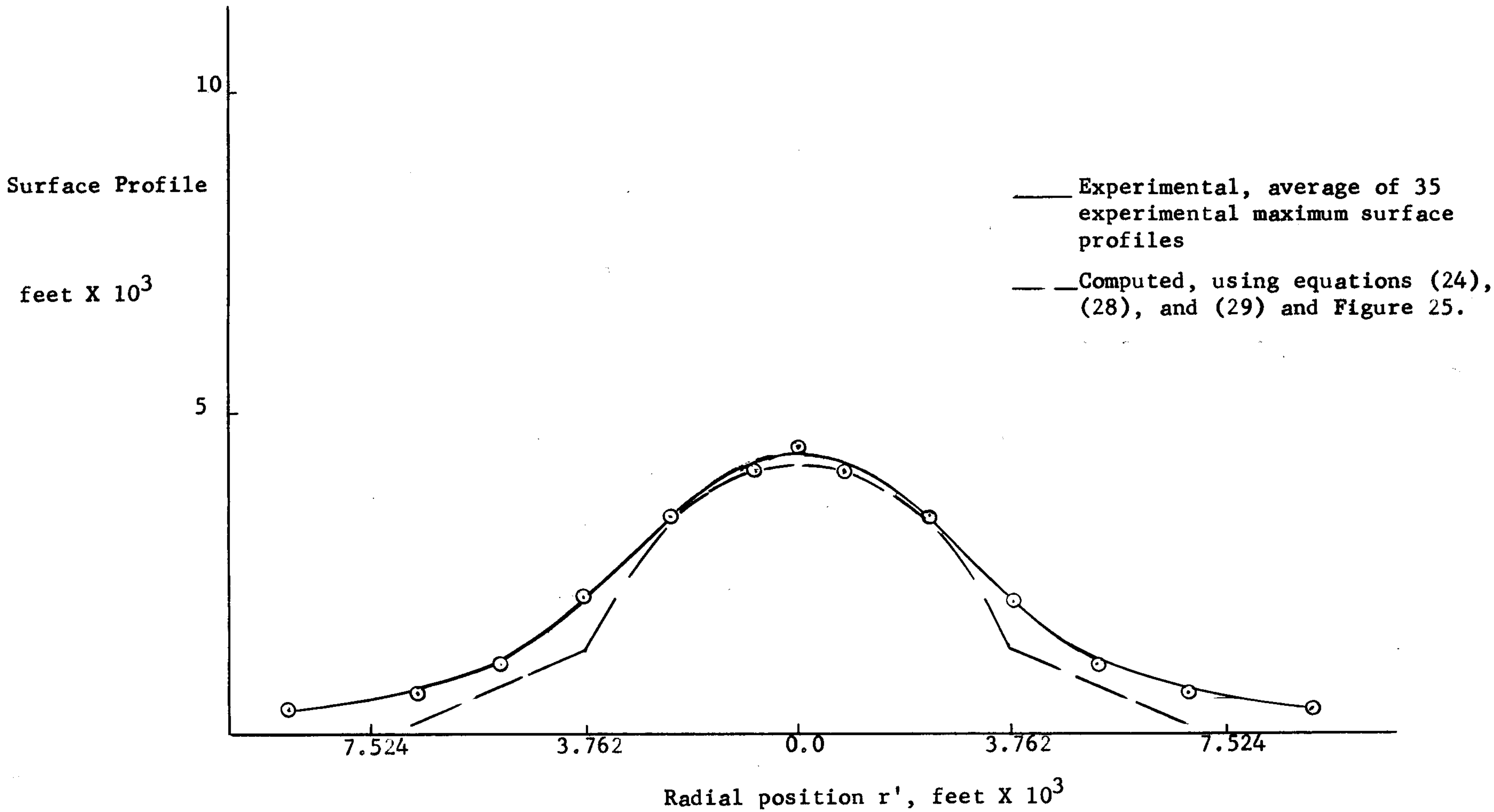

Figure 18. Comparison of Experimental Surface Profile with Profile Computed with Correlation Procedure for Reynolds Number of 565 and Bubble Diameter of 0.007524 Feet. Nitrogen Gas in Distilled Water.

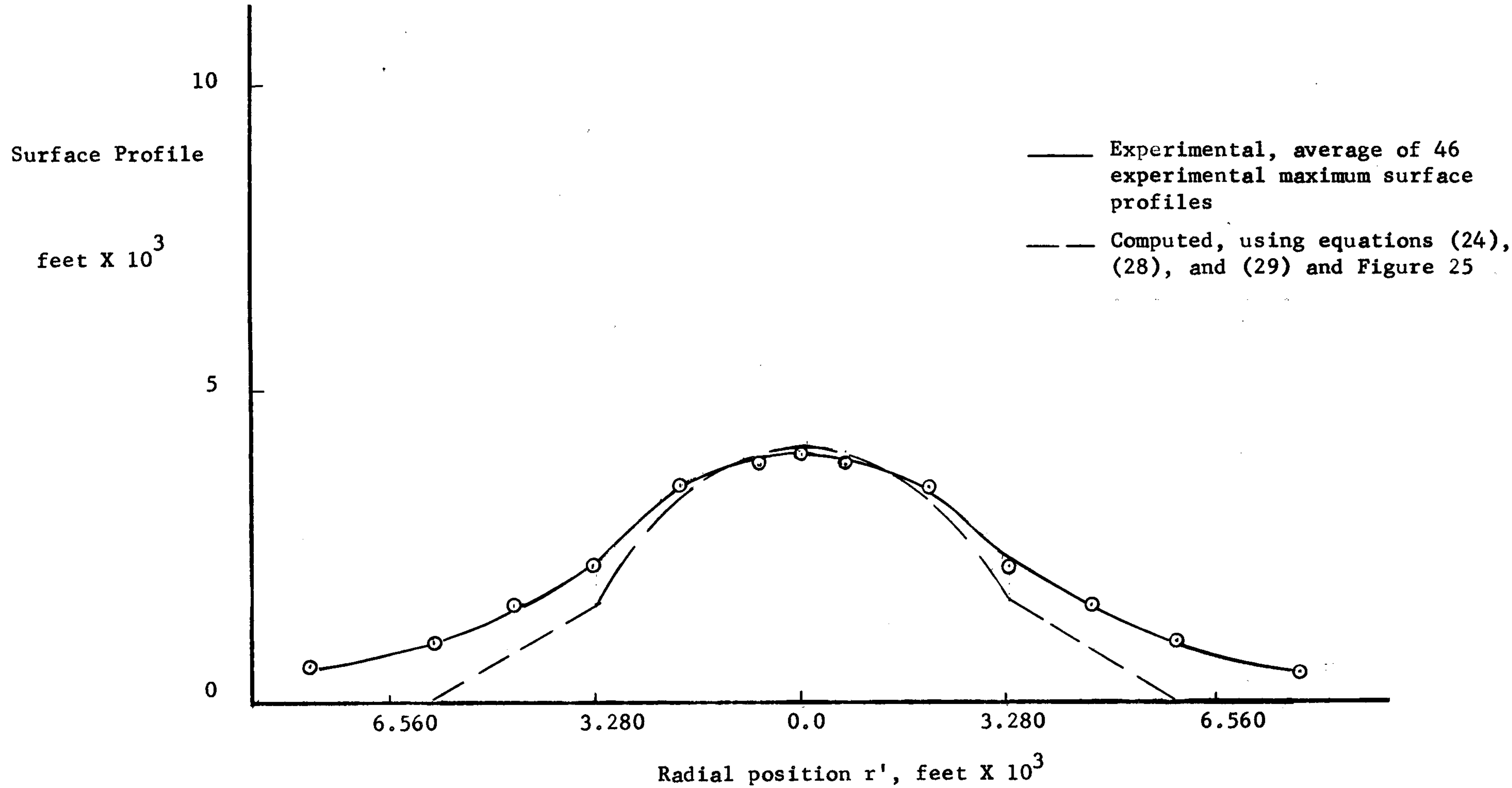

Figure 19. Comparison of Experimental Surface Profile with Profile Computed with Correlation Procedure for Reynolds Number of 514 and Bubble Diameter of 0.006560 Feet. Nitrogen Gas in Distilled Water.

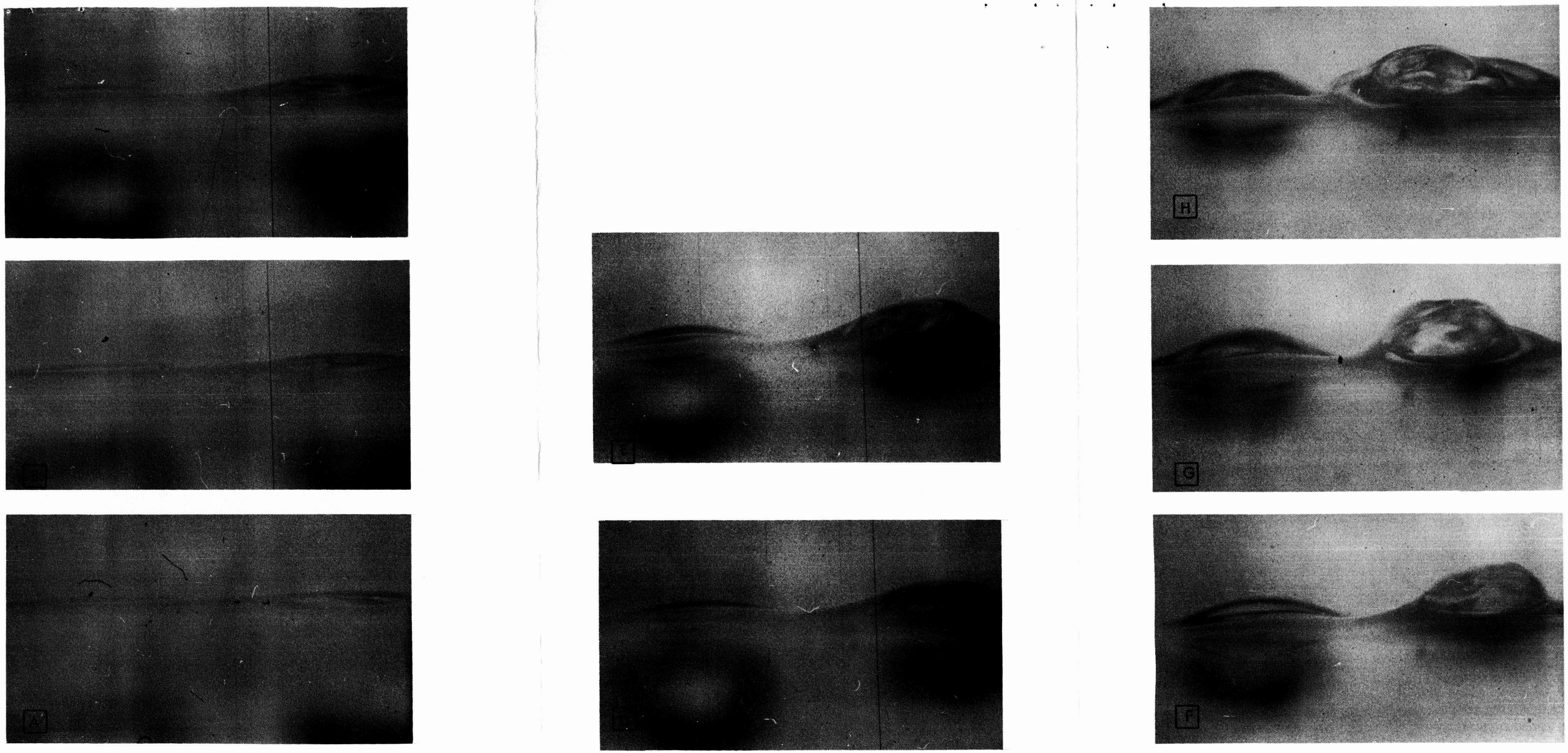

Figure 20. Surface Disturbance Caused by Two Bubbles of Nitrogen Gas Rising in Distilled Water 1/100 Second Apart. Taken from Frames of High Speed, 16 mm, Motion Picture Film. Time Interval Between Pictures of 1/200 Second.

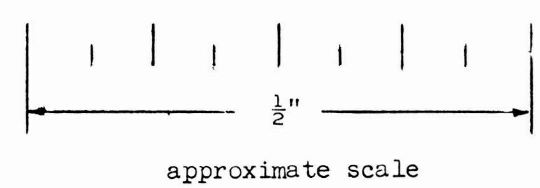

Experimental Surface Profiles for Two Horizontally Interfering Bubbles

It is very difficult to produce simultaneously two bubbles which will rise together and strike the surface at the same instant within two to four bubble radii apart. However, some success has been achieved. Figure 20 gives a sequence from the motion picture film which shows two bubbles interfering horizontally. The resulting profile is similar in shape to that predicted by analytical calculation and given in Figure 10. The correlation procedure has not yet been applied to this case.

APPENDIX I

Development of Equations Related to the Potential Solution

The potential function for the fluid motion produced when a sphere of radius a moves with a uniform velocity U is given by Prandtl and Tietjens (78) as

$$\Phi_s = \frac{Ua^3 \cos\theta}{2R'^2} \tag{30}$$

where the angle θ and the radial coordinate R' are as shown in Figure 21.

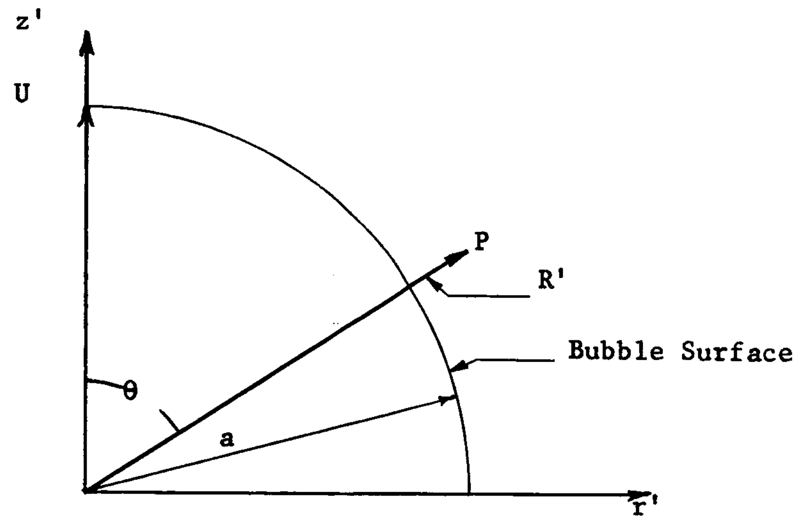

Figure 21. Coordinate System Potential Flow

The radial (R') and tangential components of velocity are given by $\frac{\partial \Phi_s}{\partial R'}$ and $\frac{\partial \Phi_s}{R' \partial\theta}$ respectively. Thus,

$$V_o = \frac{\partial \Phi_s}{\partial R'} = \left[- \frac{Ua^3}{R'^3} \right] \cos\theta \tag{31}$$

$$U_o = \frac{\partial \Phi_s}{R \partial \theta} = \left[- \frac{Ua^3}{2R'^3} \right] \cos\theta \tag{32}$$

Defining the dimensionless variable $R = \frac{R'}{a}$, equations (31) and (32) become

$$\frac{V_o}{U} = - \frac{\cos\theta}{R^3} \tag{31a}$$

and

$$\frac{U_o}{U} = - \frac{\sin\theta}{2R^3} \tag{32a}$$

Two approaches could be taken to determine expressions for the velocity components in the r' and z' directions. One would be to transform equations (31a) and (32a) into cylindrical coordinates r', z' and then add vectorially their components in the r' and z' directions. The other approach, which is the most direct, would be to transform the potential function given by equation (30) into cylindrical coordinates and then determine the velocity components by taking the appropriate derivatives. This latter method was used, and the results were verified by the first approach.

The following coordinate transformations are used to transform equation (3) into cylindrical coordinates r', z':

$$R' = (r'^2 + z'^2),^{\frac{1}{2}} \tag{33a}$$

$$\cos\theta = \frac{z'}{(r'^2 + z'^2)^{\frac{1}{2}}} , \tag{33b}$$

and

$$\sin\theta = \frac{r'}{(r'^2 + z'^2)^{\frac{1}{2}}} . \tag{33c}$$

Rewriting equation (30) in cylindrical coordinates, we have:

$$\Phi_c = \frac{Ua^3}{2} \cdot \frac{z'}{(r'^2 + z'^2)^{\frac{1}{2}}} \cdot \frac{1}{\left[(r'^2 + z'^2)^{\frac{1}{2}}\right]^2} \tag{30a}$$

Simplifying,

$$\Phi_c = \frac{Ua^3}{2} \cdot \frac{z'}{(r'^2 + z'^2)^{3/2}} . \tag{11}$$

By definition

$$V_o = \frac{\partial \Phi_c}{\partial r} = -\frac{3Ua^3}{2} \cdot \frac{r'z'}{(r'^2 + z'^2)^{5/2}} \tag{34}$$

$$U_o = \frac{\partial \Phi_c}{\partial z} = -\frac{Ua^3(z'^2 + r'^2/2)}{(r'^2 + z'^2)^{5/2}} \tag{35}$$

By defining $r = \frac{r'}{a}$ and $z = \frac{z'}{a}$, equations (34) and (35) may be written as

$$V_o = -\frac{3}{2} \frac{Urz}{(r^2 + z^2)^{5/2}} \tag{12}$$

$$U_o = -\frac{U(z^2 - r^2/2)}{(r^2 + z^2)^{5/2}} . \tag{13}$$

Now the relationship for $\bar{v}^2(r,z)$ for use in equation (9) may be determined. For the potential solution

$$\bar{v}^2 = V_o^{\,2} + U_o^{\,2} . \tag{8c}$$

Equations (8c), (12), and (13) may be combined to give

$$\overline{v}^2 = \frac{9/4U^2r^2z^2}{(r^2 + z^2)^5} + \frac{U^2\left[z^2 - r^2/2\right]^2}{(r^2 + z^2)^5} .$$

Simplifying the above expression,

$$\overline{v}^2 = \frac{9/4U^2r^2z^2 + U^2(z^4 - z^2r^2 + r^4/4)}{(r^2 + z^2)^5} ,$$

$$\overline{v}^2 = \frac{U^2(z^4 + 5/4r^2z^2 + r^4/4)}{(r^2 + z^2)^5} ,$$

$$\overline{v}^2 = \frac{U^2(4z^2 + r^2)(z^2 + r^2)}{4(r^2 + z^2)^5} ,$$

$$\overline{v}^2 = \frac{U^2(4z^2 + r^2)}{4(r^2 + z^2)^4} . \qquad (36)$$

Thus, the relation

$$F(r) = \int_{\sqrt{1-r^2},\ 0}^{H} \overline{v}^2(r,z)dz , \qquad (9)$$

may be written for the potential flow model as

$$F(r) = \int_{\sqrt{1-r^2},\ 0}^{H} \frac{4z^2 + r^2}{4(r^2 + z^2)^4} \, dz . \qquad (14)$$

APPENDIX II

Integration of Equation (14)

Considering a fixed value of r, the expression

$$\int_{\sqrt{1-r^2},\ 0}^{\infty} \frac{4z^2 + r^2}{4(r^2 + z^2)^4}\, dz$$

can be written as

$$\int_{\sqrt{1-r^2},\ 0}^{\infty} \frac{4z^2 + r^2}{4(r^2 + z^2)^4}\, dz = \int_{\sqrt{1-r^2},\ 0}^{\infty} \frac{z^2}{(r^2 + z^2)^4}\, dz + \frac{r^2}{4} \int_{\sqrt{1-r^2},\ 0}^{\infty} \frac{dz}{(r^2 + z^2)^4} . \quad (37)$$

The two integrals on the right side of equation (37) may be integrated by successive application of the integration by parts technique. Thus:

$$\int_{\sqrt{1-r^2},\ 0}^{\infty} \frac{z^2}{(r^2 + z^2)^4}\, dz = \left[- \frac{z}{6(r^2 + z^2)^3} \right]_{\sqrt{1-r^2},\ 0}^{\infty} + \frac{1}{6} \int_{\sqrt{1-r^2},\ 0}^{\infty} \frac{dz}{(r^2 + z^2)^3} ,$$

$$\int_{\sqrt{1-r^2},\ 0}^{\infty} \frac{z^2}{(r^2 + z^2)^4}\, dz = \left[- \frac{z}{6(r^2 + z^2)^3} + \frac{z}{24r^2(r^2 + z^2)^2} \right]_{\sqrt{1-r^2},\ 0}^{\infty}$$

$$+ \frac{z}{24r^2} \int_{\sqrt{1-r^2},\ 0}^{\infty} \frac{dz}{(r^2 + z^2)^2} ,$$

$$\int_{\sqrt{1-r^2},\;0}^{\infty} \frac{z^2}{(r^2+z^2)^4}\,dz = \left[-\frac{z}{6(r^2+z^2)^3} + \frac{z}{24r^2(r^2+z^2)^2} + \frac{3z}{48r^4(r^2+z^2)}\right]_{\sqrt{1-r^2},\;0}^{\infty}$$

$$+ \frac{3}{48r^4}\int_{\sqrt{1-r^2},\;0}^{\infty} \frac{dz}{(r^2+z^2)} ,$$

$$\int_{\sqrt{1-r^2},\;0}^{\infty} \frac{z^2}{(r^2+z^2)^4}\,dz = \left[-\frac{z}{6(r^2+z^2)^3} + \frac{z}{24r^2(r^2+z^2)^2} + \frac{3z}{48r^4(r^2+z^2)}\right.$$

$$\left. + \frac{3}{48r^5}\arctan\frac{z}{r}\right]_{\sqrt{1-r^2},\;0}^{\infty} , \qquad (38)$$

and

$$\frac{r^2}{4}\int_{\sqrt{1-r^2},\;0}^{\infty} \frac{dz}{(r^2+z^2)^4} = \left[\frac{z}{24(r^2+z^2)^3}\right]_{\sqrt{1-r^2},\;0}^{\infty} + \frac{5}{24}\int_{\sqrt{1-r^2},\;0}^{\infty} \frac{dz}{(r^2+z^2)^3} ,$$

$$= \left[\frac{z}{24(r^2+z^2)^3} + \frac{5z}{96r^2(r^2+z^2)^2}\right]_{\sqrt{1-r^2},\;0}^{\infty}$$

$$+ \frac{15}{96r^2}\int_{\sqrt{1-r^2},\;0}^{\infty} \frac{dz}{(r^2+z^2)^2} ,$$

$$\frac{r^2}{4}\int_{\sqrt{1-r^2},\ 0}^{\infty}\frac{dz}{(r^2+z^2)^4} = \left[\frac{z}{24(r^2+z^2)^3}+\frac{5z}{96r^2(r^2+z^2)}+\frac{15z}{192r^4(r^2+z^2)}\right]_{\sqrt{1-r^2},\ 0}^{\infty}$$

$$+\ \frac{15}{192r^4}\int_{\sqrt{1-r^2},\ 0}^{\infty}\frac{dz}{(r^2+z^2)} ,$$

$$\frac{r^2}{4}\int_{\sqrt{1-r^2},\ 0}^{\infty}\frac{dz}{(r^2+z^2)^4} = \left[\frac{z}{24(r^2+z^2)^3}+\frac{5z}{96r^2(r^2+z^2)^2}+\frac{15z}{192r^4(r^2+z^2)}\right.$$

$$\left. +\ \frac{15}{192r^5}\ \arctan\frac{z}{r}\right]_{\sqrt{1-r^2},\ 0}^{\infty} . \qquad (39)$$

After obtaining a common denominator and combining terms of equations (38) and (39), equation (37) becomes for $r > 0$:

$$\int_{\sqrt{1-r^2},\ 0}^{\infty}\frac{4z^2+r^2}{4(r^2+z^2)^4}\,dz = \left[-\ \frac{3z}{24(r^2+z^2)^3}+\frac{9z}{96r^2(r^2+z^2)^2}+\frac{27z}{192r^4(r^2+z^2)}\right.$$

$$\left. +\ \frac{27}{192r^5}\ \arctan\frac{z}{r}\right]_{\sqrt{1-r^2},\ 0}^{\infty} , \qquad (37a)$$

and for r = o

$$\int_{\sqrt{1-r^2},\ 0}^{\infty} \frac{4z^2 + r^2}{4(r^2 + z^2)^4}\, dz = \int_{1}^{\infty} \frac{dz}{z^6} = \left[- \frac{1}{5z^5} \right]_1^{\infty} = 0.20 \qquad (37b)$$

APPENDIX III

Discontinuity in $\frac{F(r)}{U^2}$ Derived from Potential Solution of Velocity Field

Applying Leibnitz' formula for differentiation of an integral to

$$K = \int_{f(r)}^{H} g(z,r)dz, \tag{40}$$

where

$$g(z,r) = \frac{4z^2 + r^2}{4(r^2 + z^2)^4}$$

and

$$f(r) = \sqrt{1-r^2} \quad ,$$

we obtain

$$\frac{dK}{dr} = g(H,r)\frac{dH}{dr} - g\left[f(r),r\right]\frac{df(r)}{dr}$$

$$+ \int_{f(r)}^{H} \frac{\partial}{\partial r}\left[g(z,r)\right] dz. \tag{18}$$

Performing the mathematical operations shown in equation (18), we obtain:

$$\frac{dH}{dr} = 0 \quad \text{(since H is constant)},$$

$$g\left[f(r),r\right] = \frac{4-3r^2}{4} \quad ,$$

$$\frac{df(r)}{dr} = \frac{d}{dr}(1-r^2)^{\frac{1}{2}} = -\frac{r}{(1-r^2)^{\frac{1}{2}}} \quad ,$$

$$-g\left[f(r),r\right]\frac{df(r)}{dr} = \left[-\frac{4-3r^2}{4}\right] \cdot \left[-\frac{r}{(1-r^2)^{\frac{1}{2}}}\right] = \frac{4r-3r^3}{4(1-r^2)^{\frac{1}{2}}} \quad ,$$

and

$$\frac{\partial}{\partial r}\left[g(z,r)\right] = \frac{\partial}{\partial r}\left[\frac{4z^2 + r^2}{4(r^2 + z^2)^4}\right] = \frac{2r(4z^2 + r^2)}{(r^2 + z^2)^5} + \frac{r}{2(r^2 + z^2)^4}$$

$$\frac{\partial}{\partial r}\left[G(z,r)\right] = -\frac{3r(5z^2 + r^2)}{2(r^2 + z^2)^5} .$$

Inserting the above into equation (18), we have

$$\frac{dK}{dr} = \frac{4r-3r^3}{4(1-r^2)^{\frac{1}{2}}} - \int_{\sqrt{1-r^2}}^{H} \frac{3r(5z^2 + r^2)\,dz}{2(r^2 + z^2)^5} . \qquad (19)$$

Performing the integration shown in equation (19), we obtain

$$\frac{dK}{dr} = \frac{4r-3r^3}{4(1-r^2)^{\frac{1}{2}}} - \left[-\frac{3rz}{4(z^2 + r^2)^4} + \frac{6z}{16r(z^2 + r^2)^3} \right.$$

$$+ \frac{1005z}{384r^3(z^2 + r^2)^2} + \frac{3015z}{768r^5(z^2 + r^2)}$$

$$\left. + \frac{3015}{768r^6} \arctan\frac{z}{r} \right]_{\sqrt{1-r^2}}^{H} . \qquad (41)$$

Inserting the limits of integration, equation (41) becomes

$$\frac{dK}{dr} = \frac{4r-3r^3}{4(1-r^2)^{\frac{1}{2}}} - \left[-\frac{3rH}{4(H^2 + r^2)^4} + \frac{6H}{16r(H^2 + r^2)^3} \right.$$

$$+ \frac{1005H}{384r^3(H^2 + r^2)^2} + \frac{3015H}{768r^5(H^2 + r^2)}$$

$$+ \frac{3015}{768r^6} \arctan\frac{H}{r} + \frac{3r\sqrt{1-r^2}}{4} - \frac{6\sqrt{1-r^2}}{16r} - \frac{1005\sqrt{1-r^2}}{384r^3}$$

$$\left. - \frac{3015\sqrt{1-r^2}}{768r^5} - \frac{3015}{768r^6} \arctan\frac{\sqrt{1-r^2}}{r} \right] . \qquad (42)$$

Taking the limit of equation (42) as $r \to 1$, we see that the first term approaches infinity while the terms inside of the braces approach a finite number. Thus

$$\lim_{r \to 1} \frac{dK}{dr} = \infty \quad .$$

APPENDIX IV

Development of Equations Related to the Real Fluid Solution

At any point P in the perturbed region Chao (11) defines the radial velocity component v_o and the tangential velocity component u_o of the fluid in spherical coordinates, to be:

$$v_o = V_o + v'_o \qquad (43a)$$

$$u_o = U_o + u'_o \quad . \qquad (43b)$$

In equations (43a) and (43b) V_o is the radial velocity component and U_o the tangential velocity component derivable from potential theory, and v'_o is the radial velocity component and u'_o the tangential velocity component of the perturbed velocity as derived by Chao (11).

Dividing equations (43a) and (43b) by U, the bubble rise velocity, yields:

$$\frac{v_o}{U} = \frac{V_o}{U} + \frac{v'_o}{U} \qquad (43c)$$

and

$$\frac{u_o}{U} = \frac{U_o}{U} + \frac{u'_o}{U} \quad . \qquad (43d)$$

As shown in Appendix I,

$$\frac{V_o}{U} = -\frac{\cos\theta}{R^3} \qquad (31a)$$

and

$$\frac{U_o}{U} = -\frac{\sin\theta}{2r^3} \quad , \qquad (32a)$$

where R and θ are defined in Figure 22.

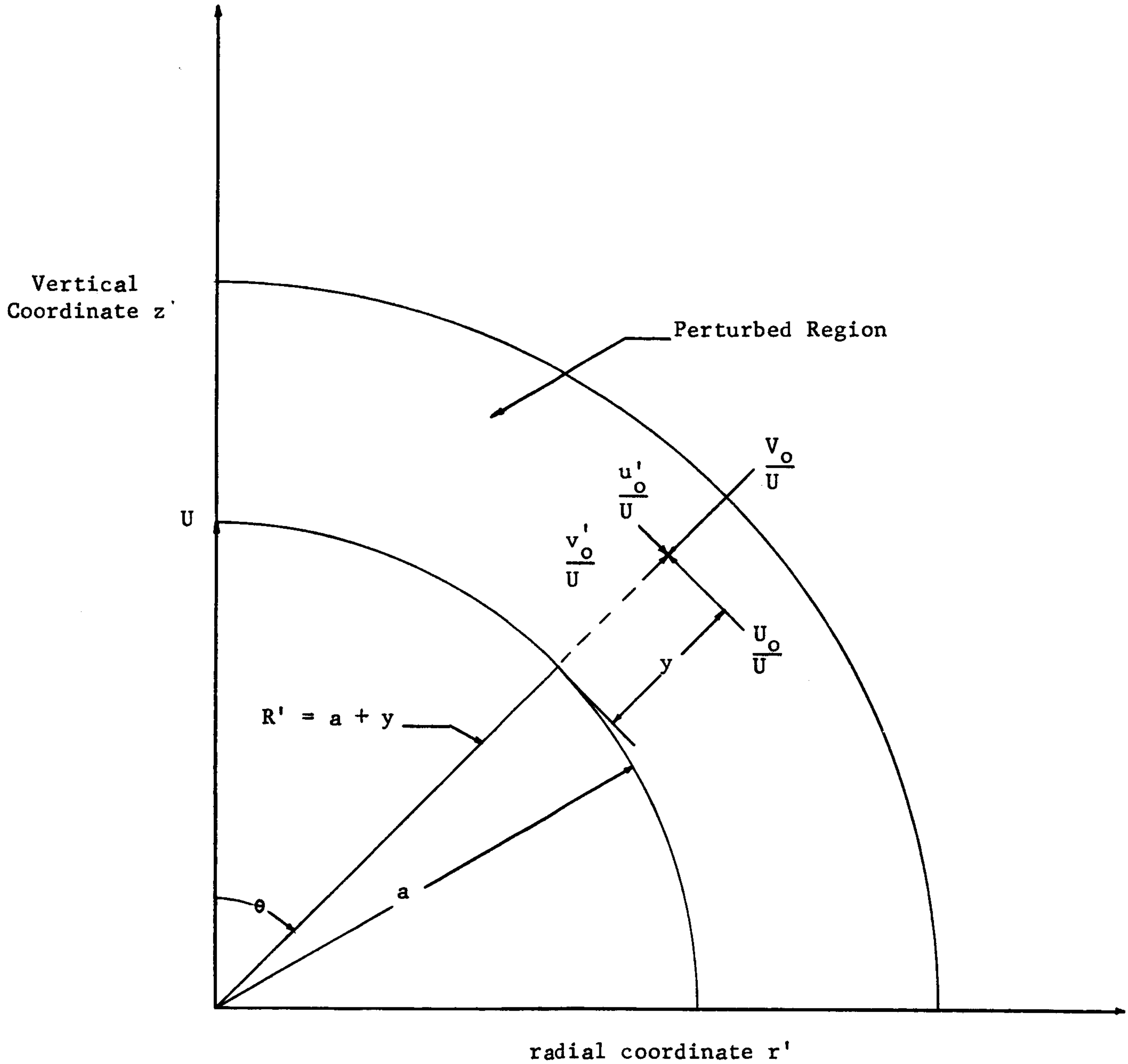

Figure 22. Radial and Tangential Velocity Components for the Potential Solution and Perturbed Solution

The perturbed components of velocity at P, given by Chao, are:

$$\frac{v_o}{U} = \frac{4}{3N_{Re}}\left[\frac{1 + 4\,\mu_g/\mu_L}{1 + \left[(\rho_g/\rho_L)(\mu_g/\mu_L)\right]^{\frac{1}{2}}}\right]\cdot\left[\left(\frac{1}{2} + \left[\frac{1-\cos\theta}{\sin^2\theta}\right]^2\right)\operatorname{erf}\zeta_o\right.$$

$$\left. + \; 2\left(1 - \left[\frac{1-\cos\theta}{\sin^2\theta}\right]^2\right)\zeta_o \;\operatorname{ierfc}\zeta_o\right] \qquad (44)$$

and

$$\frac{u'_o}{U} = -\frac{2\sqrt{3}}{(N_{Re})^{\frac{1}{2}}}\left(\frac{1 + 4\,\mu_g/\mu_L}{1 + \left[(\rho_g/\rho_L)(\mu_g/\mu_L)\right]^{\frac{1}{2}}}\right)$$

$$\cdot\left(\frac{(2/3 - \cos\theta + 1/3\,\cos^3\theta)^{\frac{1}{2}}}{\sin\theta}\right)\left(\operatorname{ierfc}\zeta_o\right). \qquad (45)$$

where the symbols are defined as:

N_{Re} = bubble Reynolds number = $\frac{2Ua}{\nu_L}$

a = bubble radius

μ_g = gas viscosity

μ_L = liquid viscosity

ρ_g = gas density

ρ_L = liquid density

ν_L = liquid kinematic viscosity = μ_L/ρ_L

$$\zeta_o = \frac{(3N_{Re})^{\frac{1}{2}}}{4}\;\frac{\sin^2\theta}{(2/3 - \cos\theta + 1/3\,\cos^3\theta)^{\frac{1}{2}}}\cdot\frac{y}{a},\quad y \geq 0 \qquad (46)$$

$$\operatorname{erf}\zeta_o = \frac{2}{\sqrt{\pi}}\int_0^{\zeta_o} e^{-\beta^2}\,d\beta \qquad \operatorname{erfc}\zeta_o = 1 - \operatorname{erf}\zeta_o,$$

$$\operatorname{ierfc}\zeta_o = \int_{\zeta_o}^{\infty}\operatorname{erfc}\beta\;d\beta\;.$$

Substituting equations (31a) and (32a) into equations (43c) and (43d), we obtain:

$$\frac{v_o}{U} = - \frac{\cos\theta}{R^3} + \frac{v_o'}{U} \tag{47}$$

and

$$\frac{u_o}{U} = - \frac{\sin\theta}{2R^3} + \frac{u_o'}{U} \quad , \tag{48}$$

where

$\frac{v_o'}{U}$ and $\frac{u_o'}{U}$ are given by equations (44) and (45).

To convert the right hand side of equations (47) and (48) from spherical coordinates (R,θ) to cylindrical coordinates (r,z) the following coordinate transformations (see Figure 23) are used:

$$R = (r^2 + z^2)^{\frac{1}{2}} \quad ,$$

$$\cos\theta = \frac{z}{(r^2 + z^2)^{\frac{1}{2}}} \quad ,$$

and

$$\sin\theta = \frac{r}{(r^2 + z^2)^{\frac{1}{2}}} \quad .$$

Transforming equations (47) and (48) into cylindrical coordinates, the following expressions for each term are obtained:

$$\frac{V_o}{U} = - \frac{\cos\theta}{R^3} = - \frac{z}{(r^2 + z^2)^2} \quad , \tag{31b}$$

$$\frac{U_o}{U} = - \frac{\sin\theta}{2R^3} = - \frac{r}{2(r^2 + z^2)^2} \quad , \tag{32b}$$

$$\frac{v_o'}{U} = \frac{4}{3N_{Re}} \left[\frac{1 + 4\mu_g/\mu_L}{1 + \left[(\rho_g/\rho_L)(\mu_g/\mu_L)\right]^{\frac{1}{2}}} \right] \cdot \left[\left[\frac{1}{2} + \frac{\left(1 - \frac{z}{(r^2 + z^2)^{\frac{1}{2}}}\right)^2}{\left(\frac{r^2}{(r^2 + z^2)}\right)^2} \right] \operatorname{erf} \zeta_o \right.$$

$$\left. + 2 \left[1 - \frac{\left(1 - \frac{z}{(r^2 + z^2)^{\frac{1}{2}}}\right)^2}{\left(\frac{r^2}{(r^2 + z^2)}\right)^2} \right] \zeta_o \operatorname{ierfc} \zeta_o \right] , \tag{44a}$$

and

$$\frac{u_o'}{U} = - \frac{2\sqrt{3}}{(N_{Re})^{\frac{1}{2}}} \left[\frac{1 + 4\mu_g/\mu_L}{1 + \left[(\rho_g/\rho_L)(\mu_g/\mu_L)\right]^{\frac{1}{2}}} \right]$$

$$\cdot \left[\frac{\frac{2}{3} - \frac{z}{(r^2 + z^2)^{\frac{1}{2}}} + \frac{1}{3} \frac{z^3}{(r^2 + z^2)^{3/2}}}{\frac{r}{(r^2 + z^2)^{\frac{1}{2}}}} \right] \operatorname{ierfc} \zeta_o , \tag{45a}$$

where

$$\zeta_o = \frac{(3N_{Re})^{\frac{1}{2}}}{4} \left[\frac{\frac{r^2}{(r^2 + z^2)}}{\left[\frac{2}{3} - \frac{z}{(r^2 + z^2)^{\frac{1}{2}}} + \frac{1}{3} \frac{z^3}{(r^2 + z^2)^{3/2}}\right]} \right]^{\frac{1}{2}} \cdot \left[(r^2 + z^2)^{\frac{1}{2}} - 1 \right] . \tag{46a}$$

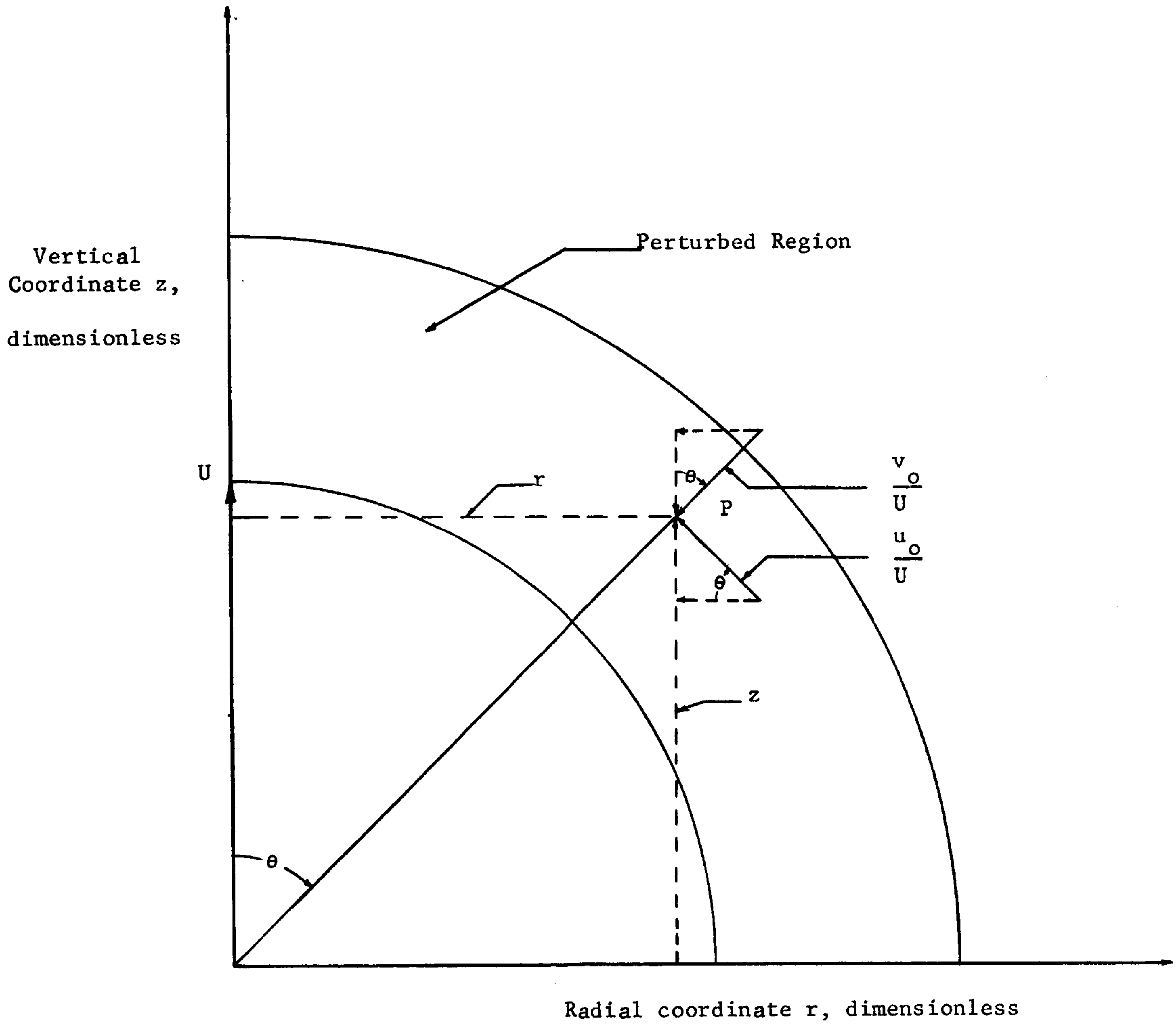

Figure 23. Velocity Components of $\frac{v_o}{U}$ and $\frac{u_o}{U}$ in the r and z Directions

After simplification

$$\frac{v'_o}{U} = \frac{4}{3N_{Re}} \left[\frac{1 + 4\mu_g/\mu_L}{1 + [(\rho_g/\rho_L)(\mu_g/\mu_L)]^{\frac{1}{2}}} \right]$$

$$\cdot \left[\left[\frac{1}{2} + \left(\frac{r^2 + z^2 - z(r^2 + z^2)^{\frac{1}{2}}}{r^2} \right)^2 \right] \operatorname{erf} \zeta_o \right.$$

$$\left. + 2 \left[1 - \left(\frac{r^2 + z^2 - z(r^2 + z^2)^{\frac{1}{2}}}{r^2} \right)^2 \right] \zeta_o \operatorname{ierfc} \zeta_o \right], \tag{44b}$$

$$\frac{u'_o}{U} = -\frac{2\sqrt{3}}{(N_{Re})^{\frac{1}{2}}} \left[\frac{1 + 4\mu_g/\mu_L}{1 + [(\rho_g/\rho_L)(\mu_g/\mu_L)]^{\frac{1}{2}}} \right]$$

$$\cdot \left[\frac{\left[2/3(r^2 + z^2)^{3/2} - zr^2 - 2/3z^3 \right]^{\frac{1}{2}}}{r(r^2 + z^2)^{\frac{1}{4}}} \right] \operatorname{ierfc} \zeta_o, \tag{45b}$$

and

$$\zeta_o = \frac{(3N_{Re})^{\frac{1}{2}}}{4} \frac{r^2(r^2 + z^2)^{\frac{1}{2}} - r^2}{\left[\frac{2}{3}(r^2 + z^2)^2 - z(r^2 + z^2)^{3/2} + \frac{1}{3} z^3 (r^2 + z^2)^{\frac{1}{2}} \right]^{\frac{1}{2}}} \tag{46b}$$

As shown on Figure 23, $\frac{v_o}{U}$ and $\frac{u_o}{U}$ can now be evaluated at any point P as functions of r and z by using

$$\frac{v_o}{U} = \frac{V_o}{U} + \frac{v'_o}{U} \tag{43c}$$

and

$$\frac{u_o}{U} = \frac{U_o}{U} + \frac{u'_o}{U} \tag{43d}$$

where

$\frac{V_o}{U}$ is calculated from equation (31b),

$\frac{v'_o}{U}$ is calculated from equation (44b),

$\frac{U_o}{U}$ is calculated from equation (32b),

and

$\frac{u'_o}{U}$ is calculated from equation (45b).

The last step remaining is to determine expressions for the velocity components in the r and z directions for use in equation (20). Defining new velocity components for Point P, UC and VC, where UC is the sum of the z components of $\frac{v_o}{U}$ and $\frac{u_o}{U}$ and VC is the sum of the r components of $\frac{v_o}{U}$ and $\frac{u_o}{U}$ it can be seen from Figure 23 that:

$$VC = \frac{u_o}{U}\cos\theta + \frac{v_o}{U}\sin\theta \tag{49}$$

and

$$UC = \frac{v_o}{U}\cos\theta - \frac{u_o}{U}\sin\theta, \quad \text{or} \tag{50}$$

since

$$\cos\theta = \frac{z}{(r^2 + z^2)^{\frac{1}{2}}} \text{ and } \sin\theta = \frac{r}{(r^2 + z^2)^{\frac{1}{2}}},$$

$$VC = \frac{u_o}{U} \cdot \frac{z}{(r^2 + z^2)^{\frac{1}{2}}} + \frac{v_o}{U} \cdot \frac{r}{(r^2 + z^2)^{\frac{1}{2}}} \tag{49a}$$

$$UC = \frac{v_o}{U} \cdot \frac{z}{(r^2 + z^2)^{\frac{1}{2}}} - \frac{u_o}{U} \cdot \frac{r}{(r^2 + z^2)^{\frac{1}{2}}} \tag{50a}$$

where

$\frac{u_o}{U}$ and $\frac{v_o}{U}$ are given by equations (43d) and (43c).

Relations (49a) and (50a) may be used with the following equation,

$$F(r) \quad = \quad \overline{V^2}H \quad = \int_{\sqrt{1-r^2},\ 0}^{H} \left[(UC)^2 + (VC)^2 \right] \, dz$$

to determine the time mean kinetic energy distribution for the real fluid analysis.

APPENDIX V

Computer Program for Integration of Equation (20)

NOMENCLATURE

FOR COMPUTER PROGRAM ONLY

US	VISCOSITY OF GAS
UL	VISCOSITY OF LIQUID
RL	DENSITY OF LIQUID
REY	BUBBLE REYNOLDS NUMBER
R	RADIAL COORDINATE, NON-DIMENSIONAL
Z	VERTICAL COORDINATE, NON-DIMENSIONAL
UOP	PERTURBED TANGENTIAL VELOCITY COMPONENT
VOP	PERTURBED RADIAL VELOCITY COMPONENT
UO	POTENTIAL TANGENTIAL VELOCITY COMPONENT
VO	POTENTIAL RADIAL VELOCITY COMPONENT
UC	VERTICAL VELOCITY COMPONENT FOR THE REAL FLUID SOLUTION, DEFINED BY EQUATION 50
VC	SOLUTION, DEFINED BY EQUATION 49
EF	ZETA SUB ZERO, DEFINED BY EQUATION 46
EEF	ERF OF ZETA SUB ZERO
O,P,Q, S,T,U	COEFFICIENTS IN CURVE FIT TO DETERMINE ERF OF ZETA SUB ZERO
EEEF	IERFC OF ZETA SUB ZERO
U,V,W,X	COEFFICIENTS IN CURVE FIT TO DETERMINE IERFC OF ZETA SUB ZERO

```
C   C   KINETIC ENERGY REAL FLUID SOLUTION
        DIMENSION Y(999)
        UG=.0000122
        UL=.00076
        RG=.077
        RL=62.35
        O=1.129793
        P=-2.04716
        Q=1.3295
        S=-.3143
        T=-.0096
        U=.00997
        V=.278393
        W=.230389
        X=.000972
        YY=.078108
     98 READ 20,K1,K2,K3,BBB
     20 FORMAT(3I5,F10.4)
        DZ=0.05
        DO 7 IR=K1,K2,K3
        R=IR
        R=(R-1.0)/BBB
        K=1
        IF (R-1.0) 80,81,81
     80 Z=(1.0-R*R)**0.5
        GO TO 1
     81 Z=0.0
      1 REY=100.0
        B=(SQRTF(3.0*REY))/4.0
        C=(R*R)*(SQRTF((R*R)+(Z*Z)))-(R*R)
        D=(2.0/3.0)*(((R*R)+(Z*Z))**2.0)
        E=Z*(((R*R)+(Z*Z))**1.5)
        F=(1.0/3.0)*(Z*Z*Z)*(((R*R)+(Z*Z))**.50)
        EF=B*(C/SQRTF(D-E+F))
        VEF=V*EF
        WEF=W*(EF**2)
        XEF=X*(EF**3)
        YEF=YY*(EF**4)
        EEF=1.0-(1.0/((1.0+VEF+WEF+XEF+YEF)**4.0))
        IF(EF-2.6) 100,108,108
    100 EEEF=O+(P+(Q+(S+(T+U*EF)*EF)*EF)*EF)*EF
        AA=(-2.0*(3.0**.50))/(REY**.50)
        CC=4.0/(3.0*REY)
        AK=(1.0+(4.0*(UG/UL)))/(1.0+(((RG/RL)*(UG/UL))**.50))
        QQ=(R*R)+(Z*Z)
        AB=((2.0/3.0)*(QQ**1.5))-(Z*R*R)
        AC=(-2.0/3.0)*(Z*Z*Z)
        AE=R*(QQ**.25)
        UOP=AA*AK*(((AB+AC)**.50)/AE)*EEEF
        BB=(QQ-(Z*(QQ**.50)))/(R*R)
        BC=(.50+(BB**2.0))*EEF
        BD=2.0*(1.0-(BB**2.0))*EF*EEEF
        VOP=CC*AK*(BC+BD)
```

```
      GO TO 118
  108 UOP=0.
      VOP=0.
      QQ=(R*R+Z*Z)
  118 UO=-(R/2.0)/(QQ**2.0)
      US=UO-UOP
      VO=-Z/(QQ**2.0)
      VS=VO+VOP
      UC=(VS*(Z/(QQ**.50)))-(US*(R/(QQ**.50)))
      VC=(US*(Z/(QQ**.50)))+(VS*(R/(QQ**.50)))
      Y(K)=(UC**2)+(VC**2)
      IF (Y(K)-0.000001) 3,3,2
    2 Z=Z+DZ
      K=K+1
      IF(VOP)1,108,1
    3 N=K
      FN=N/2
      M=FN*2.0
      IF (K-N) 4,10,4
   10 Z=Z+DZ
      K=K+1
      GO TO 1
    4 EVEN=0.0
      FODD=0.0
      ME=K-1
      MO=K-2
      DO 5 J=2,ME,2
    5 EVEN = EVEN + Y(J)
      DO 6 J=3,MO,2
    6 FODD=FODD + Y(J)
      SUM = DZ*(Y(1)+Y(K)+2.0*EVEN+4.0*FODD)/3.0
    7 PRINT 8,R,SUM,ZS,Z
      GO TO 98
    8 FORMAT (F5.2,2E18.8,F20.8)
      END
21   401    10    100.0
```

APPENDIX VI

Origin of Spray Droplets Above Liquid Surface

Figure 24 gives a sequence of pictures taken from the motion picture film showing an interesting phenomenon associated with the breaking of the gas bubbles. These pictures are also spaced in time by 1/200 of a second. After causing a surface distortion as shown in Figure 11, the bubbles normally relax into a position as shown in frames 24a, 24b, and 24c. Convection currents generated by the rising bubbles slowly carry these bubbles toward the walls of the vessel. Usually they break within 1 to 2 seconds.

The disappearance of one of these bubbles begins with the membrane above the liquid surface breaking, as shown in frame 24d. Notice that a void in the liquid is created when this membrane breaks. Liquid quickly fills this void, within 1/200 of a second, as shown in frame 24e. This action is so violent that a small geyser of liquid is produced as shown in frame 24f. Occasionally a drop of liquid is expelled upward as in frames 24g and 24h. This phenomenon accounts for all the spray above the liquid observed in this research.

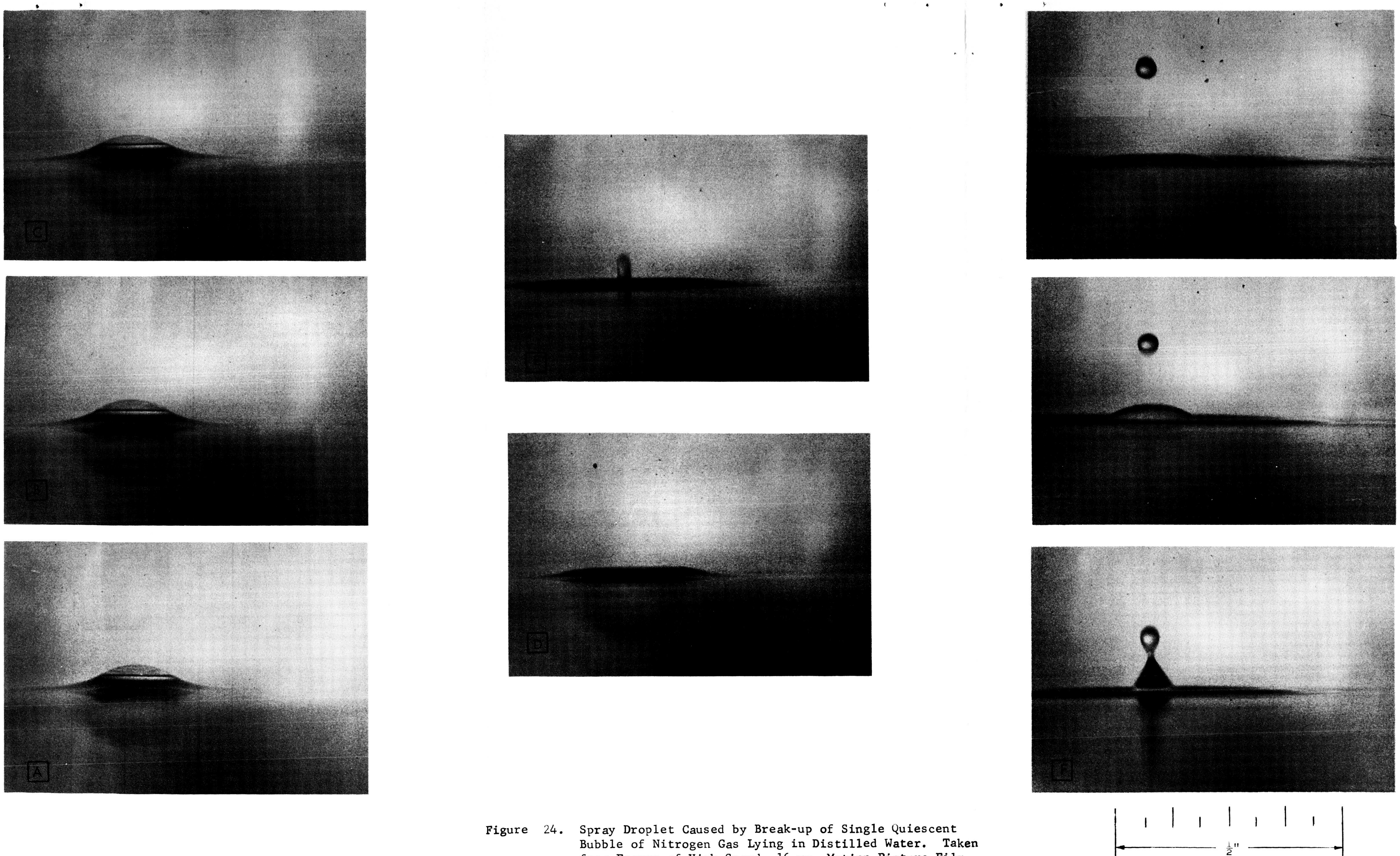

approximate scale

Figure 24. Spray Droplet Caused by Break-up of Single Quiescent Bubble of Nitrogen Gas Lying in Distilled Water. Taken from Frames of High Speed, 16 mm, Motion Picture Film. Time Interval Between Pictures of 1/200 Second.

APPENDIX VII

Correlation of Terminal Rise Velocity of Nitrogen Bubbles Rising in Distilled Water

The bubble rise velocity versus bubble radius correlation of Haberman and Morton (37) for an air-distilled water system has been replotted as Reynolds number N_{Re} versus bubble diameter and is given as the solid line in Figure 25. This correlation appears as Figure 4 of Haberman and Morton.

The data taken from the high speed motion picture film include the terminal rise velocity and the equivalent diameter of the gas bubbles. These data were used to determine the applicability of the Haberman and Morton correlation to our work. Figure 25 also shows a comparison of our nitrogen gas-distilled water data with the air-distilled water correlation of Haberman and Morton.

A best fit line through the data of this research is given as the dashed line. This is probably about as good a comparison as is possible considering the variation in the correlation depending on the quality of the water as shown in the Haberman and Morton article. Also, the impurities found in air as contrasted to our use of pure nitrogen gas could account for a portion of the difference. Haberman and Morton do not show the extent of the scatter of their data, therefore a quantitative comparison is impossible. However, we have arbitrarily used the Haberman and Morton curve for the calculations given elsewhere in this report.

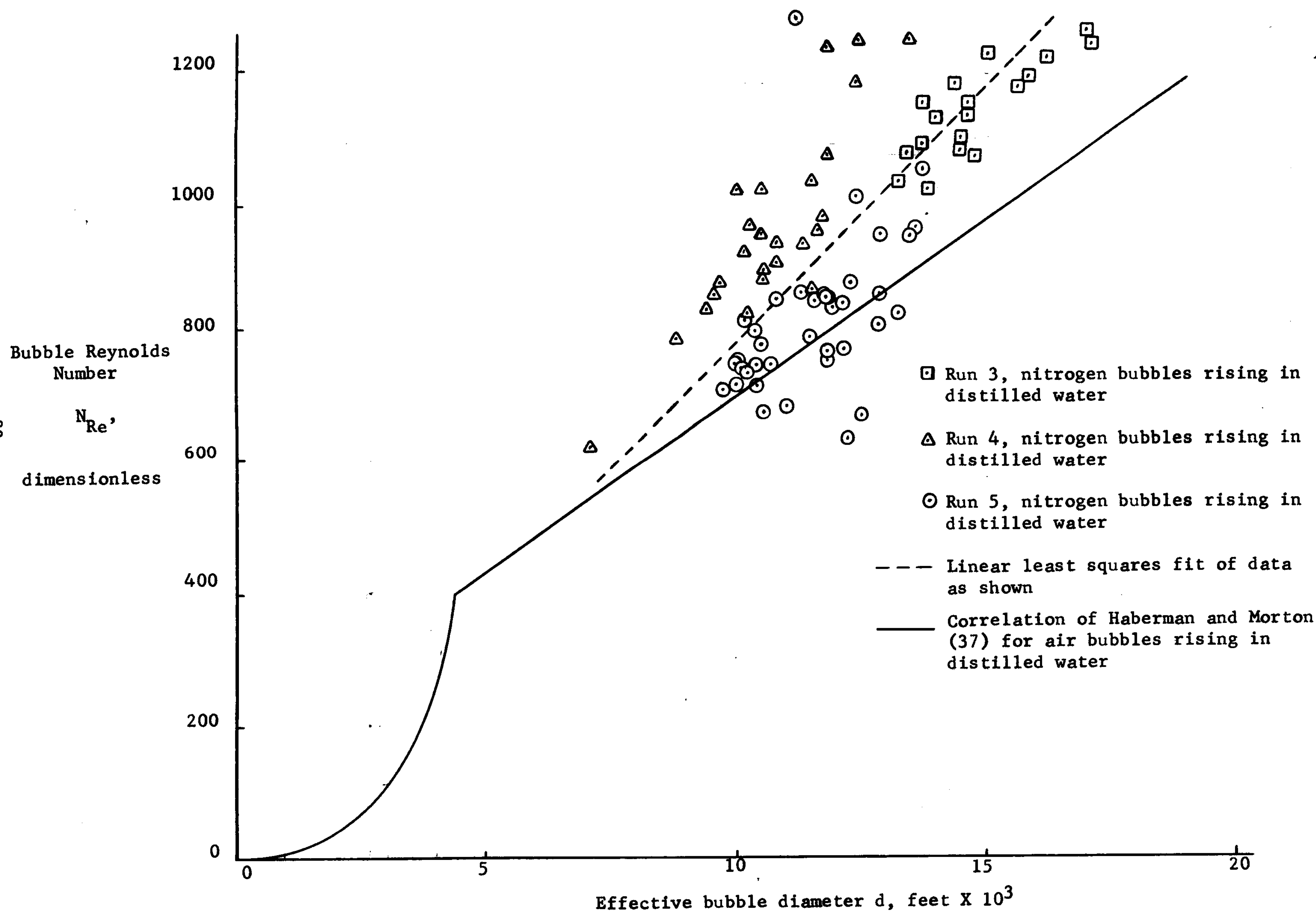

Figure 25. Comparison of Terminal Rise Velocity Data of this Research with the Correlation of Haberman and Morton (37).

APPENDIX VIII

Description of Equipment

The experimental system used in obtaining the data given in this report is shown in Figures 26 and 27. The photograph shows all the equipment presented in the schematic diagram except the bank of photoflood lamps, which are behind the translucent screen to the right. The lighted area on the screen which is a result of the lights may be seen in the photograph.

The locally constructed 155 mm lens is readily apparent between the camera body and the tank. The photograph shows the camera in position to begin recording.

The image of the gas inlet nozzle appears in two faces of the tank wall. This is the largest nozzle that has been used. A stream of a large number of bubbles is shown leaving the nozzle. The twelve brass bolts which attach the nozzle plate to the bottom of the tank may be seen. These bolts seal an opening large enough to accept any nozzle configuration that might be necessary in this research. The nozzle configuration shown is simply a single large nozzle. There is also the capability of changing the single nozzle without disturbing the bolts or the liquid contents.

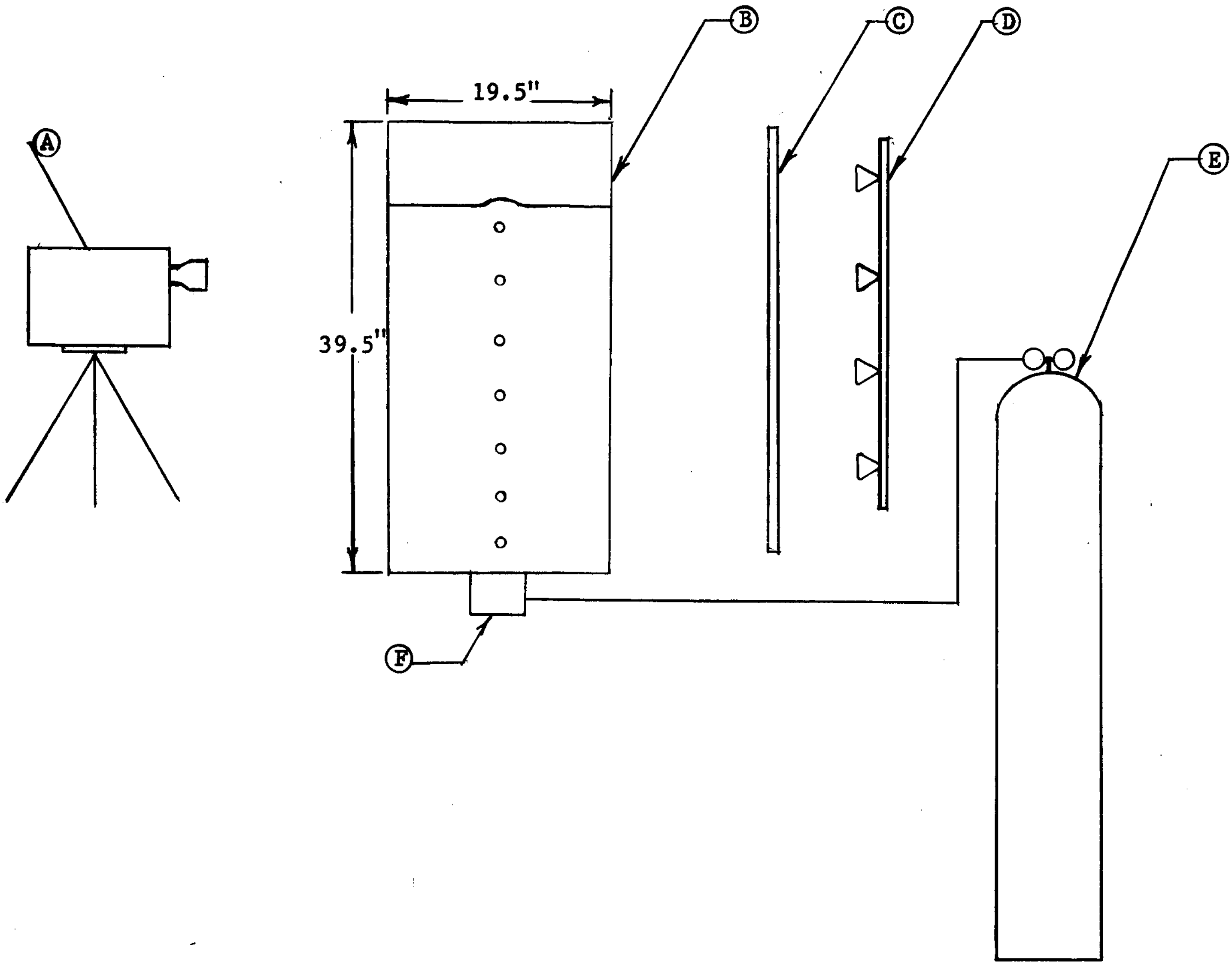

A. Cinerama Model 600 high speed photograph recorder with 155 mm lens
B. square plexiglas tank
C. sheet of translucent plexiglas for diffusing light
D. bank of four 300 watt photoflood lamps
E. tank of inert gas (N_2, He, etc.)
F. bubbler

Figure 26. Schematic Diagram of the Experimental Apparatus

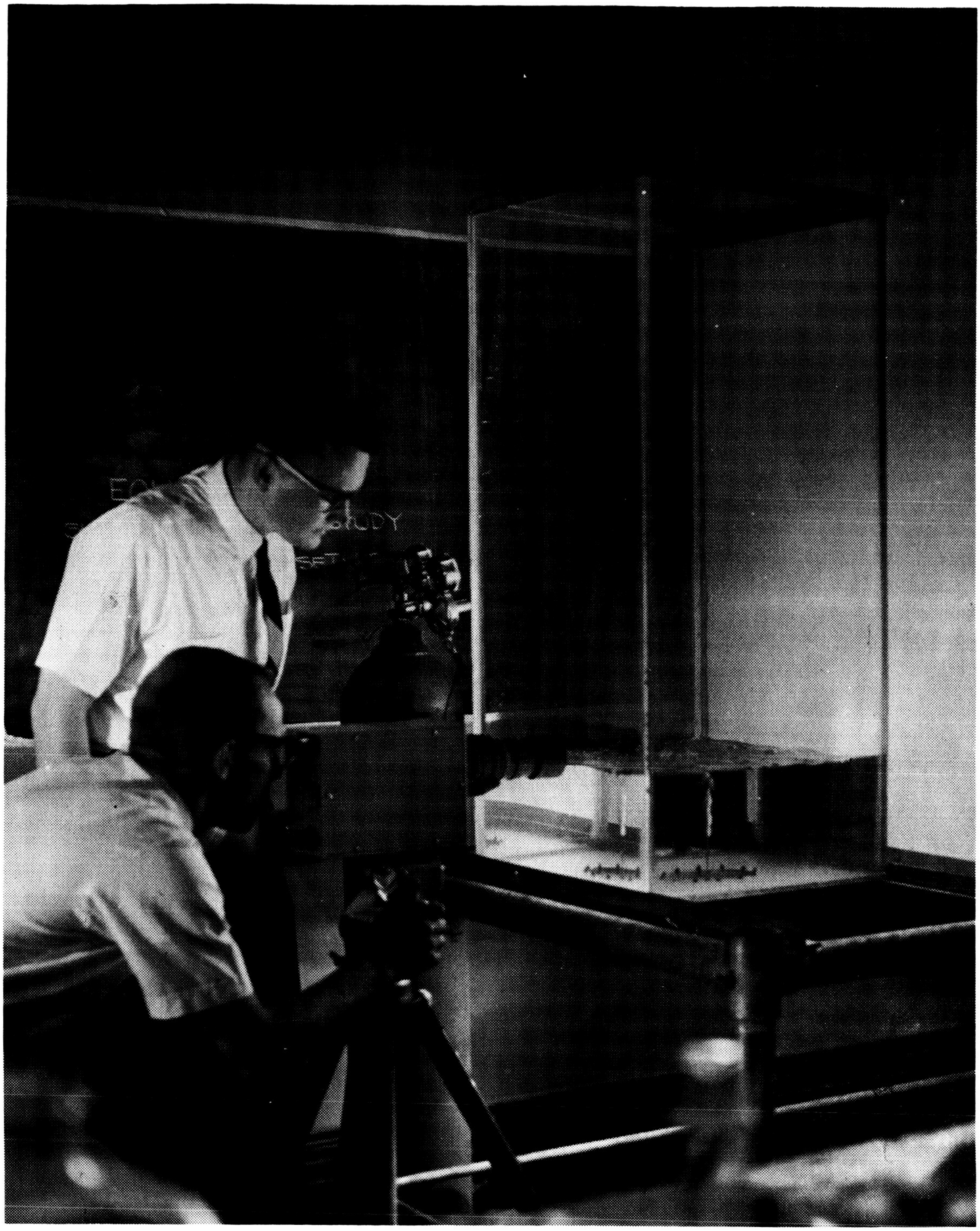

Figure 27. Photograph of Experimental Apparatus.

APPENDIX IX

Tabulation of Experimental Data

SURFACE PROFILE DATA

The numbers in the body of the table refer to the height of the free liquid surface above the dead liquid surface in feet X 10^3.

Equivalent Diameter feet X 10^3	Radial Position r, Dimensionless												
	2.4	1.8	1.4	1.0	0.6	0.2	0.0	0.2	0.6	1.0	1.4	1.8	2.4
6.634	0.4166	1.0000	1.5000	2.3333	2.9166	3.1666	3.2083	3.1666	3.0000	2.5000	1.9166	1.3333	
6.858	1.2917	1.7500	2.0417	3.1666	2.5833	3.7500	2.7583	2.6666	2.3333	1.9166	1.4166		
6.735	0.5417	1.4166	2.0833	3.2500	4.5000	5.0000	5.1666	5.0000	4.2500	2.5000	1.3333	0.6666	0.3333
6.066	0.2500	1.0000	2.0833	2.9166	3.5000	3.6666	3.7083	3.6250	3.3333	2.7500	1.6666	1.6666	0.2917
6.534			1.3333	2.6666	3.4166	3.7500	3.8333	3.7500	3.5833	4.0000	2.1250	0.4166	1.0000
6.989	0.0000	0.3333	0.7917	1.3333	2.3333	3.2500	3.5833	3.4166	3.9166	2.2500	1.3333	0.6666	0.0833
6.374	0.4166	1.1666	2.1666	1.1666	2.8333	4.1666	4.2500	4.0833	3.6666	2.6666	1.5000	0.6666	0.1666
6.109	0.4583	1.0833	1.7500	2.6666	3.4166	3.8333	3.9166	3.7500	3.4166	2.4166	1.5000	1.0000	0.5833
6.625		0.1666	1.5000	2.5833	3.1666	3.5000	3.5833	3.5417	3.1666	2.2500	1.5833	1.2500	
6.773		0.5833	1.2500	2.3333	3.5000	4.0000	4.2500	4.0833	3.7500	3.2500			
6.841			1.0833	1.9166	2.6666	3.2500	3.3333	3.1666	2.0833	0.9166			
6.041				1.1666	1.9166	2.2500	2.2917	2.2500	2.0833	1.4166	0.5833	0.1666	
6.841		0.6250	2.0000	3.3333	4.1666	4.6666	4.7500	5.5833	3.8333	2.0000	1.3333	0.9166	2.4166
6.676		0.4166	0.8333	2.0000	3.3333	3.8333	4.0000	3.9166	3.4166	2.8333	2.0000	1.3333	0.4166
6.373	0.1666	0.6666	1.3333	2.3333	3.1666	3.5833	3.6250	3.5000	3.0833	2.4166	1.5000	1.0000	0.5000
6.508	0.0000	0.4166	0.7500	1.5833	1.0833	4.2500	4.3333	4.2500	4.0000	3.5000	2.3000	1.8333	0.9166

SURFACE PROFILE DATA -- Continued

DEQ	2.4	1.8	1.4	1.0	0.6	0.2	0.0	0.2	0.6	1.0	1.4	1.8	2.4
6.411	0.3333	0.9166	1.8333	2.8333	3.6666	4.0833	4.1666	4.0833	3.8333	3.3333	2.2917	1.6666	1.3333
6.931	0.3333	0.8333	1.5000	2.2500	2.8333	3.1666	3.2500	3.1666	3.5833	1.5000	0.7500	0.4166	
6.130	0.2917	0.8333	1.6666	2.5833	3.7500	4.1666	4.2500	4.1666	3.6666	2.7500	1.8333	1.0000	0.7500
6.936	0.5000	1.0833	2.0000	2.6666	3.0417	3.5000	3.7083	3.4166	2.2500	1.2500	0.9166	0.4166	0.0833
6.193	1.0000	1.3333	1.8333	2.6666	3.5000	4.0000	4.0833	3.9166	3.5833	2.6666	1.8333	1.1666	0.5833
6.596		0.7500	1.3333	2.6666	3.4166	3.6666	3.7500	3.6666	3.4166	2.7500	1.8750	1.0833	0.4166
6.183	1.0000	1.5000	1.8333	2.8333	3.7500	4.0000	4.0833	4.0000	3.5833	3.0833	2.1666	1.4166	1.0000
6.804	0.2500	0.4166	0.8333	1.5000	2.5000	3.2500	3.4166	3.2500	2.8333	2.0833	1.4166	1.0000	0.4166
6.741	0.4166	1.0000	1.3333	2.1666	3.0000	3.8333	3.9166	3.8333	3.4166	2.3333	1.4166	1.0833	0.6250
6.773	0.0833	0.4166	1.1666	1.9583	3.2500	4.0000	4.2500	4.1666	3.6666	2.6666	1.6666	1.0833	0.7500
6.712					4.5000	4.8333	4.9166	4.7500	4.1666	3.0000	1.3333	1.2500	
6.938		0.0000	0.5000	1.4166	3.1666	3.5000	3.5883	3.5000	3.0833	2.5833	1.8333	1.0833	0.4166
6.218	0.8333	1.5000	2.2500	3.1666	3.6666	3.9166	3.9583	3.8333	3.5000	2.7500	2.0000	1.3333	0.5000
6.560	0.9166	1.3333	1.5000	2.0833	2.6666	2.2583	3.0000	2.9583	2.6666	2.1666	1.7500	1.1666	0.7500
6.478		0.4166	0.6666	1.8333	3.6666	4.8333	5.0833	5.0000	4.6666	3.5000	1.9166	0.2166	0.1666
6.322	0.4166	0.6666	1.7500	3.7500	3.5833	4.0000	4.0833	4.0000	3.5000	2.6666	2.0000	1.3333	0.7500
6.466	0.2500	0.7500	1.6666	2.7500	3.5000	4.0000	4.0833	4.0000	3.3333	2.6666			
6.021	0.0000	0.9166	2.2500	3.5000	4.3333	4.5833	4.6666	4.5000	3.9166	2.5000	0.9166	0.2500	0.0000
6.820			0.2500	1.5000	2.8333	3.0000	3.0833	3.0417	2.6666	2.0000	1.2500	0.5000	0.0873
6.305	0.5000	1.0833	1.9166	3.0833	4.0000	4.5000	4.6250	4.5000	4.2500	3.5833	2.7500	2.0833	1.3333

SURFACE PROFILE DATA -- Continued

DEQ	2.4	1.8	1.4	1.0	0.6	0.2	0.0	0.2	0.6	1.0	1.4	1.8	2.4
6.635		0.5000	0.8333	1.6666	2.5833	3.0833	3.2500	3.1666	2.9166	2.5000	1.9166	1.0833	0.5833
6.632	0.3333	0.8333	1.5833	2.3333	3.0000	3.4166	3.5000	3.4166	3.0833	2.4166	1.6666	1.0833	0.5000
6.998	0.0000	0.2500	1.7500	2.9166	3.8333	4.0000	4.0833	3.9166	3.2500	1.9166	0.9166	0.4166	0.0833
6.147	0.6666	1.0833	1.7500	2.5833	3.2500	3.7500	3.9166	3.7500	3.5833	3.5833	1.5000	0.9583	0.6660
6.275		0.6666	1.5000	2.1666	2.9166	3.0833	3.1250	3.0000	2.5833	2.0000	1.3333	0.7500	0.0833
6.769	0.2500	0.3750	0.7500	1.8333	3.2500	3.7917	3.8750	3.8333	3.5000	3.0000			
6.519	0.5833	1.2500	2.3333	3.3333	4.0000	4.2500	4.3333	4.2500	3.9166	3.1666	2.0000	1.1666	
6.227	0.0000	1.0000	2.0833	3.2500	3.9166	4.3333	4.4166	4.2500	3.6666	2.3333	1.4583	0.7500	0.2500
6.670	0.5833	1.2917	2.3333	3.0833	3.6666	4.0000	4.0833	4.0000	3.4166	2.6666	1.5833	0.9166	0.5000
6.700	0.1666	0.6666	1.5000	3.3333	4.3333	4.8333	4.9166	4.8333	4.4166	3.4166	1.9166	1.0000	
Average:6.560	*	*	*	*	*	*	3.9131	3.7971	3.3645	2.3208	1.5678	0.9158	0.4497

*The values equidistant from the center were combined to get a single average given in the right columns.

SURFACE PROFILE DATA

The numbers in the body of the table refer to the height of the free liquid surface above the dead liquid surface in feet X 10^3.

Equivalent Diameter feet X 10^3	Radial Position r, Dimensionless												
	2.4	1.8	1.4	1.0	0.6	0.2	0.0	0.2	0.6	1.0	1.4	1.8	2.4
7.372	0.4166	0.7500	1.3333	2.0000	2.5000	2.7500	2.8333	2.7500	2.0000	0.5000	0.3333	0.2500	0.0833
7.708	0.0000	1.5000	2.9166	3.4166	4.5833	5.0833	5.2083	5.0833	4.0833	2.0000	0.9166	0.5833	0.2917
7.654		0.2500	0.6666	1.6666	3.0000	3.7500	3.8333	3.7500	3.0833	2.0000	0.8333	0.3333	0.0000
7.693		0.6666	1.3333	2.6666	4.0000	4.3333	4.5000	4.3333	3.7500	2.0000	0.9166	0.5833	
7.659	0.1666	0.5000	1.3333	3.6666	5.0833	5.7500	5.9166	5.5833	4.0000	1.5000			
7.884	0.2500	1.0000	1.8333	2.9133	3.4166	3.7500	3.7917	3.6666	3.0833	1.6666			
7.626				1.9166	3.8333	4.5833	4.6666	4.5833	3.7500	2.5000	1.0833	0.5000	
7.456	0.2083	0.5000	1.3333	2.4166	2.5000	3.9573	4.0000	3.9166	3.6666	2.5833	1.5833	1.1250	0 . 7500
7.909		0.0000	1.1666	2.0000	2.6666	3.8750	3.9166	2.8750	2.5833	2.0833	0.8333	0.5000	0.0833
7.515			0.9166	1.7500	2.6666	3.3333	3.4983	3.3333	2.5833	1.5000	0.7500	0.1666	0.0000
7.427	0.2500	0.5833	1.2500	2.3333	3.0833	3.5833	3.6250	3.5833	3.2500	2.1666	1.5000	0.9166	0.5833
7.062	0.4166	0.7500	1.1666	1.9166	3.2500	4.2500	4.3333	4.1666	3.6666	2.4166	0.9166	0.5000	0.3333
7.925	0.5000	0.5833	0.7500	2.0000	4.0833	4.5833	4.6666	4.5833	4.0000	2.5833	0.6666	0.2500	0.0833
7.886			0.3333	1.0833	3.3333	4.5833	4.6666	4.6250	4.2500	1.9166	0.8333	0.4166	0.0000
7.173	0.5000	C.9166	2.0000	3.2500	4.0000	4.3750	4.5000	4.3333	3.5000	1.4166			
7.624		0.1666	0.4583	1.9166	3.1666	3.7083	3.7583	3.7083	2.0833	1.8333	1.0000	0.7500	0.5833
7.142			0.6666	1.8333	2.6666	3.4166	3.5417	3.4166	3.1666	2.5833	1.7500	0.8333	0.2500
7.576		0.3333	0.7500	2.1250	3.7500	4.9166	5.0000	4.9166	4.0000	2.8750	2.0000	1.2500	0.4166

SURFACE PROFILE DATA -- Continued

DEQ	2.4	1.8	1.4	1.0	0.6	0.2	0.0	0.2	0.6	1.0	1.4	1.8	2.4
7.199	0.6666	0.5833	1.1666	2.5000	3.5000	3.8333	3.9166	3.7917	3.2500	2.1250	1.0000	0.2500	0.1666
7.286				1.1666	3.6666	3.7166	3.8333	3.7500	2.8333	1.3333	0.4166		
7.609					0.9166	3.0417	3.2500	3.0833	2.5833	1.8333	0.8333	0.3333	0.0000
7.106	0.2500	0.5000	0.8333	1.5000	2.8333	3.4166	3.5000	3.4166	3.0833	2.5000	1.6666	0.9166	0.4166
7.871				2.0000	3.1666	3.5000	3.5833	3.4166	2.9166	1.5833			
7.707	0.5000	0.7500	1.5000	2.2500	3.0000	3.2500	3.3333	3.2500	2.1666	1.0833	0.7500	0.5000	
7.055	0.5833	0.9166	1.8333	3.0000	4.0000	4.3333	4.4166	4.3333	3.7500	2.6666	1.2500	0.6666	0.2500
7.005	1.0833	1.6666	1.9166	2.0833	3.0000	3.5000	3.6666	3.4166	2.7500	2.2500	1.9166	1.4166	0.5833
7.997	0.0000	0.4166	0.8333	2.2500	3.8333	4.3750	4.8333	4.2500	3.5833	2.3333	1.0000	0.5000	
7.479	0.0000	0.6666	1.4166	2.0000	2.6666	3.3333	3.4166	3.2500	3.0833	2.0833			
7.641	0.1666	0.4166	1.0833	2.3333	3.9166	4.5833	4.8333	4.6666	4.1666	2.3333	1.6666	1.2500	1.0000
7.383	0.4166	1.1666	2.000	3.0833	3.8333	4.2500	4.3333	4.2500	3.5833	2.3333	1.3333	0.7500	0.5000
7.737			0.0833	0.3333	2.3333	4.0833	4.3333	4.2500	3.9166	3.0000	1.0833		
7.593	0.3333	0.6666	1.0000	2.0833	3.0833	3.6666	3.8333	3.6666	3.1666	1.7500	0.7500	0.5000	0.3333
7.263			0.1666	1.3333	2.5833	2.9166	3.0000	2.8333	2.5000	1.5833	0.3333		
7.789	0.0833	0.5833	1.7500	3.0417	3.8333	4.4166	4.5000	4.3333	3.0000	1.9166	1.0833	0.7500	0.1666
7.161	0.2500	0.5000	1.0000	2.3333	3.6666	4.5417	4.6666	4.5000	3.5833	2.1666	0.9133	0.3333	0.0000
Average: 7.523	*	*	*	*	*	*	4.5381	3.9633	3.3018	2.1988	1.1031	0.6157	0.0366

*The values equidistant from the center were combined to get a single average given in the right columns.

SURFACE PROFILE DATA

The numbers in the body of the table refer to the height of the free liquid surface above the dead liquid surface in feet X 10^3.

Equivalent Diameter feet X 10^3	Radial Position r, Dimensionless												
	2.4	1.8	1.4	1.0	0.6	0.2	0.0	0.2	0.6	1.0	1.4	1.8	2.4
11.775		0.1666	0.6666	1.5000	5.5000	5.8333	6.6666	5.8333	4.8333	3.0833	1.0000		
11.620		0.7500	1.0833	2.7500	5.6666	6.8333	7.0000	6.5833	4.3333				
11.014	0.7500	0.7500	1.0833	2.4166	4.4166	5.8333	6.0000	5.8333	5.2500	3.5833	1.7500	1.0833	0.8333
11.085			0.9166	2.3333	5.0833	7.0000	7.5000	7.1666	5.7500	2.5000	1.0833	0.5000	0.0833
11.553				0.9166	3.5000	4.9166	5.0833	4.7500	3.4166	1.9166	1.0000	0.5000	
11.197	0.2500	0.6666	0.9166	1.8333	3.7500	4.8333	4.9166	4.8333	4.0833	2.9166	1.6666	0.9166	0.1666
11.776			1.0000	3.1666	5.5833	6.5000	6.6666	6.3333	4.4166	1.5000	0.6666	0.4166	
11.443		0.6666	1.7500	2.9166	3.9166	4.6666	4.8333	4.7500	4.0833	2.7500	1.2500		
11.194			0.6666	2.1666	4.5833	5.6666	5.8333	5.5833	4.3333	2.2500	1.2500	0.8337	0.4583
11.989	0.1666	0.3333	1.0000	2.4166	3.6666	4.2500	4.5000	4.4166	4.0833	2.3333	1.0000	0.2500	
11.770	0.2083	0.4166	1.4166	4.0833	6.0000	6.6666	6.7500	6.0833	3.6666	1.4166			
11.197		0.1666	1.1666	2.2500	3.8333	4.5000	4.8333	5.6666	2.7500	1.3333	0.4166		
Average: 11.468	*	*	*	*	*	*	5.8470	5.6041	4.4792	2.3621	1.1381	0.4903	0.3645

* The values equidistant from the center were combined to get a single average given in the right columns.

SURFACE PROFILE DATA

The numbers in the body of the table refer to the height of the free liquid surface above the dead liquid surface in feet X 10^3.

Equivalent Diameter feet X 10^3	Radial Position r, Dimensionless												
	2.4	1.8	1.4	1.0	0.6	0.2	0.0	0.2	0.6	1.0	1.4	1.8	2.4
16.457		2.8333	2.9549	3.3333	5.5833	7.0000	7.1666	6.9166	6.0417	4.6666	3.0833	1.7500	0.8333
15.983	2.2500	3.6666	4.2500	4.9166	5.6250	6.0833	6.0833	6.0833	5.0000				
15.601			2.7500	4.2500	6.1666	7.3333	7.5833	7.4166	6.6666	5.4166	3.3333	2.2500	
16.160		1.7500	3.2500	4.8333	7.3333	8.5833	8.6666	8.4166	7.5833	4.5000	2.7500	2.0833	
16.141		1.3333	2.4166	2.0833	7.4166	9.0000	9.1666	9.0833	8.6666	7.1666	4.5833	2.6666	1.9166
16.453			3.5833	5.5000	8.6666	10.666	10.833	10.750	10.333	9.0000	7.2500	4.4166	1.9166
16.024	0.7500	2.1666	3.0833	4.8333	10.833	13.083	13.250	13.167	12.917	11.833	10.583	8.0000	2.9166
16.052		2.5833	4.1666	7.0000	8.5833	9.0833	9.1666	9.0833	8.1666	4.5833	2.3333	1.4166	
16.011		2.0833	2.1666	3.2500	6.1666	8.0333	8.1666	8.1666	7.3333	5.7500	3.7500	2.5000	1.5000
16.437		1.5833	4.6666	6.7500	8.0000	8.4166	8.5833	8.5833	8.1666	7.5200	5.9166	4.1666	
Average: 16.132	*	*	*	*	*	*	8.8666	8.8655	7.8400	5.8400	4.0600	2.9611	1.4912

*The values equidistant from the center were combined to get a single average given in the right columns.

SURFACE PROFILE DATA

The numbers in the body of the table refer to the height of the free liquid surface above the dead liquid surface in feet X 10^3

Equivalent Diameter feet X 10^3	Radial Position r, Dimensionless												
	2.4	1.8	1.4	1.0	0.6	0.2	0.0	0.2	0.6	1.0	1.4	1.8	2.4
17.480		3.2500	5.000	5.7500	9.1666	9.9166	10.000	9.8333	7.9166	6.8333			
17.210				6.3333	9.0000	10.083	10.166	10.166	8.9166	6.6666	4.2500	3.6666	
17.756		2.8333	4.4166	6.7500	8.9166	10.500	10.750	10.417	9.0833				
17.389				7.9166	9.2500	13.750	14.583	14.250	12.250	8.7500	4.3333	3.7500	
17.275				8.3333	9.5000	13.916	14.333	14.083	12.833	9.0833	4.9166	2.7500	
17.316			1.1667	4.4166	6.8333	7.9166	8.0000	7.9166	6.2500	3.0000	0.8333		
17.360				8.4166	12.250	12.500	13.416	12.667	11.667	6.4166	2.9166	1.0833	
17.819		2.0833	3.2500	17.000	10.667	12.166	12.333	12.250	10.000	5.9166			
17.667			2.8333	6.9166	9.2500	10.416	10.416	10.416	9.3333	7.5000	4.5000	3.2500	2.0000
17.437		1.7500	2.2500	3.5000	4.9166	5.8333	6.0000	5.9166	5.0833	4.0833	3.4166	2.8333	
17.802		0.9166	2.0833	3.6666	9.1666	14.167	14.500	14.500	12.750	9.6666	4.2500	2.8333	
17.346			1.8333	2.2500	9.4166	12.083	12.083	11.833	9.5000				
17.577			3.1666	5.2500	7.2500	7.8333	8.0000	7.6666	5.4166				
17.437			1.3333	2.5000	6.0000	7.2500	7.2500	7.2500	5.9166	2.6666	1.9166	1.4166	0.7500
17.541			1.6666	6.0000	13.167	12.417	12.500	12.417	10.583	5.2500	3.9166	3.8333	
17. 884		2.8333	5.0000	5.7500	7.9166	11.000	11.166	11.000	8.8333	5.8333	1.4166	0.0000	
17.026		0.9166	2.4166	7.8333	10.417	11.667	12.417	11.667	10.833	6.0833			
Average: 17.489	*	*	*	*	*	*	11.053	10.803	9.0713	6.1624	3.0440	2.2922	

*The values equidistant from the center were combined to get a single average given in the right columns.

APPENDIX X

Determination of Bubble Equivalent Diameter

The equivalent bubble diameter is defined as the diameter of a sphere whose volume is equal to the actual volume of the bubble. To determine the bubble volume, the following procedure was followed:

(1) The solid geometric shape of a given bubble was assumed to be ellipsoidal, with A, B, and C as the radii in the x, y, and z directions respectively.

(2) Suitable values for A and C were obtained from selected frames of the high speed motion picture film, e.g., Figure 11L, page 35.

(3) Since the radius B could not be obtained from the film, its value was assumed to be the average of A and C.

(4) The bubble volume was calculated from

$$VOL = \frac{4}{3}\pi ABC \quad . \tag{51}$$

(5) The volume determined in step (4) above was set equal to the volume of a sphere, and the bubble equivalent diameter calculated from:

$$DEQ = \frac{6.VOL}{\pi}^{1/3} \quad . \tag{52}$$

APPENDIX XI

Literature Survey

A literature search was made to obtain the reported research relating to formation, growth, ascent velocity, shape, and size distribution of gas bubbles in liquids. The search included the following sources of information.

1. <u>Chemical Abstracts</u>
   1940 - July 1964

2. <u>Engineering Index</u>
   1938 - July 1964

3. <u>Applied Mechanics Reviews</u>
   January 1960 - July 1964

4. <u>Chemical Titles</u>
   January 1961 - July 1964

5. <u>Science Abstracts</u>
   Section A, 1940 - 1961

6. <u>Applied Science and Technology Index</u>
   1958 - March 1964

A listing of the technical articles which were obtained is given in the Bibliography.

An attempt was made to improve the usefulness of this lengthy list by distributing the articles into the following categories:

A. Formation of Gas Bubbles in Liquids

B. Size, Shape, and Volume Change of Gas Bubbles in Liquids

C. Rate of Rise of Gas Bubbles in Liquids

D. Swarms of Gas Bubbles in Liquids

E. Experimental Apparatus and Procedures

F. Foreign Publications of Possible Interest Which are to be Translated

G. Publications of Peripheral Interest

The titles of the categories give a good description of their content with the exception of Category G.

A number of articles were located which reported research related to gas bubbles in liquids, but were of doubtful interest to the particular problem which is of interest in this investigation. However, in order to present as complete a literature survey as possible, these references are given in Category G, entitled Publications of Peripheral Interest.

A. Formation of Gas Bubbles in Liquids. Articles which are applicable to this category are given in the Bibliography under the following numbers: 6, 7, 13, 14, 15, 16, 29, 40, 43, 44, 45, 46, 47, 53, 54, 55, 60, 70, 77, 94, 95, 97, 104.

B. Size, Shape, and Volume Change of Gas Bubbles in Liquids. Articles which are applicable to this category are given in the Bibliography under the following numbers: 2, 8, 10, 13, 17, 20, 22, 26, 28, 37, 42, 44, 56, 59, 60, 61, 63, 69, 71, 74, 75, 76, 80, 84, 101, 103, 104, 105, 106.

C. Rate of Rise of Gas Bubbles in Liquids. Articles which are applicable to this category are given in the Bibliography under the following numbers: 11, 13, 17, 22, 37, 38, 48, 53, 66, 68, 71, 82, 85, 92, 93, 101, 102.

D. Swarms of Gas Bubbles in Liquids. Articles which are applicable to this category are given in the Bibliography under the following numbers: 53, 60, 99.

E. Experimental Apparatus and Procedures. Articles which are applicable to this category are given in the Bibliography under the following numbers: 3, 6, 13, 14, 16, 17, 20, 28, 37, 38, 40, 43, 46, 49, 51, 52, 53, 60, 62, 67, 70, 71, 77, 81, 85, 92, 95, 98, 99.

F. Foreign Publications of Possible Interest which are to be Translated. Articles which are applicable to this category are given in the Bibliography under the following numbers:

German Articles - 12, 35, 36, 50, 89, 90

French Articles - 1, 5

Russian Articles - 33

G. Publications of Peripheral Interest. Articles which are applicable to this category are given in the Bibliography under the following numbers: 4, 9, 18, 19, 21, 23, 25, 25, 27, 30, 31, 32, 34, 39, 41, 57, 58, 64, 65, 72, 73, 78, 79, 83, 86, 87, 88, 96, 100.

BIBLIOGRAPHY

1. Angelino, H., Charzat, C., and Williams, R., "Evolution de bulles de gaz dans des liquides at des systems fluidises," Chemical Engineering Science 19, 289-304 (1964).

2. Barlow, E. J. and Langlois, W. E., "Diffusion of Gas from a Liquid into an Expanding Bubble," I.B.M. Journal of Research and Development 6, No. 3, 329-337 (July 1962).

3. Barton, J. C., Donnelly, R., Green, J. A. S., and Lewis, F. A., "Cinematographic Study of the Evolution of Hydrogen Bubbles During Overpotential Measurements," Naturwissenschaften 51, No. 1, 9 (1964).

4. Bauer, H. F., "Fluid Oscillations in the Containers of a Space Vehicle and their Influence upon Stability," NASA TR R-187, NASA, Washington, D.C., February 1964.

5. Behar, M. and Semeria, R., "Contribution to the Study of the Behavior of Gas Bubbles in a Liquid," Compt. Rend. Acad. Sci. Paris 255, No. 10, 1331-1333 (September 1962).

6. Benzing, R. J. and Myers, J. E., "Low Frequency Bubble Formation at Horizontal Circular Orifices," Industrial and Engineering Chemistry 47, No. 10, 2087-90 (1955).

7. Bernath, L., "Theory of Bubble Formation in Liquids," Industrial and Engineering Chemistry 44, No. 6, 1310-1313 (1952).

8. Berry, V. J., "Effect of a Liquid Phase Velocity on the Growth and Collapse of Gas Bubbles," J. Chemical Physics 20, 1045 (1952).

9. Birkhoff, G. and Caywood, T.E., "Fluid Flow Patterns," Journal of Applied Physics 20, 646-649 (1949).

10. Birkhoff, G., Margulies, R. S., and Horning, W.A., "Spherical Bubble Growth," The Physics of Fluids 1, No. 3, 201-204 (1958).

11. Chao, B. T., "Motion of Spherical Gas Bubbles in a Viscous Liquid at Large Reynolds Numbers," The Physics of Fluids 5, No. 1, 69-79 (1962).

12. Coester, von Erwin, "Die Steigegeschwindigkeit von Gasblasen in Flussigkeiten unterschiedlicher Viskositat und Oberflachenspannung," Zeitschrift fur angewandte Physik 13, No. 5, 254-259 (1961).

13. Datta, R. L., Napier, D. H., and Newitt, D. M., "The Properties and Behavior of Gas Bubbles Formed at a Circular Orifice," Transactions Institution of Chemical Engineers, 14-26 (February 14, 1950).

14. Davidson, J. F. and Schuler, B. O. G., "Bubble Formation at an Orifice in a Viscous Liquid," Transactions Institution Chemical Engineers 38, 144-154 (1960).

15. Davidson, J. F. and Schuler, B. O. G., "Bubble Formation at an Orifice in an Inviscid Liquid," Transactions Institution Chemical Engineers 38, 335-342 (1960).

16. Davidson, L. and Amick, E. H., "Formation of Gas Bubbles at Horizontal Orifices," American Institute of Chemical Engineering J. 2, No. 3, 337-342 (1956).

17. Davies, R. M. and Taylor, G., "The Mechanics of Large Bubbles Rising through Extended Liquids and through Liquids in Tubes," Proc Roy Soc A 200, 375-90 (1950).

18. Dean, R. B., "The Formation of Bubbles," Journal of Applied Physics 15, 446-451 (1944).

19. de Becze, D. and Liebmann, A. J., "Aeration in the Production of Compressed Yeast," Industrial and Engineering Chemistry 36, 882 (1944).

20. Dergarabedian, P., "The Rate of Growth of Vapor Bubbles in Superheated Water," Journal of Applied Mechanics 20, No. 4, 537-545 (1953).

21. Dukhin, S. S. and Deriagin, B. V., "Method of Calculating the Precipitation of Disperse Particles from a Stream on an Obstacle," Kolloidn. Zh. 20, No. 3, 309-311 (1958).

22. Epstein, P. S. and Plesset, M. S., "On Stability of Gas Bubbles in Liquid-Gas Solutions," Journal of Chemical Physics 18, No. 11, 1505-1509 (1950).

23. Eversole, W. G., Wagner, G. H., and Stackhouse, E., "Rapid Formation of Gas Bubbles in Liquids," Ind. and Eng. Chem. 33, 1459 (1941).

24. Fedoseev, V. A., "Dispersion of a Stream of Superheated Liquid," Kolloidn. Zh. 20, No. 4, 463-466 (1958).

25. Forster, H. K., "Diffusion in a Moving Medium with Time Dependent Boundaries," A. I. Ch. E. Journal 4, 535 (1958).

26. Forster, H. K., "On the Conduction of Heat into a Growing Vapor Bubble," Journal of Applied Physics 25, 1067-1068 (1954).

27. Forster, H.K. and Zuber, N., "Growth of Vapor Bubbles in a Superheated Liquid," Journal of Applied Physics 25, 474 (1954).

28. Foulk, C. W. and Miller, J. N., "Experimental Evidence in Support of the Balanced-Layer Theory of Liquid Film Formation," Industrial and Engineering Chemistry 23, No. 11, 1283-88 (1931).

29. Fox, F. E. and Herzfeld, Karl F., "Gas Bubbles with Organic Skin as Cavitation Nuclei," The Journal of the Acoustical Society of America 26, No. 6, 984-989 (1954).

30. Gleim, V. G., Shelomov, I. K., and Shidlovskii, "Processes Leading to Generation of Droplets in the Rupture of Bubbles at Liquid-Gas Interfaces," Zh. Prikl. Khim. 32, No. 1, 222-226 (1959).

31. Glotov, V. P., Kolobaev, P.A. and Neuimin, G.G., "Investigation of the Scattering of Sound by Bubbles Generated by an Artificial Wind in Sea Water and the Statistical Distribution of Bubble Sizes," Akusticheskii Zhurnal 7, No. 4, 421-427 (1961).

32. Goldsmith, H. L. and Mason, S. G., "The Movement of Single Large Bubbles in Closed Vertical Tubes," Journal of Fluid Mechanics 14, No. 1, 42-58 (1962).

33. Gorodetskaya, A., "The Rate of Rise of Bubbles in Water and Aqueous Solutions at Great Reynolds Numbers," Zhur. Fiz. Khim 23, 71-77 (1949).

34. Gorring, R. L. and Datz, D. L., "Bubble Rise in a Packed Bed Saturated with Liquids," A. I. Ch. E. Journal 8, No. 1, 123-126 (1962).

35. Grassmam, P., and Lemaire, L. H., "Zur Darstellung Aweiphasiger Stromungsvorgange,"Chemie-Ing.-Techn. 30, No. 7, 450-454 (1958).

36. Grassmann, P. and Reinhart, A., "Zur Ermittlung der Sinkgeschwindigkeit von Tropfen under der Steiggeschwindigkeit von Blasen," Chemie-Ing.-Techn. 33, No. 5, 348-9 (1961).

37. Haberman, W. L. and Morton, R. K., "An Experimental Investigation of the Drag and Shape of Air Bubbles Rising in Various Liquids," Navy Department - The David W. Taylor Model Basin, September 1953.

38. Hartunian, R. A. and Sears, W. R., "On the Instability of Small Gas Bubbles Moving Uniformly in Various Liquids," Fluid Mechanics 3, Pt. 1, 27-47 (1957).

39. Harrison, M., "An Experimental Study of Single Bubble Cavitation Noise," The Journal of the Acoustical Society of America 24, No. 6, 776-782 (1958).

40. Hayes, W. B., Hardy, B. W., and Holland, C. D., "Formation of Gas Bubbles at Submerged Orifices," A.I.Ch.E. Journal 5, No. 3, 319-24 (1959).

41. Hill, T., "Concerning the Dependence of the Surface Energy and Surface Tension of Spherical Drops and Bubbles on Radius," J. Amer. Chem. Soc. 72, 3923-3927 (1950).

42. Hovestreijdt, J., "The Influence of the Surface Tension Difference on the Boiling of Mixtures," Chemical Engineering Science 18, 631-639 (1963).

43. Hughes, R. R., Handlos, A. E., Evans, H. D., and Maycock, R. L., "The Formation of Bubbles at Simple Orifices," Chemical Engineering Progress 51, No. 12, 557-563 (1955).

44. Jackson, R. W., "The Formation of Gas Bubbles from Orificies - Part 1," The Industrial Chemist 28, 346-351 (1952).

45. Jackson, R. W., "The Formation of Gas Bubbles from Orifices - Part 2," The Industrial Chemist 28, 391-398 (1952).

46. Jackson, R. W., "The Formation of Gas Bubbles from Orifices - Part 3," The Industrial Chemist 29, 16-20 (1953).

47. Jackson, R. W., "The Formation of Gas Bubbles from Orifices - Part 4, The Industrial Chemist 29, 109-118 (1953).

48. Kaparthi, R., "Terminal Velocities of Liquid Drops and Air Bubbles," Trans. Indian Inst. Chem. Eng. 11, 18-22 (1958-59).

49. Kintner, R. C., Horton, T. J., Graumann, R. E., and Amberkar, S., "Photography in Bubble and Drop Research," The Canadian Journal of Chemical Engineering 39, 235-241 (1961).

50. Kling, G., "Uber die Dynamik der Blasenbildung beim Begasen Von Flussigkeiten Unter Druck," Int. J. Heat Mass Transfer 5, 211-223 (1962).

51. Klinkenberg, A. and Mooy, H. H., "Dimensionless Groups in Fluid Friction Heat, and Material Transfer," Chemical Engineering Progress 44, No. 1, 17-36 (1948).

52. Knapp, R. T. and Hollander, A., "Laboratory Investigations of the Mechanism of Cavitation," American Society of Mechanical Engineers - Transactions 70, 419-435 (1948).

53. Krevelen, D. W. van and Hoftijzer, P. J., "Studies of Gas-Bubble Formation - Calculation of Interfacial Area in Bubble Contactors," Chemical Engineering Progress 46, No. 1, 29-35 (1950).

54. Krishnamurthy, S., Kuman, R., Datta, R. L., and Kuloor, N. R., "Correlation of Data on Bubble Formation in Viscous Liquids," Indian J. Technol. 2, No. 2, 67 (1964).

55. Krishnamurthy, P. G., Kumar, R., Datta, R. L., and Kuloor, N. R., "Formation of Air Bubbles through Nozzles at Right Angles to Liquid Column," Indian J. Technol. 2, No. 2, 68-69 (1964).

56. Ladyzhensky, R. M., "Investigation of the Shape of a Gas Bubble Ascending in a Stationary Liquid," J. Applied Chem. U.S.S.R. 29, No. 1, 217-24 (1956).

57. Lamb, Sir H., Hydrodynamics, Dover Publications, New York, 1945.

58. Langhaar, H. J., Dimensional Analysis and Theory of Models, John Wiley and Sons, New York, 1951.

59. Larsen, P. S. and Clark, J. A., "The Dynamics of Gas-Vapor Bubbles in Binary Systems," The University of Michigan, NASA Contract No. NAS8-825, 187 pp., November 1963.

60. Leibson, I., Holcomb, E. G., Cacoso, A. G., Jacmic, J.J., "Rate of Flow and Mechanics of Bubble Formation from Single Submerged Orifices," A. I. Ch. E. Journal 2, No. 3, 296-306 (1956).

61. Liebermann, L., "Air Bubbles in Water," Journal of Applied Physics 28, No. 2, 205-211 (1957).

62. Mahoney, J. F. and Wenzel, L.A., "Formation of Moderate-Size Bubbles, " A. I. Ch.E. J. 9, No. 5, 641-645 (1963).

63. Manley, D. M. J. P., "Change of Size of Air Bubbles in Water Containing a Small Dissolved Air Content," British Journal of Applied Physics 11, 38-42 (1960).

64. Marique, L. A. and Houghton, G., "Analog Computer Solution of Modified Rayleigh Equation and Parameters Affecting Cavitation," Can. J. Chem. Eng. 40, No. 3, 122-6 (1962).

65. Mellen, R. H., "An Experimental Study of the Collapse of a Spherical Cavity in Water," The J. of the Acoustical Society of America 28, No. 3, 447-454 (1956).

66. Moore, D. W., "The Boundary Layer on a Spherical Gas Bubble," Journal of Fluid Mechanics 16, No. 2, 161-176 (1964).

67. Nishikawa, K., "Photographic Study of Saturated Free Convection Stable Film Boiling," Bulletin of Japan Society of Mechanical Engineers 4, No. 13, 115-123 (1961).

68. O'Brien, M. P. and Gosline, J. E., "Velocity of Large Bubbles in Vertical Tubes," Industrial and Engineering Chemistry 27, 1436-1440, (1935).

69. Pattle, R. E., "The Aeration of Liquids, Part 1, The Solution of Gas from Rising Bubbles," Institution of Chemical Engineers Papers, 27-31 (February 14, 1950).

70. Pattle, R. E., "The Aeration of Liquids, Part II, Factors in the Production of Small Bubbles," Transactions Institution of Chemical Engineers, 32-37 (February 14, 1950).

71. Peebles, F. N. and Garber, H. J., "Studies on the Motion of Gas Bubbles in Liquids," Chemical Engineering Progress 49, No. 2, 88-97 (1953).

72. Perkins, A. S. and Westwater, J. W., "Measurements of Bubbles Formed in Boiling Methanol," A. I. Ch. E. Journal 2, No. 4, 471-476 (1956).

73. Plesset, M. S., "The Dynamics of Cavitation Bubbles," Journal of Applied Mechanics 16, 277-282 (L949).

74. Plesset, M. S. and Hsieh, Din-yu, "Theory of Gas Bubble Dynamics in Oscillating Pressure Fields," The Physics of Fluids 3, No. 6, 882-892 (1961).

75. Plesset, M. S. and Zwick, S. A., "A Nonsteady Heat Diffusion Problem with Spherical Symmetry," Journal of Applied Physics 23, No. 1 95-98 (1952).

76. Plesset, M. S. and Zwick, S. A., "The Growth of Vapor Bubbles in Superheated Liquids," Journal of Applied Physics 25, No. 4, 493-500 (1954).

77. Poutanen, A. A. and Johnson, A. I., "Studies of Bubble Formation and Rise," Can. J. Chem. Eng. 38, No. 4, 93-101 (1960).

78. Prandtl, L. and Tietjens, O. G., Fundamentals of Hydro- and Aeromechanics, Dover Publications, New York, 1934.

79. Preston, F. W. and Turnbull, J. C., "The Physics of Upward Drilling," Glass Ind. 22, 57-59 (1941).

80. Rayleigh, Lord, "On the Pressure Developed in a Liquid During the Collapse of a Spherical Cavity," Philosophical Magazine and Journal of Physics 34, 94-98 (1917).

81. Riggle, G. C. and Weisburger, J. H., "Gas Bubble and Liquid Flow Detector, an Automatic Control System for Column Chromatography," Analytical Chemistry 36, No. 6, 1167-1168 (1964).

82. Robinson, J. V., "The Rise of Air Bubbles in Lubricating Oils," J. of Physical and Colloid Chemistry 51, 431-437 (1947).

83. Roll, J. B. and Myers, J. E., "Measurement of Dynamic Surface Tension in Bubbling Systems," Journal of Chemical and Engineering Data 9, No. 2, 256-8 (1964).

84. Ruckenstein, E., "On Mass Transfer in the Continuous Phase from Spherical Bubbles or Drops," Chem. Eng. Sc. 19, No. 2, 131-146 (1964).

85. Saffman, P. G., "On the Rise of Small Air Bubbles in Water," Journal of Fluid Mechanics 1, Pt. 3, 249-275 (1956).

86. Savic, P. and Gosnell, J. W., "The Dynamics of the Expanding Vapor Bubble in a Boiling Liquid," The Canadian Journal of Chemical Engineering 40, No. 6, 238-245 (1962).

87. Scriven, L. E., "On the Dynamics of Phase Growth," Chem. Eng. Sci. 10, 1-13 (1959).

88. Senior, D. A., "A Theoretical Treatment of Combustion in a Spherical Underwater Gas Bubble," Proceedings of the Royal Society 251, 493-503 (1959).

89. Siemes, W., "Gasblasen in Flussigkeiten," Chemie - Ing.-Techn. 26, Pt. 1, No. 8/9, 479-496 (1954).

90. Siemes, W., "Gasblasen in Flussigkeiten," Chemie - Ing. - Techn. 26, Pt. 2, No. 11, 614-630 (1954).

91. Siemes, W. and Borchers, E., "Zur Blasengrosse in Blasenaulen," Chem. Eng. Sci. 12, No. 2, 77-87 (1960).

92. Smirnov, N. I. and Ruban, V. L., "Velocity of Movement of Drops in a Median in the Laminar Region," J. Appl. Chem. U.S.S.R. 25, No. 7, 1357-1361 (1952).

93. Smirnov, N. I. and Ruban, V. L., "Droplet Motion in Media," J. Appl. Chem. U.S.S.R. 26, No. 1, 95-99 (1953).

94. Spells, K. E., "Bubble Formation by Rapid Air Flow Through Slots Submerged in Water," Trans. Instn. Chem. Engrs. 32, No. 3, 167-173 (1954).

95. Spells, K. E. and Bakowski, S., "A Study of Bubble Formation at Single Slots Submerged in Water," Trans Instn. Chem. Engrs., 38-51 (Feb. 14, 1950).

96. Strenge, P. H., Orell, A., and Westwater, J. W., "Microscopic Study of Bubble Growth During Nucleate Boiling," A. I. Ch.E. Journal 7, No. 4, 578-583 (1961).

97. Takagi, S., "Theory of the Formation of Bubbles," Journal of Applied Physics 24, No. 12, 1453-1461 (1953).

98. Tuson, K. R., "Single Exposure Photography of a High Speed Event," British Journal of Applied Physics 6, No. 3, 99-100 (1955).

99. Verschoor, H., "Some Aspects of the Motion of a Swarm of Gas Bubbles Rising through a Vertical Liquid Column," Transactions Institution of Chemical Engineers 52-62 (Feburary 14, 1950).

100. von Glahn, U. and Polcyn, R. P., "On the Effect of Head Addition in Empirical Correlation of Void Fractions for Steam-Water Flow," NASA TN D 1440, NASA, Washington, D. C., November 1962.

101. Walters, J. K. and Davidson, J. F., "The Initial Motion of a Gas Bubble Formed in an Inviscid Liquid," J. Fluid Mechanics 12, Pt. 3, 408-416 (1964).

102. White, E. T. and Beardmore, R. H., "The Velocity of Single Cylindrical Air Bubbles through Liquids Contained in Vertical Tubes," Chem. Eng. Sci. 17, 351-361 (1962).

103. Yang, Wen-Jei and Clark, J. A., "On the Application of the Source Theory to the Solution of Problems Involving Phase Change. Part 1 - Growth and Collapse of Bubbles," Transactions of the A.S.M.E. 86, No. 2 Series C, 207-212 (1964).

104. Zuber, N., "The Dynamics of Vapor Bubbles in Nonuniform Temperature Fields," J. Heat and Mass Transfer 2, No. 1-2, 83-105 (1961.)

105. Zwick, S. A., "Growth of Vapor Bubbles in a Rapidly Heated Liquid," The Physics of Fluids 3, No. 5, 685-692 (1960).

106. Zwick, S. A. and Plesset, M. S., "On the Dynamics of Small Vapor Bubbles in Liquids," Journal of Mathematics and Physics 33, No. 4, 308-330 (1955).